Acceptance Testing and Energy-based Mission Reliability in Unmanned Ground Vehicles

by

Amir A Sadrpour

A dissertation submitted in partial fulfillment
of the requirements for the degree of
Doctor of Philosophy
(Industrial and Operations Engineering)
in the University of Michigan
2014

Doctoral Committee:

Professor Jionghua Jin, Co-Chair
Professor A. Galip Ulsoy, Co-Chair
Associate Professor Ella M. Atkins
Assistant Professor Mariel Lavieri

I dedicate this dissertation to my parents Sholeh and Hadi for their endless support, encouragements and love.

ACKNOWLEDGEMENTS

It gives me great pleasure in acknowledging the support and encouragement of my advisers professor Judy Jin and professor A. Galip Ulsoy for mentoring me throughout the period of my Ph.D. studies. Without their support and mentorship, the completion of this dissertation would not have been possible. I want to especially thank the other members of the committee, Professor Ella Atkins and Professor Mariel Lavieri for their valuable comments, suggestions and guidance over the past three years.

I would like to thank Dr. Timothy Johnson, Dr. Kerby Shedden, Dr. Vijay Nair, and Dr. Douglas Schaubel for their inspiring courses and guidance and for helping me to develop my background in statistics which inspired many of the topics in this dissertation.

My special gratitude also goes to Dr. Kamran Paynabar who as a friend and mentor always provided me with constructive feedback and Pegah for her moral support. Also, I am thankful of the undergraduate students, Jongsoo Choi, Yongxian He, and Rafael Martinez who helped with various aspects of my research.

Finally, I would like to express my extreme gratitude to my parents and brother for encouraging me with their best wishes throughout my education.

My research was supported in part by the Ground Robotic Reliability Center (GRRC), Automotive Research Center (ARC), the United States Army Tank Automotive Research, Development and Engineering Center (TARDEC), and by University of Michigan through Graduate Student Instructorship.

TABLE OF CONTENTS

DEDICATION ii

ACKNOWLEDGEMENTS iii

LIST OF FIGURES vii

LIST OF TABLES ix

ABSTRACT x

CHAPTER

I. Introduction 1

1.1 Research Motivation 1
1.2 Research Goals, Challenges and Contributions 3
1.2.1 Simulation-based Acceptance Testing for Unmanned Ground Vehicles 3
1.2.2 Mission Energy Prediction for Unmanned Ground Vehicles 6
1.2.3 Dynamic Energy-Reliable Path Planning for Unmanned Ground Vehicles 9
1.2.4 The Role of Operator Style on Mission Energy Requirements for Tele-Operated Unmanned Ground Vehicles 11
1.3 Outline of Dissertation 12

II. Simulation-based Acceptance Testing for Unmanned Ground Vehicles . . 15

2.1 Introduction 15
2.2 Proposed Methodology 18
2.3 Study of Torque Saturation & Rollover Failures 19
2.3.1 Static and Dynamic Simulation Framework 21
2.3.2 Statistical Hypothesis Test for Simulation Comparison 24
2.3.3 Identifying the Test Range for the Joint Torque Saturation Failures 27
2.3.4 Study of Rollover Failure 28
2.4 Study of the Suspension System & Flip Over Failures 29
2.4.1 Static and Dynamic Simulation Framework 30
2.4.2 Statistical Hypothesis Test for Simulation Comparison 32
2.4.3 Statistical Assessment of Safe Operating Speed Using Dynamic Simulation 34

III. Mission Energy Prediction for Unmanned Ground Vehicles 37

3.1 Introduction 37

3.2 Methodology . . . 40
3.2.1 Overview of Methodology . . . 40
3.2.2 Vehicle Dynamic Model . . . 41
3.3 Approach 1: Linear Regression in the Absence of Prior Knowledge . . . 43
3.3.1 Linear Regression for Power Prediction . . . 43
3.3.2 EWMA Control Chart Monitoring . . . 44
3.3.3 Prediction of Mission Energy Requirement . . . 44
3.4 Approach 2: Bayesian Estimation and Prediction in the Presence of Prior Knowledge . . . 46
3.4.1 Bayesian Estimation . . . 46
3.4.2 Prior Updating for Future Missions Based on Past Measurements 49
3.4.3 Prediction of Mission Energy Requirement . . . 50
3.4.4 Application Scope of Proposed Methods . . . 50
3.5 Experimental Validation of the Model . . . 51
3.5.1 Measurement System Capability Analysis . . . 53
3.5.2 Model Linearity with Respect to Velocity . . . 54
3.5.3 Model Linearity with Respect to Road Grade . . . 55
3.5.4 Effect of Road Surface Condition on Power Consumption . . . 56
3.5.5 Estimating the Internal Power Consumption . . . 57
3.5.6 Prior Knowledge . . . 58
3.6 Experimental and Simulation Studies . . . 58
3.6.1 Experimental Study 1: Impact of Mission Prior Knowledge on Energy Prediction . . . 60
3.6.2 Experimental Study 2: Effect of Mission Imprecise Prior Knowledge on Energy Prediction . . . 62
3.6.3 Simulation Study: In-advance Parameter Updating Using the Vehicle Surrogate Model . . . 63
A Appendix . . . 67
A.1 Velocity Prediction . . . 67
A.2 Energy Prediction with Linear Regression Model (RLS approach) . 67
A.3 Energy Prediction with Bayesian Regression Model . . . 68
A.4 Surface Type Grouping Using Tukey's Test . . . 70
A.5 Energy Prediction Confidence Interval . . . 70

IV. Dynamic Energy-Reliable Path Planning for Unmanned Ground Vehicles 71

4.1 Introduction . . . 71
4.1.1 Problem Statement . . . 71
4.2 Methodology Overview . . . 74
4.3 Methodology . . . 75
4.3.1 Vehicle Model . . . 75
4.3.2 Problem Definition . . . 77
4.3.3 Bayesian Prediction of Energy Requirement . . . 78
4.3.4 Pruning of Undesirable Paths . . . 81
4.3.5 Exploration Feasibility & Exploration Budget . . . 81
4.3.6 Exploration Budget Assignment . . . 82
4.3.7 Exploitation . . . 84
4.4 Simulated Case Study . . . 84
A Appendix . . . 88
A.1 Parameter Estimation for Random Slope . . . 89
A.2 Predictive Distribution of Output . . . 90
A.3 Posterior Updating Using Similarities . . . 92
A.4 Covariance of Energy Requirement of Road Segments . . . 92
A.5 Estimating the Reduction in Uncertainty . . . 93

V. The Role of Operator Style on Mission Energy Requirements for Tele-Operated Unmanned Ground Vehicles 94

5.1 Introduction 94
5.2 Simulation Model 96
5.2.1 Optimal Velocity 96
5.2.2 Vehicle Longitudinal/Lateral Model 98
5.2.3 Simulink Model 98
5.3 Response Surface Design 99
5.4 Simulation Results 101
5.4.1 Model Selection 101
5.4.2 Simulation Results 102
5.5 Recommendations for Reduction of Mission Energy Requirements 104

VI. Concluding Remarks 107

6.1 Summary of Major Work and Results 107
6.2 Summary of Major Contributions 109
6.3 Future Research 112

BIBLIOGRAPHY 117

LIST OF FIGURES

Figure

1.1 Outline of dissertation . . . 13
2.1 Proposed methodology . . . 20
2.2 Multi-body dynamic simulation model . . . 21
2.3 Schematic of a two-link robot arm . . . 21
2.4 Static and dynamic simulation torque profiles . . . 24
2.5 Statistical comparison between dynamic and static simulations . . . 26
2.6 Boundaries of safe-operation for robot arm . . . 27
2.7 Example of robot tilt orientations . . . 28
2.8 Boundaries of safe-operation for rollover . . . 28
2.9 UGV crossing a bumpy road . . . 29
2.10 Free body diagram of the UGV . . . 30
2.11 Static simulation results . . . 31
2.12 The effect of road roughness on force profiles . . . 33
2.13 Statistical test for comparison of dynamic and static simulations . . . 34
2.14 Loss of contact is an early indication of other failures . . . 35
2.15 Boundaries of safe operation for suspension breakdown . . . 36
3.1 Overview of methodology for prediction of mission energy . . . 41
3.2 UGV on a mission with no prior knowledge . . . 43
3.3 Percent of total energy associated with the driving style . . . 45
3.4 Drive cycle based on a scaled EPA US06 . . . 45
3.5 UGV on a mission comprised of s road segments. . . . 48
3.6 Experimental data for measurement system capability test . . . 53
3.7 Power versus speed plot on sidewalk for linearity test . . . 55
3.8 Power versus speed plot on grass for linearity test . . . 55
3.9 Power versus grade for sidewalk and asphalt roads . . . 56
3.10 Boxplot of power consumption on different road surfaces . . . 57
3.11 The short mission is composed of two road segments. . . . 59
3.12 The long mission (a round trip) is composed of four road segments. . . . 59
3.13 The PackBot used on grass and sidewalk surfaces . . . 61
3.14 UGV power profile . . . 61
3.15 Energy prediction mean vs. time using the Bayesian, RLS, and naive approaches . 62
3.16 Categorizing the first road segment as flat-grass instead of downhill-sidewalk . . . 64
3.17 End-of-mission energy prediction vs. time . . . 66
4.1 Methodology overview . . . 75
4.2 The energy requirement distributions of a simple network . . . 76
4.3 The convex structure of the objective function in exploration allocation . . . 83
4.4 Scaled EPA drive cycle was used in simulation studies . . . 85
4.5 Network of Simulation Study . . . 87
4.6 Initial energy requirement distributions of paths & path two energy distribution . . 87
4.7 Updated energy distributions using exploration . . . 88

5.1 Optimal velocity characterization 97
5.2 The simulation model of the operator and vehicle. 99
5.3 Impact of reference velocity on energy requirements 104
6.1 The proposed future research direction 113

LIST OF TABLES

Table		
2.1	Comparison of dynamic and static simulations	19
2.2	The robot arm orientation	22
2.3	Parameters used in the static and dynamic simulations	31
3.1	Experimentally established prior knowledge	48
3.2	Driving style prior information (average speed)	48
3.3	Sample of power measurements for measurement capability test.	54
3.4	Features presented in the study	60
3.5	Parameters of Experimental Study 1.	62
3.6	Strategies for in-advance updating of road combined parameter	64
3.7	Simulation parameters	65
3.8	Prior information for simulation study	65
4.1	Parameters of the simulated case study.	86
5.1	Factors and their levels in the simulation study.	101
5.2	Significant factors and their coefficients	103
5.3	Summary of recommendations for improving mission energy requirements.	105
5.4	Recommendations for improving mission energy requirements based on the type of control.	105

ABSTRACT

Acceptance Testing and Energy-based Mission Reliability in Unmanned Ground Vehicles (UGVs)

by

Amir Sadrpour

Co-Chair: Dr. Judy Jin

Dr. A. Galip Ulsoy

The objective of this research is to explore and develop new methodologies and techniques to improve UGV mission reliability. This dissertation focuses on two research issues that are critical in the following UGV deployment phases: (1) prior to field deployment to remove design deficiencies; and (2) during field usage to prevent mission failures.

Four specific research topics are accomplished. The first topic focuses on simulation-based acceptance testing. A general framework is proposed to integrate dynamic and static simulations. Statistical hypothesis testing is used to compare static and dynamic simulations to determine when a simple static simulation can be used to replace the complex dynamic simulation. Results show that the static simulation can be used when a failure mechanism is not significantly affected by the dynamic characteristics of the vehicle. The remaining research topics aim at prevention of operational failures due to unexpected energy depletion. A model-based Bayesian prediction framework integrated with a dynamic vehicle model is proposed in the second research topic, which improves traditional approaches for estimation and prediction. The Bayesian framework combines mission prior knowledge with real-time measurements for adaptive prediction of end-of-mission energy requirement. Experimental studies were conducted, which validated and demonstrated the advantages of the framework on roads with different surface types and grades.

The third research topic, entitled real-time energy reliable path planning, builds upon the above mentioned prediction framework to identify the most energy reliable path in a stochastic

network with unknown and correlated arc lengths. Since traditional sequential optimization techniques cannot be directly applied to this problem, a heuristic approach based on two stage exploration/exploitation is proposed to identify the most reliable path. The framework, which minimizes the cost of exploration, outperforms traditional path planning approaches.

In the final research topic, the impact of operator driving style on mission energy requirements is investigated using statistical response surface. While the previous topics help with overall mission planning regardless of the operator's driving style, here, improving the driving style to increase energy availability is studied. The optimal drive cycle that minimizes energy consumption and procedures for reduction of energy consumption are proposed.

CHAPTER I

Introduction

1.1 Research Motivation

Unmanned ground vehicles (UGVs) are entering the economic mainstream, and are being used more extensively in military as well as commercial applications (Tilbury and Ulsoy, 2011). However, studies of mobile robots used in Urban Search and Rescue (US&R) and Military Operations in Urban Terrain (MOUT) have shown a mean time between failures (MTBF) in the field of 6 to 20 hours, far below the desired 96 hours as established by Test and Evaluation Coordination Office at the Department of Defense (Kramer and Murphy, 2006). Despite the current limitations and deficiencies in their reliability, UGVs are still expected to be a less expensive and safer alternative for space missions, mining, agriculture, rescue operations, and military applications (Hagras et al., 1999, 2002; Larsson et al., 2010). Given the prevalence of UGVs, their reliability has a wide-reaching, significant impact on the economy, our security efforts overseas, and our standard of living.

Limited research has been done in reliability and failure analysis of UGVs. In Carlson et al. (2004), a novel taxonomy of UGV failures is introduced which classifies them into two major categories: physical and human operational failures. The physical failures are further categorized based on the UGV subsystems, while human failures are attributed to faulty design or human-robot interactions. However, limited study was presented in the area of human-robot interactions. Understanding failures mechanism is the first step for improving UGV performance and reliability.

The key causes of failures can be attributed to manufacturing, design, and operations. This thesis focuses on failures caused by (1) exceeding the vehicle design limitations (i.e., design failures), and (2) misuse during field operations (i.e., operational failures). The design failures are addressed by investigating the limitations of design to meet typical operational requirements. Boundaries of safe operation are developed as a guideline for operating within the limits of the vehicle design.

For the purpose of demonstration, a few commonly encountered scenarios, such as lifting objects using the UGV manipulator arms, were studied. The methodology can be readily extended to other typical scenarios, such as the vehicle dragging capability and stair climbing scenarios.

In the area of operational failures, there are many failure modes that can be considered. This thesis focuses on preventing unanticipated battery depletion failure by predicting the energy requirement in a typical surveillance mission. The motivation for studying this failure mode is its linkage to challenging operational factors such as uncertain and diverse road conditions and operator driving style. Also, there is very little research on power system failures, and the limited available literature mainly focuses on failures at the component level, attributing 9-25% of overall reported failures to the power systems (Carlson and Murphy, 2005; Kramer and Murphy, 2006). To achieve this research objective, it was necessary to carry out three research topics: (1) prediction of a mission energy requirement for a pre-specified mission scenario, (2) performing real-time path planning using adaptive predictions, and (3) studying the impact of operator driving style on the mission energy requirement. Similar to the design stage, the methodologies developed here can be extended to other failure modes and types of vehicles. For instance, a similar Bayesian framework can be extended to unmanned aerial or underwater vehicles.

While the scope of potential research opportunities is broad, the perspective of the research in this dissertation is to ensure UGV mission reliability by developing strategies for reducing and preventing UGV failures during the design and operation stages, which includes: (a) Discovery and removal of UGV's design deficiency in order to meet the dispersed requirements of various mission tasks and operating conditions. Unlike industrial robots and conventional vehicles, UGVs are typically designed with limited choices and brands. Consequently, the available UGVs may have to work in geographically dispersed areas or different operating conditions (Gage, 1995), which should be fully considered in the design and testing specifications. (b) Prevention of mission failures by adaptively adjusting the UGV remaining mission tasks according to the online monitoring of the UGV's operational and environmental condition changes. Because of the inevitable uncertainty of environmental conditions, UGVs may often encounter an unanticipated environmental change that may significantly affect its expected mission reliability. As a typical example, the UGV's battery energy requirement may vary for different operating time/distances, which is also closely affected by road conditions and operators' driving styles (speed, acceleration, etc.). Consequently, mission energy requirements cannot be fully predicted before its execution. Moreover, different UGVs, even with the same design specifications, may still have inherent performance variations caused by different manufacturing processes. Therefore, it is critical to accurately predict the remaining

lifetime or mission reliability based on real-time monitoring of UGV's operating status under the specific environmental condition. (c) To prevent unanticipated mission failures during the mission execution, an adaptive planning of UGV's remaining mission tasks becomes necessary. A typical patrol mission may consist of several alternative paths that the vehicle selects from to reach the destination (i.e., exploitation). The energy requirements of the paths may not be known in advance, but by exploring shortly on the roads, more precise estimates can be obtained. Due to limited energy storage, a limited amount of exploration can be conducted. Thus, path planning needs to balance between the amount of energy spent on exploration and exploitation. (d) To investigate the impact of teleoperation on energy consumption of a small UGV to answer critical questions such as: does the variations in the operators' driving style significantly change the energy consumption in a surveillance mission? In the above mentioned research topics, the mission energy requirement is predicted without interfering with the operator's activities using real-time measurements. In the final research topic, by playing a more proactive role in the operations, the goal is to alter the driving style or improve the operator-vehicle interface to reduce the energy requirements in a typical surveillance mission. To do so, factors in the driving style that significantly impact the energy requirements are identified, and procedures to make the driving style more energy efficient are proposed.

1.2 Research Goals, Challenges and Contributions

In this section, research topics highlighted in the previous section are briefly discussed in the following subsections. For each topic, an overview of research objectives, motivations, literature review and the proposed methodology are provided.

1.2.1 Simulation-based Acceptance Testing for Unmanned Ground Vehicles

Even with a sharp increase in the number of UGVs in military operations, studies show average failure rates to be much worse than the desired benchmarks (Kramer and Murphy, 2006). Some of the failures are due to manufacturing or subtle interactions between components; these failures can be detected and prevented prior to field deployment. However, other failures are due to uncertain operating environments, misuse by operators, and insufficient understanding of failure modes. Therefore, it is important to develop an acceptance test to provide better understanding of the failure modes and to ensure that such systems meet their reliability goals. Although such testing methods are widely used in various engineering applications, there is still no general guidance for UGV acceptance tests in terms of mission reliability.

The goal of Chapter II is to suggest research ideas and develop methods to perform an acceptance test for small UGVs. Some of the earliest works on UGV reliability and acceptance testing were done by Carlson and Murphy (2003), Carlson and Murphy (2005), Carlson et al. (2004), and Stancliff and Dolan (2005). Murphy discussed a methodology similar to a final factory acceptance test, i.e., a test usually performed by a manufacturer prior to shipping. In Kramer and Murphy (2006), the role of endurance testing for rescue and safety robots is discussed. The test uncovered failures under certain conditions as well as key design and manufacturing issues. Endurance and agility tests were also conducted at the US Army Aberdeen Test Center (ATC) on small size UGVs. The robots were tested under a variety of actual operating conditions to validate their design reliability (Tricomo, 2009).

In terms of performance standards, the Department of Homeland Security Science and Technology Directorate initiated an effort in 2004 with National Institute of Standards and Technology (NIST) to develop comprehensive standards to support development, testing, and certification of effective robotic technologies for Urban Search & Rescue operations (Messina and Jacoff, 2006). These standards address robot mobility, sensing, navigation, and human system interaction (Jacoff et al., 2009). Recently, Pepper et al. (2007) used the standardized physical tests in NIST to validate the UGV's simulation models under given scenarios.

There are major limitations that almost all of the above acceptance and performance testing share. Due to the limited testing facilities and apparatus, often only a small range of operational requirements can be physically tested. Additionally, conducting physical tests can be time consuming and tedious requiring expert operators. Moreover, there are many uncontrollable or hard-to-control factors in physical tests such as variations in different operators' knowledge and operating skills, environmental condition changes, etc., which may lead to inevitable variations in the physical testing results.

In contrast to the physical tests, the simulation-based tests, as a complementary tool to physical tests, can be very time efficient since they can be fully automated and a full scale or broader variety of scenarios can be easily integrated into the simulation. Simulation-based evaluation methods have played an increasing role in complementing physical tests in other industries, such as aerospace and automotive (Norris, 1995; Guonian et al., 2010). The results can be used to systematically identify the boundaries of safe operation range for vehicles under various scenarios. Our simulation-based acceptance testing is based on two models: dynamic and static simulation models. Dynamic simulation can include a variety of environmental conditions and uncertainties which makes its results more accurate. However, the dynamic simulation models are more time consuming and costly to

construct. Static simulation, on the other hand, is more straightforward and quick to construct, but does not include operational variations and uncertainty. Using the static simulation, we can readily derive UGV boundaries of safe operation through closed form static equations, while, in the dynamic case, these boundaries are obtained by exploring the large space of dynamic parameters and environments through simulations.

The static simulation is more time efficient, but it may not always be an acceptable approximation for the dynamic simulation when the failure mechanism in a scenario is significantly affected by the dynamic characteristics of the UGV. Comparisons between the simulation results is typically done qualitatively in an ad-hoc manner by visual inspection of results or through expert inputs.

Some major challenges in this research include: (1) how to develop efficient models that can incorporate operational variations into the simulation; (2) how to develop quantitative methods to capture the effect of operational variations and environmental uncertainties; (3) how to develop comprehensive guidelines for safe operating conditions considering the diverse robot configurations and the wide range of applications.

The main approach of Chapter II is to propose a systematic method to quantitatively ensure when a static simulation analysis is satisfactory for acceptance testing of UGVs. For this purpose, dynamic and static simulation results are compared by proposing a statistical hypothesis testing, which is used to systematically judge whether both simulations will make a consistent decision on the failure state for a given acceptance testing scenario. The purpose of using a statistical hypothesis test is to consider the inherent performance variation due to operational or environmental uncertainties.

Two sets of commonly encountered UGV failure scenarios are investigated: the first set studies joint torque saturation and rollover when the UGV attempts to lift various loads; and the second set focuses on the suspension system and flip over failures when the UGV is operated on bumpy terrains with mild roughness. The results from the simulations show that while a static simulation model can be appropriately used for determining the required joint motor torques of UGVs under slow operation speeds, dynamic simulation model is needed to determine the maximum allowable moving speeds for UGVs to be safely operated on bumpy terrains.

In summary, the original contributions of Chapter II are as follows: (1) development of a simulation-based acceptance test for UGVs to complement the physical tests, (2) use of statistical tests to systematically determine if a static simulation is sufficient to replace dynamic simulation for each acceptance test scenario, (3) enhanced understanding of the safe operation boundaries of UGVs to avoid typical UGV failures.

1.2.2 Mission Energy Prediction for Unmanned Ground Vehicles

One of the key factors that limit the utility of small tele-operated battery-powered UGVs is the available on-board energy. Typical mission durations are currently on the order of 1-2 hours, while it is often desirable to carry out much longer missions (e.g., 8-10 hours) between lengthy recharging stops. For a typical UGV, the primary source of energy consumption is the vehicle locomotion. For example, typical relative order-of-magnitude power requirements for a hypothetical mission might be 100W for propulsion, 10W for computation, and 1W for communication. Furthermore, the power requirement for propulsion can vary dramatically with road conditions, road grade, as well as operators' driving styles.

The goal of Chapter III is to develop a method for UGV mission energy prediction, to provide an online estimate of the expected mission energy requirement. As an example, the energy requirement for conducting a surveillance mission in real-time is carried out. A typical surveillance mission consists of various tasks and several alternative paths that a UGV can traverse. Since each battery has limited energy storage capacity, it is essential to predict the expected energy requirements for alternative paths.

This research study has the following challenges. (1) The random terrain characteristics (i.e., surface type and average grade) and their energy requirements may not be known in advance. (2) The terrain characteristics of each path can be different from one phase of the mission to another, resulting in different energy requirements throughout segments of the mission. (3) Different UGVs, even with the same design specifications, may still have inherent performance variations caused by manufacturing variations. Consequently, the mission energy requirement cannot be fully predicted before the mission execution. (4) Small UGVs are typically tele-operated and rely on electric rechargeable batteries for their operations. Each battery has limited energy storage capacity. Thus, it is essential to obtain an accurate prediction of the expected mission energy requirement during the mission execution and update this prediction adaptively via real-time performance measurements (e.g., vehicle power consumption and velocity).

The majority of reliability studies have focused on (real-time) sensory measurements for reliability and failure prediction. For instance, past endurance tests on small UGVs have shown that some operational failures can be prevented by real-time monitoring of key performance measures (Kramer and Murphy, 2006). Prognostics and health monitoring is an approach that permits the reliability of a system to be evaluated in actual operating conditions and has been discussed in Vichare et al. (2007), Lu et al. (2001b), Gorjian et al. (2009), and Lu et al. (2001a). The limitation of such methods

is that they have not incorporated mission prior knowledge, such as duration of tasks, nature and difficulty of tasks ahead or operating style of the users, in their reliability assessments.

Most UGVs use rechargeable batteries for their operations. One approach to predict the battery end of cycle is to consider the history of its discharge rate. For instance, particle filters have been used to predict the battery end of cycle (Saha et al., 2007; Saha and Goebel, 2008; Saha et al., 2009a). However, the above prediction methods only use real-time data to determine the prediction of battery end of cycle. Consequently, ignorance of the intensity of tasks ahead may lead to an over- or underestimation of the battery end of cycle. More recently, particle filters have been used to predict the battery end of cycle for unmanned aerial vehicles (UAVs) (Saha et al., 2011), in which the mission load profile obtained through offline experimentation is used to further improve the prediction of particle filters. However, since the environment with which the UAV interacts is not directly modeled, some inevitable changes in the actual mission profile, such as an increase in the duration of tasks, is difficult to incorporate in the prediction.

Incorporating mission prior knowledge in prediction can improve prediction accuracy significantly. For instance, consider a surveillance mission with the goal of traveling from a start point to a final point where a UGV needs to traverse two road segments to accomplish this mission. The first road segment is downhill with an asphalt road surface, and the second road segment is on average flat and is a grass surface. Without knowledge of the future terrains that the vehicle will face, one can assume that at any point in the mission, the future power requirement is similar to the past. Thus, by collecting and monitoring the instantaneous power consumption of the vehicle, the average power consumption from past measurements may be used to predict future power consumption. When the vehicle traverses the first road segment (i.e., downhill/asphalt), the power consumption is substantially less than when it traverses the second road segment (flat/grass). Consequently, if the average power measurements from the first road segment were used to predict future energy requirements, the resultant predictions will considerably underestimate the true energy requirement of the mission. Our goal is to improve the predictions by integrating the available prior knowledge of road segment terrains with real-time sensory measurements.

The first original contribution of this research topic is to propose a physical model based Bayesian prediction approach. The proposed model structure considers terrain characteristics, and allow us to integrate mission prior information with real-time measurements for online energy prediction (Sadrpour et al., 2013c; Ulsoy et al., 2012). The expected prior knowledge consists of qualitative information about the road conditions and road grades, which can reasonably be expected to be known prior to a mission. For instance, Google Earth and Geocontext Center for Geographic Analysis

provide topographic profiles (i.e., grade profiles) for any custom-made paths at any location on the Earth's surface (Google-Earth, 2013; Geocontext, 2013). Although at the early stages of a mission, the uncertainty of prior knowledge might be large, this uncertainty is reduced based on online updating using the Bayesian framework.

The second contribution of this work is to conduct comprehensive physical and statistical testing to experimentally validate the proposed model and prediction approach. The majority of the existing simulation validations of robotic systems are either based on inspection and qualitative comparison between the simulated model behavior and the real vehicle or based on the visual inspection of graphs from collected measurements. The objective of these studies is to determine if the gross behavior of both the physical and simulated platforms are similar (Balakirsky et al., 2009). For instance, validation studies of multi-body dynamic simulations (Sadrpour et al., 2011) have been presented in (Balakirsky et al., 2009; Pepper et al., 2007; Carpin et al., 2007; Taylor et al., 2007; Carpin et al., 2006; Chen et al., 2009; Rossetti et al., 1998; Mei et al., 2005). Pepper et al. (2007) mainly relies on visual inspection in a few scenarios, to test whether the simulated vehicle behaves in a similar way as the physical robot and does not take advantage of real-time sensory information. In Carpin et al. (2007), validation focuses on aspects such as mission completion time on different road segments, but quantitative comparison among completion times is not performed.

Simulation and validation of human robot interactions (HRI) is presented in Wang et al. (2005), but due to insufficient data, statistical comparisons between the simulated and physical platforms were not conducted. Validation of simulations/simulators involving medical robots have been considered in (Seixas-Mikelus et al., 2010; Lendvay et al., 2008). While Seixas-Mikelus et al. (2010) focuses on face validity (i.e., a measure of the realism of the simulator) of a Robotic Surgery Simulator, Lendvay et al. (2008) goes a step further and presents the first demonstration of face and construct validity of a virtual-reality robotic simulator. Some preliminary statistical analysis based on confidence intervals for HRI was presented in Crandall et al. (2005); however, most validation studies were based on simulations.

Although validation studies of UGV simulations have been the focus of several past studies, the majority of those analyses only provide qualitative results based on the visual inspection of differences between simulation results and the behavior of the physical robot. Chapter III presents a comprehensive quantitative and statistical validations study, which is the first of its kind for UGVs.

1.2.3 Dynamic Energy-Reliable Path Planning for Unmanned Ground Vehicles

Surveillance missions that involve tele-operated battery-powered UGVs often encounter a situation where a UGV has to choose between alternative paths to complete its mission. Since each battery has a limited energy storage capacity, it is essential to predict the expected energy requirement of alternative paths to help the operator choose the most energy efficient path with high certainty. The goal of surveillance missions studied here is to start from a known location on a map and reach a destination point using one of the available alternative paths. The mission is represented by a network where arcs symbolize road segments and nodes represent intersections of road segments. The cost of each arc is the energy required to traverse the arc. This energy requirement is affected by unknown factors such as road surface condition and grade. Thus, the energy requirement of each road segment is a random variable with an unknown distribution.

The objective of Chapter IV is to identify the path with the highest probability of successfully completing the mission using the information available at any given time. One failure mode of our interest is the unanticipated depletion of the UGV's stored energy, which results in a failure to occur before reaching the destination point.

The most reliable path planning can be considered as a variation of a larger class of problems known as shortest path problems (SPP). Deterministic shortest path problems (Powell, 2011; Denardo, 2003) as well as stochastic shortest path problems (SSPP) with known distributions have been extensively studied (Powell, 2011; Fan et al., 2005). In our research, the assumption of known path cost distributions is relaxed. Moreover, unlike shortest path problems, this research integrates the uncertainty of path costs in the planning stage. A stochastic most reliable path problem with normally and correlated random costs were investigated in Seshadri and Inivasan (2010), however, the distributions of costs were assumed to be precisely known prior to the mission.

When the distributions of costs of paths are not known, adaptive learning through exploration becomes an essential part of decision making (Sutton and Barto, 1998). The exploration is comprised of collection of a limited amount of data from an arc in the network to learn its cost distribution more precisely. An exploration policy based on the Knowledge Gradient (KG) was used in a stochastic shortest path problem in which the cost distributions of arcs were not known (Ryzhov and Powell, 2011). However, in Ryzhov and Powell (2011), exploration could be performed on any arc in the network at any given time. This exploration policy cannot be applied to our problem since the UGV can only collect sequential measurements from the road segment that it traverses at a given time. Also, unlike their problem, the exploration cost increases when additional sampling information is

needed from a previously explored road segment. To collect the additional information from a road segment, the UGV must revisit the segment and traverse further than the original point of initial measurements to obtain new observations.

In the traveling salesman problem (TSP), unlike SPP or SSPP, the objective is to minimize the cost of visiting all the nodes in a network only once and returning to the initial location (Applegate et al., 2011). Several papers investigate variations of TSP for UGV path planning with energy considerations. In Wei et al. (2012), a path planning problem is discussed for mobile robots with the objective of minimizing the energy requirement, which is similar to TSP having the capability of recharging using docking stations with deterministic arc costs. A TSP in a dynamic environment for mobile robots was considered in Sipahioglu et al. (2008). They monitor changes in the network, such as when a node becomes active or inactive, and dynamically change the path. The paper assumes that such information from any arbitrary part of the network can be obtained, and at the time of decision making, it uses a deterministic cost model.

Another class of energy efficient path planning for small unmanned vehicles deals with a coverage task problem. In a coverage task, the UGV is required to move through an area and travel within a certain distance of each point. Broderick et al. (2012) investigates an energy efficient coverage task using optimal control. Unlike a shortest path formulation, the UGV must visit every point on the map. Coverage tasks have also been studied in Mei et al. (2004) with a focus on minimizing the energy for locomotion by tuning the vehicle velocity and trajectory. However, their models are deterministic and do not consider the impact of terrain variations on power consumption.

Chapter IV presents a unique path planning problem for UGVs, with the following characteristics and challenges: (1) The arc cost distributions are not fully known *a priori*. (2) The arc costs can be correlated. (3) The distributions of arc costs can be updated online by real-time measurements. (4) UGVs can only collect measurements from the road segment that they traverse.

The contribution of this research topic is the development of a novel dynamic energy-reliable path planning approach that divides the planning decisions into two stages of exploration and exploitation. At the exploration stage, a unique energy efficient strategy is developed to determine how many measurements to collect during exploration to reduce the prediction uncertainty and bias. Real-time measurements are used to dynamically determine the allocated energy for exploration and to assess and update mission feasibility. In the exploitation stage, the UGV traverses the most reliable path chosen from the exploration stage. Our simulation results show that the proposed approach outperforms commonly used offline methods in which a path is selected using only the mission prior knowledge, as well as a method that does not use the exploration, and only relies on exploitation.

1.2.4 The Role of Operator Style on Mission Energy Requirements for Tele-Operated Unmanned Ground Vehicles

One of the key factors that limit the utility of small tele-operated battery-powered UGVs is the available on-board energy. The UGV energy consumption is affected by several factors such as (Sadrpour et al., 2012, 2013a,b,d): (1) road surface condition, (2) driving style, (3) the on-board electronic equipment, and (4) vehicle internal resistance. Since most UGVs are tele-operated, Chapter V investigates the impact of remote operating style on energy requirements in a typical patrol mission for a small UGV, while the other factors have been addressed in Chapters III and IV.

The impact of driving style on emissions and fuel consumption has been extensively studied for conventional vehicles (Holmen and Niemeier, 1998; DiGenova et al., 1994). Evidence that aggressive driving and high velocity increases emissions and fuel consumption, was presented in Vojtíšek et al. (2009), Vojtíšek et al. (2008), and Berry (2010). In Van Mierlo et al. (2004) and Reichart et al. (1998), the effect of driving style on emissions and fuel consumption was shown to result in 5%-40% difference in fuel consumption. Van Mierlo et al. (2004) indicated a fluent driving style with low engine speed, and eco-drive (2010) showed changing gears and smooth driving increase energy efficiency, while Berry (2010) pointed that harsh acceleration and high velocity reduces efficiency. Also, Ericsson (2000) used regression analysis to show that the driving pattern characteristics significantly affect the fuel consumption of conventional vehicles. Vlieger et al. (2000) concluded that fuel consumption rose by 7%-40% for aggressive drivers, and Automobile Association (2012); Barkenbus (2010), and Gos (2011) showed 10-33% reduction in fuel consumption when an eco-driving style was employed. However, due to the small size of UGVs and tele-operation, those results are not directly applicable.

There has been little work on the impact of driving style on electric vehicles (EVs) (Knowles et al., 2012). Compared to conventional vehicles, EVs have a smaller range of around 145 kilometers, and in the case of small UGVs the range shrinks to only a few kilometers. The dependency between EV range and driving style was studied in Knowles et al. (2012). The result showed a significant change in the operating range among drivers. Walsh et al. (2010) investigated energy consumption in EVs showing large variations on tracks with high opportunities for regenerative braking. They also showed that driver training can result in an average of 87% more energy regeneration on certain road conditions. However, the results cannot be extended to UGVs because regenerative braking is not currently available for most UGVs. In summary, despite the abundance of literature on conventional vehicles, the impact of remote operating style and skill on UGVs has not been addressed.

There are several challenging aspects that distinguish operations with UGVs from conventional

vehicles : (1) tele-operation induces delays beyond what is normally observed while driving other types of vehicles; (2) in conventional vehicles the operator receives direct and immediate feedback and cues when turning the wheels, accelerating, or braking. In tele-operated vehicles, the operator may have to rely only on video feedback, which provides limited situation awareness, and may suffer from a time delay; (3) in conventional vehicles, locomotion accounts for the largest percentage of energy consumption. However, due to the smaller size of UGVs, electronic equipment contributes significantly to overall power consumption, which affects the optimal driving style; (4) unlike electric or hybrid vehicles, most UGVs do not have power regenerating capabilities and the operator style has a different impact on energy consumption; (5) UGVs are frequently operated off-road in hazardous and unfamiliar conditions. The intensity of missions and lack of situation awareness make operations more prone to maneuvering mistakes that increase energy requirements.

The objective of Chapter V is to provide a better understanding of the impact of tele-operation on energy consumption of a small UGV. A simulation model is developed that incorporates factors such as vehicle reference velocity, communication and human delays, random variations in steering, stop-and-go operations and operator aggressiveness.

Two specific issues are pursued in this chapter: (1) to develop an energy optimal drive cycle based on the vehicle model, and study the impact of velocity deviations from the optimal drive cycle, and (2) to determine which factors related to operator style, and their interactions, increase the energy consumption significantly.

The main contribution of Chapter V is to present the first statistical analyses of tele-operation impact on energy consumption of a small UGV. Factors and interactions that affect the energy consumption such as vehicle reference velocity, stop-and-go operations, lateral velocity variations, human delay, and operator aggressiveness are identified, and procedures to improve energy efficiency are proposed. The analysis results show that when the operator operates the vehicle at a lower than optimal reference velocity, the energy consumption can increase by up to 100%. Additionally, when the operator is informed of the optimal velocity, the energy requirements can be still reduced by up to 6.5% by improvements in other factors affecting operator style.

1.3 Outline of Dissertation

In this dissertation, a unified approach for improving UGV mission reliability during the design and operation of UGVs is proposed. The implementation of the proposed approach is demonstrated using both experiments and simulation studies. The organization of the dissertation associated with

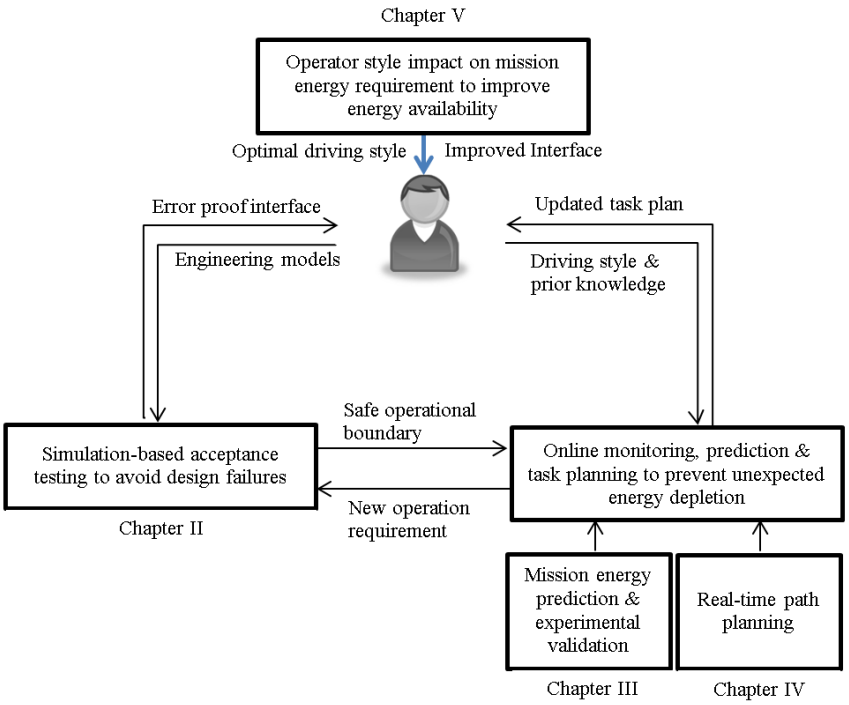

Figure 1.1: Outline of dissertation

the methodology development is shown in Figure 1.1.

Chapter I presents the research motivations and key topics to be discussed in the dissertation. Research challenges and new contributions of each research topic are also briefly introduced in this chapter.

Chapter II proposes a novel integration of dynamic simulations and static analysis to systematically obtain the safe operation boundaries, which can be further used to assess design deficiencies, plan efficient acceptance tests to remove manufacturing defects, and determine effective operator's training procedures, and design an intelligent error-proof user interface. Chapter II is based on the publications Lee et al. (2009), and Sadrpour et al. (2011).

Chapter III discusses a unique approach for prediction of mission energy requirement using prior knowledge and real-time measurements. The method integrates a vehicle longitudinal dynamic model to capture the interaction of a UGV with the terrain and uses a Bayesian recursive estimation to perform real-time estimation and prediction. Comprehensive statistical experimental studies were conducted to validate the propose model and prediction approaches. Chapter III is based on the publications Sadrpour et al. (2012), Sadrpour et al. (2013a), and Sadrpour et al. (2013b).

Chapter IV focuses on real-time most energy-reliable path planning for UGVs. Using the prediction model developed earlier, a novel approach for real-time path planning is proposed to

identify the most energy reliable path in a network with unknown and correlated cost structure. The proposed approach divides the planning decision into two stages: (1) exploration stage, deciding where and how many sensor measurements to collected to reduce the large prediction uncertainty and bias, (2) exploitation stage, deciding which path the UGV traverses, which has the highest probability of success using the information collected during the exploration stage. The work in Chapter IV is based on publications Sadrpour et al. (2013c), and Sadrpour et al. (2013d).

Chapter V investigates the impact of tele-operation on energy consumption of a small UGV. Using statistical response surface analyses, it is shown that factors such as velocity, stop-and-go operations, human operator delay and aggressiveness, and their interactions significantly increase the energy requirements in a typical mission. The effect of velocity deviation from the optimal drive cycle in terms of energy consumption is investigated, and it is demonstrated that energy requirements can increase twofold when operating the vehicle at nonoptimal velocities. Chapter V is based on the publication Sadrpour et al. (2014).

Chapter VI summarizes the major work and original contributions of the dissertation and includes suggested research topics for the future.

CHAPTER II

Simulation-based Acceptance Testing for Unmanned Ground Vehicles

2.1 Introduction

In 2004, the US army was using about 160 robots in Iraq and Afghanistan (Purdy, 2007). This number grew to approximately 4,000 in 2007 and continued to climb to about 8,000 in 2010. With the rapid increase of unmanned ground vehicle (UGV) usage in military operations, one primary concern of robotics researchers and users is UGV reliability (Tilbury and Ulsoy, 2011). Studies of mobile robots used in Urban Search and Rescue (US&R) and Military Operations in Urban Terrain (MOUT) have shown a mean time between failures (MTBF) in the field of 6 to 20 hours, well below the desired 96 hours as established by the Test and Evaluation Coordination Office (TECO), part of the Maneuver Support Center at Ft. Leonard Wood (Kramer and Murphy, 2006). Some of the failures are due to manufacturing defects or subtle interactions between components, and these failures could be detected and prevented prior to the field deployment. However, other failures are due to uncertain operating environments, misuse by operators, and insufficient understanding of failure modes. Therefore, it is important to develop an acceptance test to provide better understanding of the failure modes and to ensure that such systems meet their reliability goals. Although such testing methods are widely used in various engineering applications, there is still no general guidance for UGV acceptance tests in terms of system reliability. Thus, the purpose of this chapter is to suggest research ideas that might provide a basis for the development of an acceptance test for small UGVs or mobile robots.

Some of the earliest works on UGV reliability and acceptance testing were done by (Carlson and Murphy, 2003, 2005; Carlson et al., 2004; Stancliff and Dolan, 2005). Murphy discussed a methodology similar to a final factory acceptance test, i.e., a test usually performed by a manufacturer

prior to shipping. In contrast, this chapter discusses a methodology for simulation-based acceptance testing in which simulations are used to identify the safe operation boundaries or the worst-case scenarios in UGV operations.

The proposed simulation approach is considered as a complementary tool for improving the physical acceptance tests, which has the following advantages by overcoming some of the limitations of the physical tests:

1. The simulation approach is time and cost effective since it does not require expensive physical test facilities, expert operators to work with the UGV during the test, or various test apparatuses.

2. Simulation testing can be conducted on the full operational range of the UGV, beyond the limitations that the test facilities and apparatus may offer.

3. The simulation results can be used to develop the boundaries of safe operation for UGVs for various scenarios. These boundaries can be potentially used for (i) improving the UGV design to prevent UGVs from functional failures due to design deficiencies; (ii) developing an intelligent human-UGV interface to avoid human operational failures; (iii) providing a systematic guideline in the design of the essential physical testing scenarios for reducing the physical test time and cost.

4. It can help identify an optimal design and/or operational scheme, which exists beyond the currently available UGV products.

In this chapter, two sets of commonly encountered UGV failure scenarios are investigated: the first set studies joint torque saturation and rollover when the UGV attempts to lift various loads; and the second set focuses on the suspension system and flip over failures when the vehicle is operated on bumpy terrains with mild roughness. To determine the UGV's safe operating range, we examined both dynamic and static simulation models for a wheeled ground vehicle whose size and weight is within the typical range of a small mobile robot.

This research is intended to help users of UGVs gain a better understanding of performance and reliability of a vehicle in various operational environments. Therefore, it is important to understand failure modes associated with current UGV systems. In Carlson et al. (2004), a novel taxonomy of UGV failures is introduced which classifies failures into two major categories: physical and human operational failures. The physical failures are further studied based on the most common subsystems

used in UGV platforms: effector, sensor, control system, power, and communications. Human operational failures are subdivided into mis-design specifications and human-robot interaction.

The previous work by the Center for Robot Assisted Search and Rescue (CRASAR) includes 13 studies and 15 different models of field robots in US&R or military operations (Carlson and Murphy, 2003; Carlson et al., 2004). This study showed an overall MTBF of 8 hours and an availability of less than 50%. The effectors were the most common type of failures, 39% of overall failures, and the control system was the next with 29%.

To ensure that field robots meet such performance requirements and reliability targets, it is important to develop acceptance and performance testing standards for UGVs. Some preliminary work on UGV acceptance testing has been done by Murphy and her collaborators. In Kramer and Murphy (2006), the role of endurance testing for rescue and safety robots is discussed. It describes a methodology for endurance testing recommended for a certain class of robots. A six-hour endurance test was developed for a commercially available rescue robot. The test uncovered failures under certain conditions and the sources of the failures. In addition, the test data identified key design and manufacturing issues. Endurance and agility tests were also conducted at the US Army Aberdeen Test Center (ATC) on small size UGVs. The robots were tested under a variety of operating conditions to ensure their reliability in the field (Tricomo, 2009).

In terms of performance standards, the Department of Homeland Security (DHS) initiated an effort in 2004 to develop performance standards for US&R robots (Messina and Jacoff, 2006). In order to ensure that applicable technologies are relatively easy to use and to be integrated efficiently into existing systems, standardized test methods were needed. Therefore, the DHS Science and Technology Directorate initiated an effort in 2004 with National Institute of Standards and Technology (NIST) to develop comprehensive standards to support development, testing, and certification of effective robotic technologies for US&R applications. These standards address robot mobility, sensing, navigation, and human system interaction. Furthermore, Pepper et al. (2007) used the standardized physical tests in NIST to validate the UGV's simulation models under given scenarios.

There are major limitations that almost all of the above acceptance and performance testing share. Due to the limited testing facilities and apparatus, often only a small range of operational requirements can be physically tested. Additionally, conducting physical tests can be time consuming and tedious . Moreover, there are many uncontrollable or hard-to-control factors in physical tests such as variations in different operators' knowledge and operating skills, environmental condition changes, etc., which may lead to inevitable variations in the physical testing results.

In contrast to the physical tests, the simulation-based tests can be very time efficient since they

can be fully automated and a variety of scenarios can be easily integrated into the simulation. Moreover, simulation-based evaluation methods have played an increasing role in complementing physical tests in other industries, such as aerospace and automotive (Norris, 1995; Guonian et al., 2010). In summary, the advantages that the simulation-based acceptance testing offers makes it a complementary tool for physical acceptance testing. Therefore, this chapter investigates simulation-based acceptance testing of UGVs to provide a faster and easier method to develop performance testing and to determine robot reliability.

The rest of this chapter is organized as follows. Section 2.2 presents our simulation-based acceptance testing methodology. Section 2.3 studies two failure modes associated with UGV operations: the joint saturation of the robot actuators and the rollover failure. To perform the study, we conduct both static and dynamic simulations and compare their performances using statistical hypothesis testing. Section 2.4 presents a similar analysis concerning two other failure modes: excessive mechanical shocks and vehicle flip over.

2.2 Proposed Methodology

Acceptance tests play an important role in the verification and demonstration of key performance requirements and system reliability of UGVs. In order to establish an acceptance test, the essential performance requirements and efficient test scenarios for each of the performance requirements need to be determined. These test scenarios emulate UGV operations and user environments, and ensure that the system meets the performance requirements and reliability goals.

In this chapter, we propose a methodology for simulation-based acceptance testing which provides an efficient complement to the physical acceptance testing (see Figure 2.1). To conduct the study, static and dynamic simulations for a few typical acceptance testing scenarios are developed. The settings represent tasks that are conventional in UGV operations and missions. These test plans include several UGV failure scenarios consisting of joint torque saturation, rollover, suspension system failure and flip over failures.

Our simulation-based acceptance testing is based on two models: dynamic and static simulation models. Each simulation model offers advantages and disadvantages, and Table 2.1 provides a qualitative summary of the key differences between them. Dynamic simulation can include a variety of environmental conditions which makes its results more accurate, whereas static simulation is more straightforward and quick to construct. Using the static simulation, we can readily derive the boundaries of safe operation through closed form static equations, while, in the dynamic case,

Table 2.1: Comparison of dynamic and static simulations

Characteristic	Dynamic Simulation	Static Simulation
Complexity	Complex	Straight forward
Time/Cost	Time consuming	Quick
Accuracy	Accurate	Approximate
Failure Boundary Identification	Difficult	Quick

these boundaries are obtained by exploring the large space of dynamic parameters and environments through simulations.

The static simulation is more time efficient, but may not always be an acceptable approximation for the dynamic simulation when the failure mechanism in a scenario is significantly affected by the dynamic characteristics of the UGV. Therefore, there is a need to develop a systematic method to quantitatively ensure when a static analysis is satisfactory. For this purpose, dynamic and static simulation results are compared by proposing a statistical hypothesis testing, which is used to judge whether both simulations will make a consistent decision on the failure state for a given scenario. The purpose of using a statistical hypothesis test is to consider the inherent performance variation due to operational or environmental uncertainties. As will be discussed in the later sections, the outcome of the statistical hypothesis test, as to when static simulations can be used to approximate more complex dynamic simulations for a given scenario, can be extended to similar acceptance testing scenarios that share the same fundamental characteristics.

The simulation results can help further identify the boundaries of safe operation, which can be used as a guideline to design efficient physical tests scenarios and prevent expensive damages to a UGV during tests. Moreover, from the design perspective, the margin between the operational state and the design specification can indicate the failure probability or risk for conducting a given mission task. This will also provide us with a better understanding of failure mechanism, and guide us to improve the design of UGVs. Figure 2.1 provides a summary of the proposed methodology and its advantages, and the following sections provide the details of the analysis.

2.3 Study of Torque Saturation & Rollover Failures

In the first scenario, the robot lifts and moves an object with a known mass using its manipulator arm. The possible failure modes associated with this scenario are the inability of the arm actuators to provide the necessary torque for lifting the load, and also UGV rollover during the same lifting operation.

While it is desirable that the arm movements occur at a constant angular velocity, in reality speed

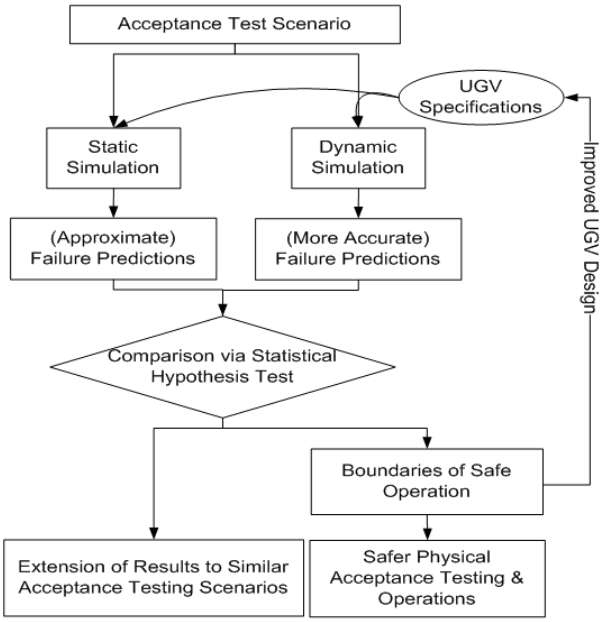

Figure 2.1: Proposed methodology for simulation-based acceptance testing and development of boundaries of safe operation.

variations occur specially at low angular velocities due to a variety of reasons such as variations in the power source, manufacturing limitations, interaction among components in the system, etc. Several papers have discussed the presence of these factors and methods to reduce the negative effect of speed and torque ripple in robot actuators by utilizing effective control systems (Ren et al., 2009; Lam et al., 2000; Godler et al., 1994). Nonetheless, even with the use of feedback control, speed variations are not entirely eliminated. Moreover, since this scenario primarily focuses on the actuator torque saturation, and speed and torque ripples influence this measure, their effect is considered in the dynamic simulation.

Electric motors are typically used in robot actuators. The accuracy of these motors mainly depends on the applications. For the purpose of this study, we assume that the actuator is using an effective control system to eliminate the major harmonic trends in the ripples. With the major trends removed, the remaining disturbances are assumed to be random. Therefore, the speed ripples are modeled using white noise. The magnitude of the ripples are considered to be around 1% of the maximum operating speed of the robot arm, i.e., 0.3 - 0.5 deg/sec for a maximum speed of about 30-50 deg/sec.

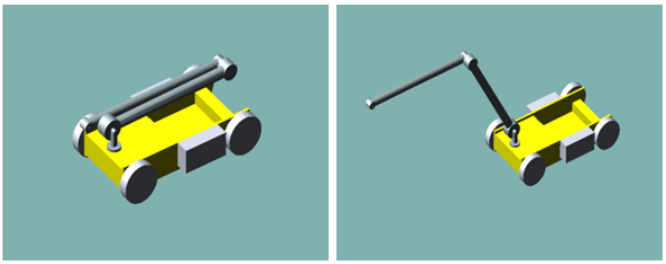

Figure 2.2: Multi-body dynamic simulation model in the 'closed-in' position and the 'manipulator extended' position

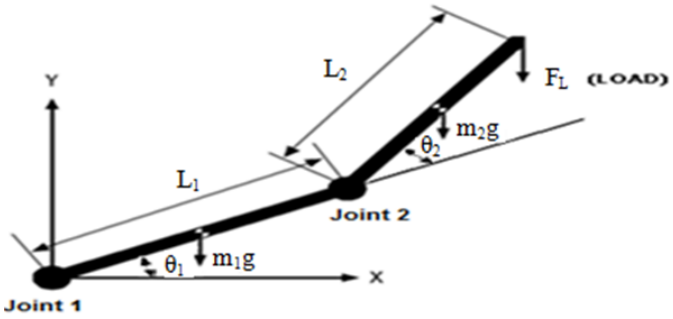

Figure 2.3: Schematic of a two-link robot arm

2.3.1 Static and Dynamic Simulation Framework

Consider a system consisting of a wheeled platform and a two-link planar robot arm as shown in Figure 2.2. It is desirable to drive each link by a separate joint motor due to ease of position control from a control logic viewpoint. The required joint torque to maintain the link in a certain position is merely the reaction moments at each joint. A two-link planar robot arm is schematically shown in Figure 2.3. Solving for the reaction moments, or required joint torque, results in the following relations

$$\tau_1 = (m_1 g \frac{L_1}{2} + m_2 g L_1 + F_L L_1)\cos(\theta_1) + (m_2 g \frac{L_2}{2} + F_L L_2)\cos(\theta_1 + \theta_2) \tag{2.1}$$

$$\tau_2 = (m_2 g \frac{L_2}{2} + F_L L_2)\cos(\theta_1 + \theta_2) \tag{2.2}$$

in which,

τ_i= The reaction moment at joint i

θ_i= The orientation of the robot arm i

F_L= Weight of the load

m_L= Mass of the load

m_i= Mass of the robot arm i

Equation (2.1) defines the reaction moment at the first joint, and (2.2) defines the reaction moment at the second joint. If θ_1 is given, τ_1 and τ_2 have maximum and minimum values with respect to θ_2 when $\frac{d\tau_1}{d\theta_2}$, $\frac{d\tau_2}{d\theta_2}$ are equal to zero.

$$\frac{d\tau_1}{d\theta_2} = \frac{d\tau_2}{d\theta_2} = -(m_2 g \frac{L_2}{2} + F_L L_2)\sin(\theta_1 + \theta_2) = 0 \tag{2.3}$$

We denote the maximum and minimum torques in the static simulation with τ_s^{max}, and τ_s^{min} respectively.

During the static simulation, the second joint angle, θ_2, is varied from 0 to 2 π, i.e., one full revolution, for each selected first joint angle. The joint torques are then calculated using the relations listed above. As we can see from the equations, the maximum and minimum for both τ_1 and τ_2 are observed at the same orientation of the robot arm. By solving Equation (2.3), we can conclude that at the worst-case orientations, the second joint angle is determined as $\theta_2 = 2\pi - \theta_1$ if $0 < \theta_1 < \pi/2$ and $\theta_2 = \pi - \theta_1$ if $\pi/2 < \theta_1 < \pi$. Given the first link angle, the orientations of the second link which result in maximum torque experienced by the robot actuators are shown in Table 2.2.

Table 2.2: The link orientations that result in maximum torque experienced by the actuators

First Joint Angle (Radian)	Second Joint Angle (Radian)	Manipulator Orientation
0	0, 2π	
π/6	11π/6	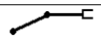
π/3	5π/3	
π/2	π/2, 3π/2	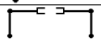
2π/3	π/3	
5π/6	π/6	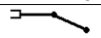
π	0, 2π	

By setting the joint torque thresholds T_1 and T_2, the safe working range of the second joint can be determined under the given first joint angle range of $0 < \theta_1 < \pi/2$.

$$T_1 \geq \tau_1, T_2 \geq \tau_2 \tag{2.4}$$

$$T_1 \geq (m_1 g \frac{L_1}{2} + m_2 g L_1 + F_L L_1)\cos(\theta_1) + (m_2 g \frac{L_2}{2} + F_L L_2)\cos(\theta_1 + \theta_2) \tag{2.5}$$

$$\cos(\theta_1 + \theta_2) \leq \frac{T_1 - (m_1 g \frac{L_1}{2} + m_2 g L_1 + F_L L_1)\cos(\theta_1)}{(m_2 g \frac{L_2}{2} + F_L L_2)} \tag{2.6}$$

$$T_2 \geq (m_2 g \frac{L_2}{2} + F_L L_2) \cos(\theta_1 + \theta_2) \tag{2.7}$$

$$\cos(\theta_1 + \theta_2) \leq \frac{T_2}{(m_2 g \frac{L_2}{2} + F_L L_2)} \tag{2.8}$$

From Equations (2.6) and (2.8), we can determine that the first joint has a narrower safe working range than the second joint under the same joint torque threshold value because the right hand side of equation (2.6) will always be smaller than that of (2.8). Similar analysis and conclusion can be obtained under the first joint angle range of $\pi/2 < \theta_1 < \pi$.

The static simulation model described above was evaluated under varying arm dimensions, masses, load size and joint angles. The model used in the static simulation has the dimensions L_1=0.55m, L_2=0.64m, m_1=2.5kg, m_2=2.5kg, m_L=4kg, which are based on the measurements taken from an actual UGV manipulator. The same parameters are used in the dynamic simulation which will be presented next.

Dynamic analysis generally provides more accurate results compared with the static study since the former takes into account the arms inertia, interaction between various components, and other disturbances such as speed variations. However, the inclusion of these factors also increases the complexity of the dynamic model, which in turn imposes a challenge for the development of analytical solutions. Therefore, in most situations, a simulation approach has to be used to perform multi-body dynamic analysis with the consideration of these factors in the model.

In the multi-body dynamic simulation, all the components are modeled in a CAD system and converted into rigid bodies for use in MSC ADAMS, a multi-body dynamic simulation software. After all the parts are assembled, the complete model is exported into MSC ADAMS. The simulation calculates information such as lateral and longitudinal forces, torques, angular velocity and acceleration at each joint. The model also accounts for all center of gravity locations in each component. Figure 2.2 shows the 3-D graphical rendering of the vehicle model in the closed-in position and the manipulator-extended position.

During the dynamic simulation, for each selected first joint angle, θ_1, the second joint angle, θ_2, is varied from 0 to 2π radian, i.e., one full revolution. This makes the manipulator move through a full range of motion and provides data for all operating states.

When the upper threshold of the joint torque for the link actuators are known, the failure of the robot manipulator will occur when the joint torque exceeds the threshold. For example, assuming that the joint torque threshold is 50 Nm, the first joint of the manipulator used in the simulation

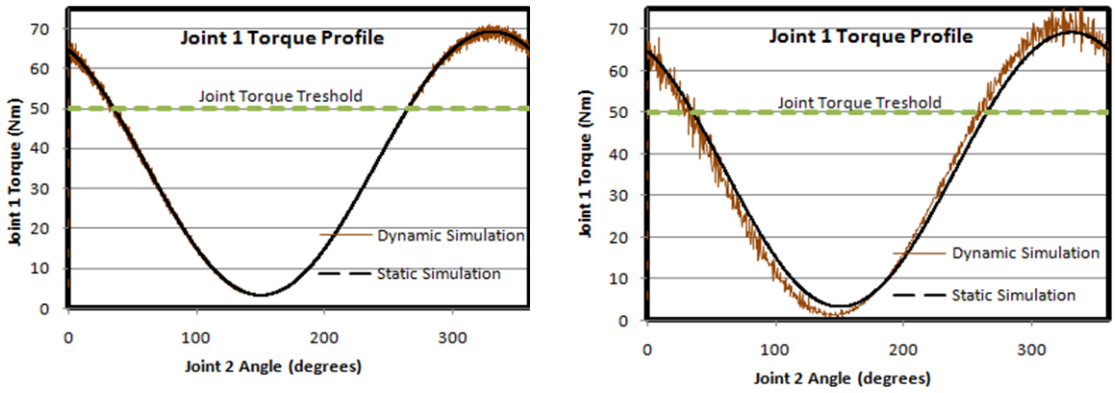

(a) (b)

Figure 2.4: Static and dynamic simulation torque profiles for the first robot joint with the first joint angle of $\pi/6$ radians. (a) Operating speed of 10 deg/sec. (b) Operating speed of 80 deg/sec.

will fail in various positions. Various manipulator orientations are evaluated using both dynamic and static simulations. The results for dynamic simulation at two angular velocities, one with a typical operating speed of 10 deg/sec and the other with a much larger speed of 80 deg/sec, along with the static simulation result at the first joint angle of $\pi/6$, with a joint torque threshold of 50 Nm is shown in Figure 2.4. As shown, speed and torque ripples create variations in the torque measurements in the dynamic simulation as expected. Due to larger moment arms, speed variations create spikes that are more pronounced near the torque maxima in the dynamic simulation. Additionally, the maximum torque in the dynamic simulation does not increase significantly within typical operating speeds of the arm. In fact, using statistical hypothesis testing, we will show that a straightforward static simulation can provide a reasonable estimation for failure detection. In the next section, we evaluate the validity of the conclusion under the selected operating speeds.

2.3.2 Statistical Hypothesis Test for Simulation Comparison

To further quantitatively assess the differences between static and dynamic simulation results and justify whether the static simulation can be used instead of dynamic simulation for predicting failures, we will use statistical hypothesis tests. In this scenario, the failure occurs when $\tau_{\mathrm{d}}^{\max}(\omega)$ exceeds the joint torque thresholds, where $\tau_{\mathrm{d}}^{\max}(\omega)$ refers to the maximum torque obtained from the dynamic simulation when the arm is traveling at ω deg/sec. Consequently, the comparison between static and dynamic simulation would be based on the accuracy of the static simulation in predicting $\tau_{\mathrm{d}}^{\max}(\omega)$ within typical operating speeds. The advantage of static analysis is its simplicity and ease of use. On the other hand, the dynamic model provides more accurate and realistic results, but it is much more complex and time consuming to construct. As a result, when comparing the dynamic

and static simulations, we would tolerate slight differences in their results by imposing a threshold for maximum allowable deviation of static results from their dynamic counterparts. This threshold is set based on the maximum deviation that is not of significance to the end user when studying a particular failure mode.

Since in this scenario the effect of speed variations are included as a part of the dynamic simulation, the maximum torque during a full revolution of robot arm, which we will refer to by $\tau_{\mathrm{d}}^{\max}(\omega)$, is a random variable whose variance is affected by the magnitude and frequency of the random speed ripples. If the maximum operating speed of the robot arm is 30 deg/sec, the magnitude of the speed ripples are considered to be around 1% of this maximum operating speed.

Statistical hypothesis test will be used to verify whether deviation of the static simulation from dynamic simulation result is significant or not. A one-sided hypothesis test on the differences between the mean of the maximum torque measurements at each angular velocity with the calculated maximum torque in static simulation is constructed as follows

$$\begin{cases} H_0 : \mu_{\tau_{\mathrm{d}}^{\max}(\omega)} - \tau_{\mathrm{s}}^{\max} \leq \Delta \\ H_1 : \mu_{\tau_{\mathrm{d}}^{\max}(\omega)} - \tau_{\mathrm{s}}^{\max} > \Delta \end{cases} \tag{2.9}$$

In which Δ is the maximum allowable difference between the static and dynamic simulation results, and $\mu_{\tau_{\mathrm{d}}^{\max}(\omega)}$ is the mean of the maximum torque measurements in the dynamic simulation. With a prior belief that the static and dynamic simulations are both capable of predicting failures accurately, the rejection of null hypothesis in (2.9) is an indication that the static simulation is no longer capable of predicting the failure at a given allowable deviation level, and the dynamic simulation should be used instead.

The null hypothesis in (2.9) is rejected if:

$$\frac{\bar{\tau}_{\mathrm{d}}^{\max}(\omega) - (\tau_{\mathrm{s}}^{\max} + \Delta)}{\frac{S_\tau}{\sqrt{n}}} \geq t_{\alpha,n-1} \tag{2.10}$$

In which, $\bar{\tau}_{\mathrm{d}}^{\max}(\omega)$ and S_τ are the sample mean and standard deviation of the maximum torque measurements. $\bar{\tau}_{\mathrm{d}}^{\max}(\omega)$ and S_τ are calculated by running the dynamic simulation for n complete revolutions, collecting the maximum torque value in each revolution, and computing the corresponding sample mean and standard deviation. Additionally, $t_{\alpha,n-1}$ is the $100(1-\alpha)^{\mathrm{th}}$ percentile of the

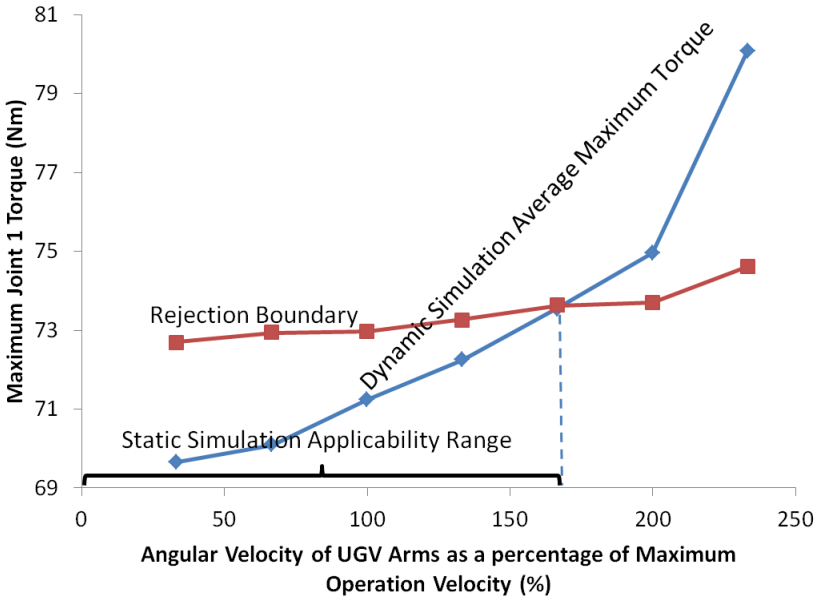

Figure 2.5: Statistical comparison between dynamic and static simulations, for the first joint angle of $\pi/6$ radians and $\Delta = \tau_{\mathrm{s}}^{\max} \times 5\%$, $n = 10$, $\alpha = 0.99$.

t distribution with $n-1$ degrees of freedom. Inequality (2.10) can be rewritten as:

$$\bar{\tau}_{\mathrm{d}}^{\max}(\omega) \geq \tau_{\mathrm{s}}^{\max} + \Delta + t_{\alpha,n-1}\frac{S_\tau}{\sqrt{n}} \tag{2.11}$$

The right hand side of inequality (2.11) provides a rejection boundary for the hypothesis test. If $\bar{\tau}_{\mathrm{d}}^{\max}(\omega)$ is larger than the rejection boundary, the hypothesis test is rejected (indicating that the deviation of static and dynamic simulations is significant and dynamic simulation should be used for failure analysis).

The result from the static analysis agrees with the result from the dynamic analysis with a typical operating speed of 10 deg/sec. Figure 2.5 depicts $\bar{\tau}_{\mathrm{d}}^{\max}(\omega)$ at various angular velocities along with the hypothesis test rejection boundary obtained from (2.11). This figure shows that the static simulation model can be used for failure analysis, rather than a more complex dynamic simulation model, due to slow operating speeds of UGV manipulator arms. However, static simulation is not always able to take the place of dynamic simulation because the joint torque increases as the robot operating speed increases due to inertial effects. With the typical maximum operating speed of about 30-50 deg/sec, as shown in Figure 2.5, static simulation provides reasonable estimates for angular velocities as high as the maximum operating speed. However, the accuracy of estimates gradually deteriorates at higher angular velocities. The hypothesis test result verifies this observation by rejecting the static simulation results at angular velocities above 150% of the maximum operating speed.

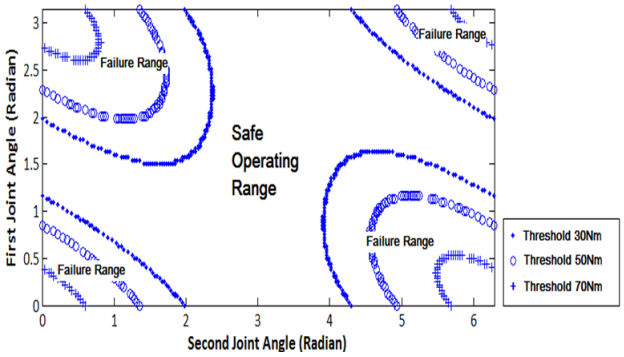

Figure 2.6: Failure range and safe operating range of the two-link planar robot arm for threshold values (30, 50, and $70Nm$) are shown in terms of first and second joint angle.

2.3.3 Identifying the Test Range for the Joint Torque Saturation Failures

In the previous section, it was shown that static simulation would provide reasonable approximation for torque saturation analysis within typical operating speeds. The developed static simulation model is further applied to identify the test range under various joint torque threshold values for the joint torque saturation failures. Assuming the threshold values are $30Nm$, $50Nm$, and $70Nm$, the failure region versus the safe operating range of the manipulator is shown in Figure 2.6. This plot will be very useful for acceptance testing planning because it shows the boundaries of operating range under different joint torque thresholds. For example, when the joint torque threshold of $50Nm$ is given, the circled line in Figure 2.6 forms a failure boundary. These failure ranges, which can potentially be costly during the actual test, should be avoided and excluded from the acceptance testing. The acceptance test scenario would then assess the UGV capabilities in the safe operating regions.

It should be noted that although both static and dynamic simulations have to be conducted for the purpose of comparison, the simulations and hypothesis tests do not need to be implemented and compared again when there are minor design changes such as changes in the length of the robot arms. Additionally, for acceptance testing scenarios that share similar characteristics, both simulations do not need to be repeated, and the previously identified simulation scheme can be used. For instance, static simulation can be used for studying operations with UGV arms whose range of operating speeds are similar to those discussed earlier without the need for constructing a dynamic simulation model. In addition, even if both simulation schemes are needed for a new acceptance testing scenario that does not share the characteristics of the previous simulated tests, the hypothesis test can largely reduce the analysis time by identifying conditions in which a static simulation can be used. In other words, instead of exploring the large space of dynamic parameters and environment by means of

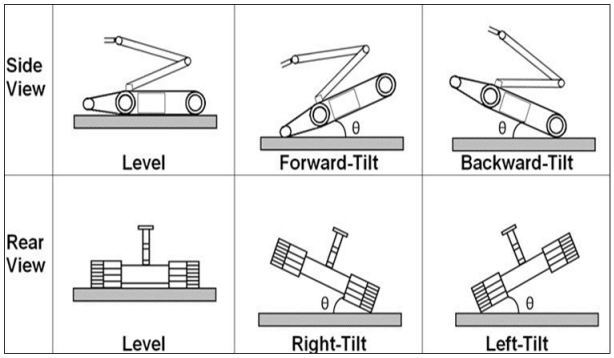

Figure 2.7: Example of initial robot orientations for test set up. Test measures the safe operation range of the tilt angle for different robot arm orientations.

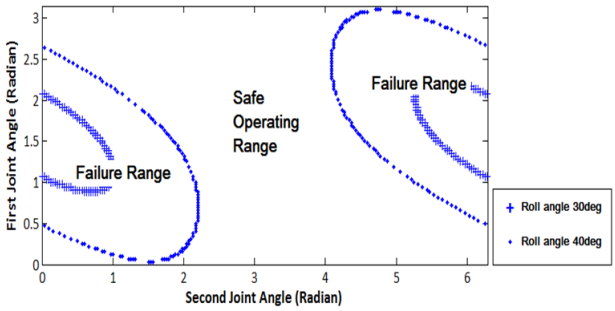

Figure 2.8: Failure range and safe operating range of the two-link planar robot arm for right-tilt (roll) angle of 30 and 40 deg are shown in terms of first and second joint angle.

dynamic simulation, the hypothesis test result may suggest that analytical static simulations can be used to quickly identify the boundaries of safe operation.

2.3.4 Study of Rollover Failure

The static simulation model discussed in the previous section can be combined with rollover failure simulation. First, additional model parameters such as platform dimensions and weight are defined. Next, equations for static analysis are derived, and this static simulation model is implemented. Several initial robot orientations can be chosen to test whether the system rolls over while the robot arm travels through its full range of motion, and those robot orientations are shown in Figure 2.7. All these orientations are evaluated, and the result for the right-tilt orientation is shown in Figure 2.8. As shown, the initial robot orientation has a significant impact on failure and its safe operating range, and this result can provide guidance for operators to avoid rollover failures. Additional test methods can be based on these initial robot orientations, including a dragging capability test and degradation in lifting capability without flippers.

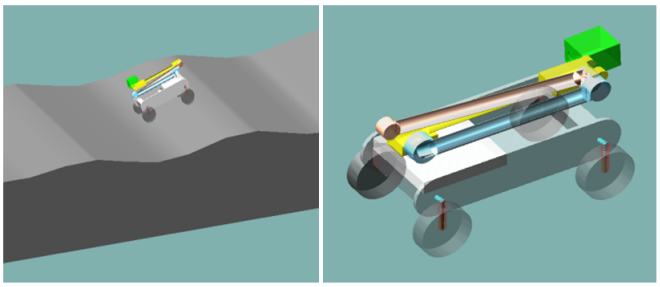

Figure 2.9: (Left) UGV crossing (left to right) a bumpy road. (Right) one-degree-of- freedom spring-damper suspension was added to the UGV model.

2.4 Study of the Suspension System & Flip Over Failures

UGVs are used in a variety of environmental conditions. As a result, it is essential to study the effect of diverse operational conditions, such as road bumpiness and roughness, on the mobility capabilities of the robot. In this scenario, the UGV moves across a bumpy road with mild roughness at various velocities. This scenario is inspired in part by the acceptance test methods for evaluating the mobility capabilities of emergency response robots conducted by NIST (Jacoff et al., 2009). Figure 2.9 shows the UGV on the road. A few interrelated failure modes can be studied under this setting as follows:

- When the forward velocity of the UGV is increased, as it drives on a rough road, the wheels intermittently lose contact with the road. The high inertia of the vehicle will raise the wheels, and can potentially lead to loss of vehicle contact with the road.

- After the loss of wheel contact with the road, if the robot velocity is further increased, the UGV will experience excessive mechanical shocks. These shocks are introduced when the robot wheels come into contact with the road again after losing contact initially. They can result in failure of the suspension or damage electronic devices on the vehicle.

- The UGV may also flip over when it moves at high velocities on a rough road surface. The loss of balance usually occurs when the UGV crosses parts of the road that have higher inclination angles.

The above failure modes are closely related. The relationships among them will be further elaborated in the final section.

2.4.1 Static and Dynamic Simulation Framework

To conduct the static simulation, a 2-D representation of the UGV is considered. The corresponding free body diagram and the static equations are shown in Figure 2.10. The numerical values of parameters used in the equations are provided in Table 2.3. For the purpose of comparison between dynamic and static simulations, the maximum suspension force on a given road will be calculated. It is assumed that the wheels are locked and only the static friction between the wheels and the road prevents the UGV from sliding.

The central mass of the vehicle is closest to the rear left wheel. Consequently, the rear left suspension experiences the largest forces due to the asymmetrical center of mass of the UGV. Since mechanical shocks are associated with large reaction forces in the suspension, special care should be directed to the rear left wheel for the failure analysis of the suspension system.

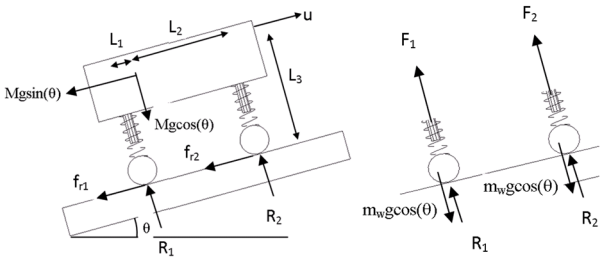

Figure 2.10: Free body diagram of the UGV

$$R_1 = \frac{Mg(L_2\cos(\theta) + L_3\sin(\theta))}{(L_1 + L_2)} \tag{2.12}$$

$$R_2 = \frac{Mg(L_1\cos(\theta) - L_3\sin(\theta))}{(L_1 + L_2)} \tag{2.13}$$

$$F_1 = R_1 - (m_w g)\cos(\theta) \tag{2.14}$$

$$F_2 = R_2 - (m_w g)\cos(\theta) \tag{2.15}$$

in which,

R_i = Reaction force of the wheel i

F_i = Suspension force associated with the wheel i

f_{ri}= Static friction between the wheels and the road

θ = Orientation/angle of the UGV on the road

m_w= Mass of the wheel

M = UGV total mass including wheels

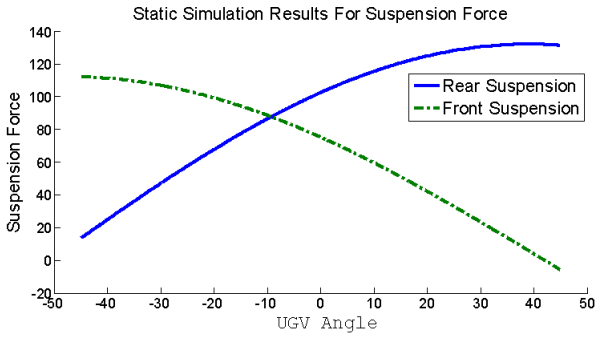

Figure 2.11: The static simulation results for the rear and front suspension force.

Table 2.3: Parameters used in the static and dynamic simulations

Parameter Name	Value
L_1	21.2 cm
L_2	28.7 cm
L_3	23 cm
UGV Mass in Static Analysis	18.47 kg
Wheel's Mass	0.166 kg
Coefficient of Static Friction	0.8
Coefficient of Dynamic Friction	0.7
Spring Constant	5000 N/m
Damping Coefficient	250 Ns/m
UGV Typical Arm Operating Speed	10 deg/sec
UGV Maximum Operating Speed	6 miles/hour
G_e	0.01
G_s	20
G_a	1×10^{-6}

Figure 2.11 shows that the orientation of the UGV on the road has a significant effect on the suspension system loads. In particular, the maximum suspension load occurs when the UGV is positioned on parts of the road with largest angles. In addition, the road roughness is too small to change the orientation of the vehicle and consequently their effect on the static simulation is negligible. The maximum angle of the UGV on the road depends on the size of the UGV, amplitude, and spatial frequency of the bumps on the road. The negative angles refer to down-slopes, and positive angles indicate upward slopes. Figure 2.11 illustrates that F_1 increases with larger up-slopes (larger positive θ), while F_2 increases with larger down-slopes (larger negative θ).

Similar to the torque saturation scenario in previous section, all the components such as road profiles were modeled in a CAD system and converted into rigid bodies for use in MSC ADAMS. The parameters used in the dynamic simulation such as coefficients of friction between the road and the UGV wheels, range of operating speeds, and suspension system details are included in Table

2.3. The road profile is assumed to follow a sine function with amplitude of $0.075m$. The simulation considers a variety of spatial frequencies for the road. Additionally, the road model includes mild roughness. The roughness of the road was generated using MSC ADAMS/CAR road generation toolbox. To summarize, the road profile follows the expression below:

$$Y(x) = 0.075 \times \sin(\omega_r x) + \varphi(G_e, G_s, G_a, x) \tag{2.16}$$

In which, ω_r is the spatial frequency of the road, and G_e, G_s, G_a are white noise elevation, slope and acceleration parameters respectively. These parameters are used for generating the road roughness according to Sayers (1988). Using the values in Table 2.3, our road profile represents a bumpy Portland-cement concrete road with a rigid to smooth-rigid roughness characteristic. Additionally, larger ω_r will decrease the distance between bumps which results in sharper road angles and higher excitation frequencies.

In order to capture the effect of mechanical shocks and road roughness, a one-degree-of-freedom suspension (spring-damper) system was added to the model. Figure 2.9 depicts the 3-D graphical rendering of the model. The properties of the suspension system such as spring and damping coefficients are provided in Table 2.3. These parameters were selected to provide a combination of low natural frequency, and large enough stiffness and damping to prevent excessive spring deformation. The spring deformation was critical due to the small size of the UGV and limitations on suspension stroke. In addition, considering the road profiles and typical operating speeds of the UGV, the excitation of the suspension system induced by movement of the UGV on the road will be smaller than the natural frequency of the suspension system.

The road roughness in the dynamic simulation results in random suspension forces. The effect of road roughness on the suspension loads is depicted in Figure 2.12. As shown the maximum force differs slightly from one road cycle to the other. As shown in the figure, the road consists of several bumps, and the road cycles are equality spaced, including one bump each.

2.4.2 Statistical Hypothesis Test for Simulation Comparison

Similar to the torque saturation scenario, the goal is to assess the static simulation effectiveness for predicting the failure. The failure mode under consideration is the suspension system breakdown, which is caused by excessive mechanical shocks. Therefore, the measure of interest in the comparisons is the maximum force that the suspension experiences on the road. The deviation of static results from the dynamic simulation outcome is determined via statistical tests. A one-sided hypothesis test

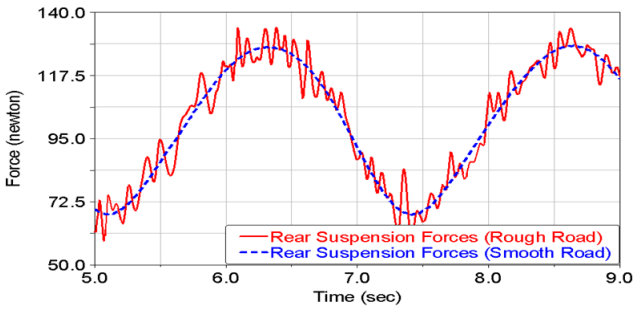

Figure 2.12: The effect of road roughness on force profiles. Comparison of rear suspension forces on a rough versus a smooth bumpy road.

on the differences between the mean of the maximum suspension forces in the dynamic simulation at different velocities with the calculated maximum force in the static simulation is constructed as follows:

$$\begin{cases} H_0 : \mu_{F_{\mathrm{d}}^{\max}(V)} - F_{\mathrm{s}}^{\max} \leq \Delta \\ H_1 : \mu_{F_{\mathrm{d}}^{\max}(V)} - F_{\mathrm{s}}^{\max} > \Delta \end{cases} \tag{2.17}$$

in which, $F_{\mathrm{s}}^{\max}$ is the maximum suspension force on a given road obtained from the static simulation, and $\mu_{F_{\mathrm{d}}^{\max}(V)}$ is the mean of the maximum force measurements in the dynamic simulation when the robot goes through one complete road cycle with a forward velocity V.

The null hypothesis in (2.17) is rejected if:

$$\frac{\bar{F}_{\mathrm{d}}^{\max}(V) - (F_{\mathrm{s}}^{\max} + \Delta)}{\frac{S_F}{\sqrt{n}}} \geq t_{\alpha,n-1} \tag{2.18}$$

in which, $\bar{F}_{\mathrm{d}}^{\max}(V)$ and S_F are the sample mean and standard deviation of the maximum force measurements. $\bar{F}_{\mathrm{d}}^{\max}(V)$ and S_F are calculated by running the dynamic simulation for n road cycles, collecting the maximum force value in each cycle, and computing the corresponding sample mean and standard deviation. Inequality (2.18) can be rewritten as:

$$\bar{F}_{\mathrm{d}}^{\max}(V) \geq F_{\mathrm{s}}^{\max} + \Delta + t_{\alpha,n-1}\frac{S_F}{\sqrt{n}} \tag{2.19}$$

The right hand side of the inequality (2.19) provides a rejection boundary for the hypothesis.

Static analysis fails to predict failure within typical operating speeds. Figure 2.13 depicts $\bar{F}_{\mathrm{d}}^{\max}(V)$ along with the hypothesis test rejection boundary obtained from (2.19). The value of Δ is assumed to be 5% of the $F_{\mathrm{s}}^{\max}$ in Figure 2.13. The statistical test shows that only for a small range of operating speeds, about a quarter of the maximum operating speed, the static simulation can provide a reasonable estimate for the maximum force in the suspension system. Additionally,

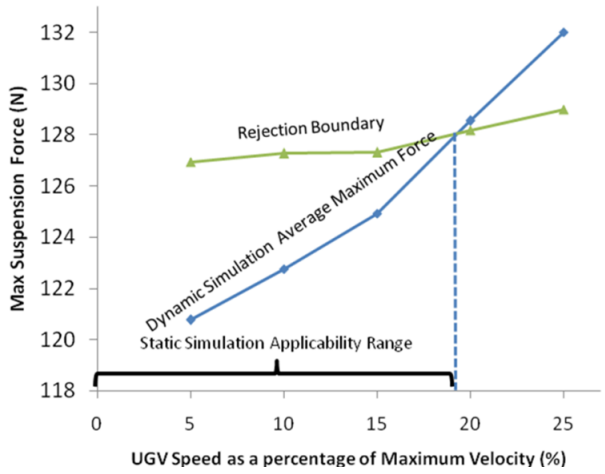

Figure 2.13: Statistical test for comparison of dynamic and static simulations for ω_r=4, $\Delta = F_{\mathrm{s}}^{\max} \times 5\%$, $n = 10$, $\alpha = 0.99$.

this figure shows that this conclusion holds for any reasonable value of Δ selected by the user, since $\bar{F}_{\mathrm{d}}^{\max}(V)$ increases rapidly at higher velocities. Typical operating speed range for the UGV is between 0 and 6 miles/hour.

2.4.3 Statistical Assessment of Safe Operating Speed Using Dynamic Simulation

In the previous section, it was shown that the static simulation fails to provide accurate results. Unlike the torque saturation scenario, the mean of dynamic forces in the bumpy road setting quickly diverged from their static counterparts within typical operating speeds. Consequently, we use the dynamic simulation to develop boundaries of safe operating speed.

As mentioned earlier, three failure modes associated with this scenario are intermittent loss of contact between the wheels and the road, excessive mechanical shocks, and finally flip over. The intermittent contact is an early indication of more severe failures such as mechanical shocks. Therefore, this event can provide suitable insight for failure prevention. Flip over, on the other hand, occurs at higher operating speeds, while severe mechanical shocks mainly take place at velocities close to the onset of flip over. Figure 2.14 shows the relation among the three events. This graph also provides a general guideline for how the UGV should be operated on various road conditions. Since intermittent loss of contact does not always result in an actual failure, (but rather is an early indication of other failures), to develop boundaries of safe operating speeds, we will focus on the failure mode associated with excessive mechanical shocks. This failure is directly correlated with the maximum force that the UGV suspension experiences on a road. The corresponding hypothesis

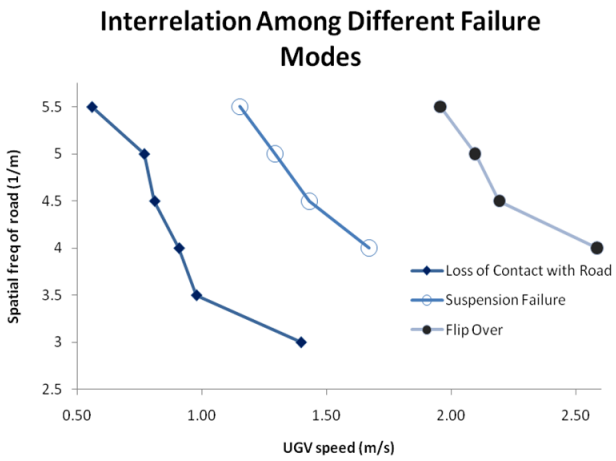

Figure 2.14: Loss of contact is an early indication of suspension system and flip over failures based on dynamic simulation.

test for failure analysis is as follows:

$$\begin{cases} H_0 : \mu_{F_d^{\max}(V)} \leq F_{\text{failure threshold}} \\ H_1 : \mu_{F_d^{\max}(V)} > F_{\text{failure threshold}} \end{cases} \tag{2.20}$$

in which, $F_{\text{failure threshold}}$ is the failure threshold above which the suspension failure takes place. The hypothesis test is rejected if:

$$\frac{\bar{F}_{\text{d}}^{\max}(V) - F_{\text{failure threshold}}}{\frac{S_F}{\sqrt{n}}} \geq t_{\alpha,n-1} \tag{2.21}$$

We can rewrite inequality (2.21) to obtain a rejection boundary for the hypothesis test as follows:

$$\bar{F}_{\text{d}}^{\max}(V) \geq F_{\text{failure threshold}} + \frac{S_F}{\sqrt{n}} t_{\alpha,n-1} \tag{2.22}$$

Figure 2.15, shows the $\bar{F}_{\text{d}}^{\max}(V)$ measurements along with the corresponding rejection boundary from (2.22). In this Figure, it is assumed that the failure occurs when the robot experiences forces in excess of $400N$, i.e.,$F_{\text{failure threshold}}$, which is more than three times as large as $\bar{F}_{\text{d}}^{\max}(V)$ at low velocities. Given the current failure limit, the allowable operating speed range on this bumpy road is about 62% of the maximum operating velocity. As a result, the failure range will include any velocities above this speed threshold. This failure range, which can result in costly damages to the UGV components, can then be excluded from the acceptance testing immediately. A similar type of analysis can be easily applied to roads with different surface roughness, bump size and road profiles.

To summarize, we showed that the dynamic simulation results provide general guidelines to how

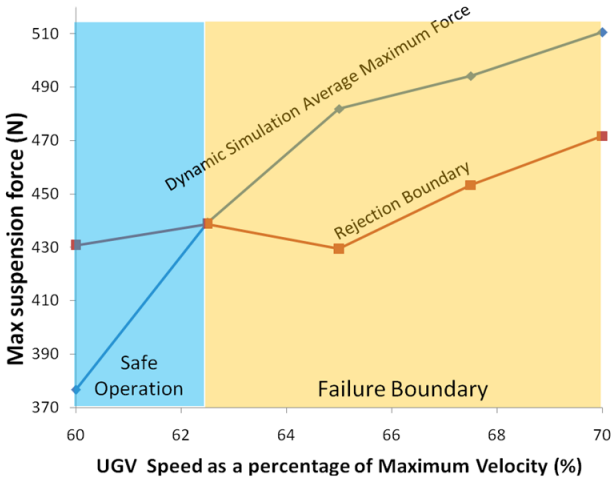

Figure 2.15: Boundaries of safe operation for suspension breakdown and flip over prevention on a typical bumpy road with mild roughness for $\omega_r = 4$ based on dynamic simulation.

the UGV should be operated on various rough bumpy roads, and can significantly help with failure prevention and design of more effective physical acceptance testing scenarios.

CHAPTER III

Mission Energy Prediction for Unmanned Ground Vehicles

3.1 Introduction

This chapter considers the problem of mission energy prediction for battery-operated unmanned ground vehicles (UGVs) undertaking a specific mission, for example, a tele-operated UGV being used for local surveillance. UGVs are entering the economic mainstream, and are being used more extensively in military as well as commercial applications (Tilbury and Ulsoy, 2011). Unlike industrial robots, they are not yet very reliable. This is primarily due to the following factors:

1. The diversity and uncertainty of their operating environments. For example, the reliability of a UGV operated in a carpeted air-conditioned building can be expected to be much better than the same UGV operated in a sandy and hot desert environment.

2. The complex interactions between the UGV and its human operator. For example, tele-operated UGVs are difficult to operate, and an untrained operator may use the UGV in ways it has not been designed for.

3. New immature technologies being used in UGVs. For example, new sensors, signal processing and artificial intelligence technologies used in UGVs may not operate well in all situations encountered.

The reliability problems associated with the current generation of UGVs have been discussed in detail in (Carlson and Murphy, 2003, 2005; Carlson et al., 2004; Kramer and Murphy, 2006; Stancliff and Dolan, 2005; Sadrpour et al., 2011). One of the key factors that limit the utility of small tele-operated battery-powered UGVs is the available on-board energy. Typical mission durations are currently on the order of 1-2 hours, while it is often desirable to carry out much longer missions (e.g., 8-10 hours) between lengthy recharging stops. For a typical UGV, the primary

source of energy consumption is the vehicle locomotion. For example, typical relative order-of-magnitude power requirements might be 100W for propulsion, 10W for computation, and 1W for communication. Furthermore, the power requirement for propulsion can vary dramatically with road conditions (i.e., paved vs. unpaved), road grade (i.e., uphill vs. downhill), as well as driving styles (i.e., velocity profiles).

To address these challenges, the goal of this research topic is to develop a method for UGV mission energy prediction, to provide the best possible estimate of available end-of-mission energy. As an example, we attempt to predict the energy requirement for conducting a surveillance mission. A typical surveillance mission consists of various tasks and several alternative paths that a UGV can select. Since each battery has limited energy storage capacity, it is essential to predict the expected energy requirements for alternative paths and to inform the operator.

A simple *naive* approach for prediction of mission energy requirement, which does not require a model, is to use the average current draw from the battery along with an estimate of the remaining duration of the mission. Assuming that the battery voltage remains almost constant throughout a mission, the product of battery average current draw, voltage and remaining duration of the mission, provides a simple estimate of the expected energy requirement of the mission. The naive approach has some major limitations, such as poor predictions when UGVs move under quite different road conditions.

Consider a surveillance mission with the goal of traveling from a base to a destination where the UGV needs to traverse two road segments to accomplish this mission. The first road segment is downhill with an asphalt road surface, and the second road segment is on average flat and is a grass surface. Without knowledge of the terrains that the vehicle will face, one can assume that at any point in the mission, the future power requirement is similar to the past (e.g., naive approach). Thus, if we can collect and monitor the instantaneous power consumption of the vehicle, the average power consumption from past measurements can be used to predict future power consumption. When the vehicle traverses the first road segment (i.e., downhill/asphalt), the power consumption is substantially less than when it traverses the second road segment (flat/grass). Consequently, if the average power measurements from the first road segment were used to predict future energy requirements, the resultant predictions would considerably underestimate the true energy requirement of the mission. Our goal is to improve the predictions by integrating the available prior knowledge of road segment terrains with real-time sensory measurements.

Past endurance tests on small UGVs have shown that some operational failures can be prevented by real-time monitoring of key performance measures (Kramer and Murphy, 2006). Prognostics and

health monitoring is an approach that permits the reliability of a system to be evaluated in actual operating conditions and has been discussed in Vichare et al. (2007), Lu et al. (2001b), Gorjian et al. (2009), and Lu et al. (2001a). The limitation of such methods is that they have not incorporated mission prior knowledge, such as duration of tasks, nature and difficulty of tasks ahead or operating style of the users, in their reliability assessments. Here, we consider mission prior knowledge and demonstrate its importance for more accurate energy requirement predictions.

Most UGVs use rechargeable batteries for their operations. One approach to predict the battery end of cycle is to consider the history of its discharge rate. For instance, particle filters have been used to predict the battery end of cycle (Saha et al., 2007; Saha and Goebel, 2008; Saha et al., 2009a). However, the above prediction methods only use real-time data to determine the prediction of battery end of cycle. Consequently, ignorance of the intensity of tasks ahead may lead to an over- or under-estimation of the battery end of cycle. More recently, particle filters have been used to predict the battery end of cycle for unmanned aerial vehicles (UAVs) (Saha et al., 2011), in which the mission load profile obtained through offline experimentation is used to further improve the prediction of particle filters. However, since the environment with which the UAV interacts is not directly modeled, some inevitable changes in the actual mission profile, such as an increase in the duration of tasks, is difficult to incorporate in the prediction.

The ultimate goal of predicting energy requirements is to determine the probability of successful completion of a mission prior to exhausting the vehicle's stored energy. Power models for motion, sonar sensing and control of mobile robots based on offline experimental results for the purpose of task planning and energy conservation are presented in Mei et al. (2004), Mei et al. (2005), and Dressler and Fuchs (2005). The models can be used in real-time if they have been calibrated prior to the mission. The limitations are that the model parameters may vary from one robot to another and from one mission to the next (and even within one mission) depending on the intensity of tasks. Power prediction in automotive applications is typically based on standard drive cycles in conjunction with a vehicle longitudinal dynamics model (Ulsoy et al., 2012). Gondor and co-workers (2007) use GPS to collect driving cycle data from drivers of Plug-In Hybrid Electric cars. An approach for predicting the residual range of an electric vehicle (EV) is proposed in Ceraolo and Pede (2001). This approach considers the history of charge, the current driving conditions, and different driving styles to estimate the vehicle residual range, which is effective if the remaining period of the mission has the same characteristics as before. This assumption can be justified for automobiles since the road grades and conditions do not drastically vary. For UGV operations, however, the road condition as well as the road grade may vary significantly from one road segment

to another. Additionally, for UGVs, more accurate prediction of energy is critical due to the much smaller quantity of stored energy compared to EVs. Conservative energy predictions can reduce the already limited operational capabilities of UGVs.

To overcome the limitations of current methods, we propose a new approach for predicting small UGV mission energy in the presence or absence of mission prior knowledge. In the absence of prior knowledge, the RLS estimation motivated by the vehicle longitudinal dynamics is used. In the presence of prior knowledge, a Bayesian prediction approach is used that integrates the prior knowledge with real-time measurements for improved predictions. The expected prior knowledge consists of qualitative information about the road condition and road grade, which can reasonably be expected to be known prior to a mission. Although at the early stages of a mission, the uncertainty of prior knowledge might be large, this uncertainty is reduced over time using the Bayesian updating framework. Additionally, the changes to a mission plan, such as an increase in the duration of the mission, can be incorporated into the adaptive prediction.

The remainder of this chapter is organized as follows: Section 3.2 presents an overview of the proposed methodology. Sections 3.3 and 3.4 describe in detail the RLS estimation and the Bayesian approaches, respectively. Section 3.5 discusses the results from several model validation experiments. Section 3.6 presents the experimental and simulation scenarios that illustrate the advantages of the proposed Bayesian approach.

3.2 Methodology

3.2.1 Overview of Methodology

Figure 3.1 shows the framework of the proposed two approaches. A Bayesian regression model is used for predicting the mission power when prior knowledge of the road segments is available. A road segment is defined as a part of the road that has a consistent average grade and a consistent surface condition. For comparison, a linear regression is used when there is no prior knowledge of the mission. In both approaches, the model parameters are recursively updated based on real-time measurements of the instantaneous UGV velocity and energy consumption. The updated model is used to predict the future power consumption. Finally, the probability of successfully accomplishing the mission can also be adaptively estimated during the mission execution.

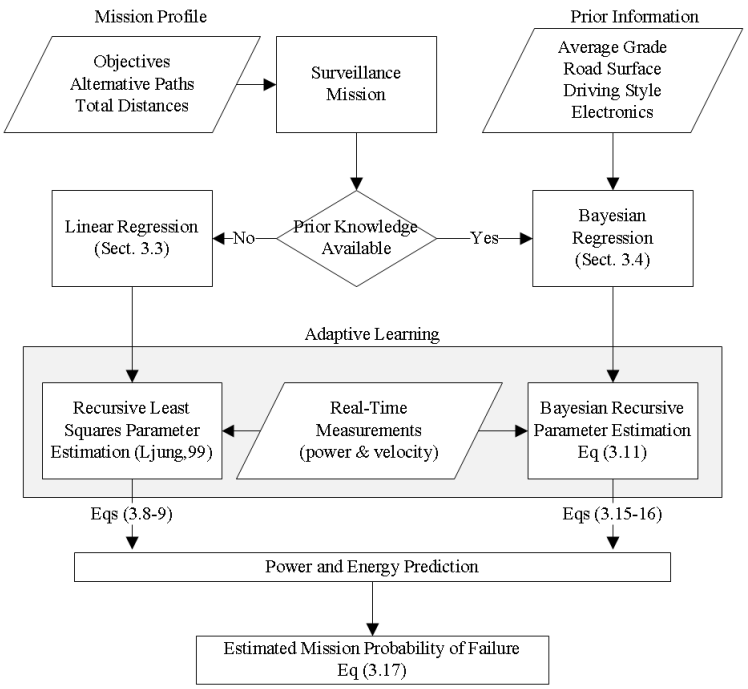

Figure 3.1: Overview of methodology for prediction of mission energy

3.2.2 Vehicle Dynamic Model

A vehicle longitudinal dynamics model, as typically used for power consumption studies in automobiles, is also utilized here (Ulsoy et al., 2012). The UGV power consumption is mainly associated with five key factors: (1) road grade (road profile), (2) road surface condition (rolling resistance), (3) driving style (velocity and acceleration profiles), (4) vehicle internal resistances, and (5) sensors and electronic equipment as follows:

$$P(t) = F(t)u(t) + b = (\underbrace{W\sin(\theta(t))}_{(1)} + \underbrace{fW\cos(\theta(t))}_{(2)} + \underbrace{ma(t)}_{(3)} + \underbrace{C_I}_{(4)})u(t) + \underbrace{b}_{(5)} + \varepsilon(t) \tag{3.1}$$

where $P(t)$ is the power at time t, $F(t)$ is the total traction force, $u(t)$ is the velocity, m is the vehicle mass, $a(t)$ is the acceleration, W is the vehicle weight, $\theta(t)$ is the road grade, f is the road rolling resistance coefficient, C_I is the internal resistance coefficient, b represents other constant sources of energy depletion, such as electronic sensors on-board the vehicle, and $\varepsilon(t)$ is the model error. Other time varying factors, which have a smaller relative significance, such as aerodynamic drag, are neglected here due to the low operating speed of small UGVs.

Equation (3.1) is nonlinear with respect to the parameter θ. Since in most applications the road

grade does not exceed 15 degrees, it can be linearized as follows:

$$P(t) = F(t)u(t) + b = (W\theta(t) + fW + ma(t) + C_I)\, u(t) + b + \varepsilon(t) \tag{3.2}$$

This linearization or the point about which we linearize the model does not introduce limitations in the methodology or the prediction approaches (see Sections 3.3.1 and 3.4.1). Equation (3.2) can be rewritten as a linear regression model:

$$P(t) - ma(t)u(t) = u(t)W(\theta(t) + f + C_I^{'}) + b + \varepsilon(t) \tag{3.3}$$

where the left side of (3.3) can be generally denoted as the response $y(t)$, i.e., $y(t) = P(t) - ma(t)u(t)$; $u(t)W$ is considered as the predictor denoted by $x(t)$; and $C = \theta(t) + f + C_I^{'}$ is the regression model parameter that combines the grade, rolling resistance coefficient, and internal frictional losses. For ease of notation and without loss of generality, we have defined $C_I^{'} = C_I/W$. Although $C_I^{'}$ is not as physically meaningful as C_I, this factorization allows us to preserve the physical meaning of θ and f, which are the major components of the prior knowledge. Thus,

$$y(t) = b + Cx(t) + \varepsilon(t) \tag{3.4}$$

In practice, the actual instantaneous UGV power consumption can be obtained in real-time by multiplying the measured current and voltage of the battery. The vehicle velocity can also be measured using a wheel velocity encoder. The acceleration can be estimated based on the difference between two consecutive velocity measurements. Generally, the exact values of rolling resistance coefficient, road grade, and vehicle internal resistance are difficult to know beforehand; however, some rough knowledge of the vehicle characteristics and road conditions, which can be generally expressed by a prior probability distribution, might be available. The modeling error term, $\varepsilon(t)$, is assumed to follow an *i.i.d.* normal distribution with zero mean and variance that is estimated by offline calibration experiments.

The proposed vehicle model has a few key properties. Equation (3.1) is a model based on vehicle-fixed coordinates, which implies movement along the heading direction of the vehicle (Ulsoy et al., 2012). Even when the vehicle heading changes, it still moves along a particular trajectory from which real-time measurements are collected allowing the predictions to account for maneuvers such as turning. If a novice operator makes frequent turns, the estimated parameters of the model will increase and adapt to reflect the driving style of the operator. A limitation of the vehicle model

is that the combined parameter, i.e., C, can algebraically become negative when a road grade is highly negative, and the road coefficient of rolling resistance is small (e.g., paved roads). In such extreme scenarios, the energy requirement for locomotion is very small, and if regenerative breaking capabilities are included in the vehicle design, a paved steep down-hill road can be used for recharging the UGV batteries. However, power regeneration is rarely used in existing UGVs. Consequently, here, C is assumed to be nonnegative. A road segment with a zero C indicates negligible power requirement for locomotion as gravitational pull is large enough to overcome the rolling resistance of the road, resulting in a very small energy requirement for propulsion.

3.3 Approach 1: Linear Regression in the Absence of Prior Knowledge

3.3.1 Linear Regression for Power Prediction

In the absence of prior knowledge, the power consumption is predicted using the regression model (3.4). Figure 3.2 shows a simple representation of a hypothetical mission. The measurements are collected at discrete time intervals that are indexed by $k = 1, 2, ..., n$. The sampling interval is Δt, and the remaining distance of the mission is denoted by R; $t_e = n\Delta t$ is the end time of the mission. The combined parameter, C, and b are both updated based on real-time power and velocity measurements using RLS estimation with forgetting factor λ_{ff} (Ljung, 1999). By tuning the forgetting factor, we increase or decrease the impact of past measurements on the estimated parameters of the model. This allows RLS to adapt more quickly to changes in the operating conditions. Unlike Bayesian estimation, RLS does not require the linearization introduced by (3.2). The parameters of model are not estimated individually, instead a combined parameter $C_n = \sin(\theta(t)) + f\cos(\theta(t)) + C'_I$ is recursively estimated, where C_n is the nonlinear version of C. Also, RLS does not assume constant linear parameters during the mission execution. The parameters of the model are estimated adaptively, which can be considered as a piecewise linear estimation approach.

Figure 3.2: UGV on a mission with no prior knowledge

3.3.2 EWMA Control Chart Monitoring

The regression model parameters can adapt to small shifts and drifts in the power consumption when RLS estimation is used, but the adaptation can be slow when an abrupt change occurs such as at the onset of transition from one road segment to another. To overcome this shortcoming, an exponentially weighted moving average (EWMA) control chart is used to monitor the prediction residuals according to Montgomery (2005). The EWMA monitoring statistic, $z(k)$, is defined as follows:

$$z(k) = \lambda_c \hat{e}(k) + (1 - \lambda_c) z(k-1) \tag{3.5}$$

$$\hat{e}(k) = y(k) - \hat{y}(k)$$

where λ_c is the EWMA weight, and $\hat{y}(k)$ is the prediction of the response at k, e.g., $\hat{y}(k) = E[y(k)|x(k), \hat{C}(k-1), \hat{b}(k-1)]$ where $\hat{C}(k-1)$ and $\hat{b}(k-1)$ are the estimated parameters at $k-1$. When an out-of-control signal is detected, the RLS covariance matrix is reset to its initial (large) value.

3.3.3 Prediction of Mission Energy Requirement

To predict the total mission energy, the future values of the velocity are required, which can be estimated based on the driving style of the UGV operator. The velocity is forecast using exponential smoothing (EWMA) with a weight λ_u as discussed in Appendix A.1. Although the variance of velocity prediction error is considered in computing the energy prediction variance, we assume that the combined parameter, i.e., $\hat{C}(k)$, and $\hat{b}(k)$ are both deterministic with values equal to the most recent estimates of C and b for energy prediction. We make this assumption considering the smaller variance of estimated parameters compared to the variance of the predicted velocity.

The effect of driving style, i.e., the $ma(t)u(t)$ term in (3.1), is considered in the estimation of the combined parameter. However, its contribution to the overall energy consumption, which is denoted as $\eta = \frac{\int ma(t)u(t)dt}{\int p(t)dt}$, is very small (i.e., less than 1%), as shown in Figure 3.3. Thus, we can assume that the approximation of $\hat{y}(k+j|k) \approx \hat{P}(k+j|k)$ is reasonable for power prediction, where $\hat{y}(k+j|k)$ and $\hat{P}(k+j|k)$ are the j-step-ahead prediction of response and power at k. More specifically, $\hat{y}(k+j|k) = E[y(k+j)|x(1:k), \hat{C}(k), \hat{b}(k)]$, where $x(1:k)$ is the vector of available measurements from 1 to k.

Generally, we have some prior knowledge about the distance that the UGV will traverse. Additionally, the position of the UGV can be tracked via GPS, and the distance that the UGV needs to

travel can be calculated. Therefore, the duration of a mission, i.e., t_e , can be estimated, denoted by $\hat{t}_e$, based on the remaining distance and real-time velocity measurements.

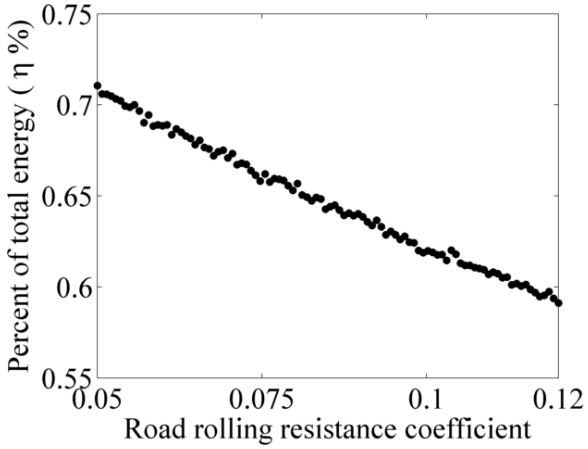

Figure 3.3: Percent of total energy associated with the driving style (i.e., $ma(t)u(t)$) term in (3.1) on a road segment with various levels of roughness and five degrees uphill grade with scaled EPA US06 speed profile shown in Figure 3.4. The power data was generated using (3.1) and the total energy was obtained using (3.6) assuming a one-second sampling time.

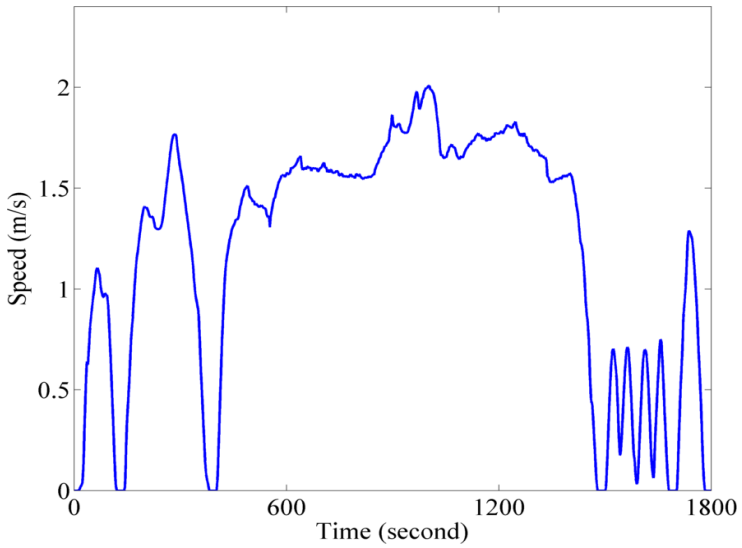

Figure 3.4: Drive cycle based on a scaled EPA US06 is used for simulation studies.

The energy consumption can be calculated by integrating the instantaneous power over the duration of the mission as follows:

$$E_m = \int_0^{t_e} P(t)dt \approx \sum_{j=1}^{n} P(j)\Delta t \tag{3.6}$$

Here, Δt is the sampling time, $t_e = n\Delta t$, and E_m is the total energy requirement for the mission,

which can be estimated by:

$$\hat{E}_m(k) = E_c(k) + \hat{E}_{rm}(k) \tag{3.7}$$

where $E_c(k)$ is the energy consumed up to time $t = k\Delta t$, and $\hat{E}_{rm}(k)$ is the expected energy requirement for the remainder of the mission. Using (3.6) and (3.7), the expected total mission energy and the corresponding variance at k can be estimated as detailed in Appendix A.2 :

$$\begin{aligned} \hat{E}_m(k) &= \left(\sum_{j=1}^{k} P(j) + \sum_{j=1}^{\hat{n}-k} \hat{P}(k+j|k) \right) \Delta t \\ &= E_c(k) + (\hat{n}-k) \left(W\hat{u}(k+1|k)\hat{C}(k) + \hat{b}(k) \right) \Delta t \end{aligned} \tag{3.8}$$

$$var(\hat{E}_m(k)) = \left(\sum_{j=1}^{\hat{n}-k} var(P(k+j|k)) \right) (\Delta t)^2 \tag{3.9}$$

Equation (3.9) can be used to calculate the 95% prediction upper and lower confidence intervals, i.e., *UCI* and *LCI*.

3.4 Approach 2: Bayesian Estimation and Prediction in the Presence of Prior Knowledge

3.4.1 Bayesian Estimation

Mission prior knowledge consists of (a) road grade information, (b) road rolling resistance information, (c) constant power consumption information due to sensors and electronic equipment, (d) vehicle internal resistance, and (e) driving style. The prior knowledge of electronic component power consumption and the vehicle internal resistance is obtained from the manufacturer or by using offline calibration experiments (Sadrpour et al., 2013a). The mission prior knowledge is also affected by the operating condition of the mission. For instance, a mission conducted at night will require infrared cameras, while in daylight there is no such need. Such information can be incorporated in the estimation of b in (3.4) using the Bayesian framework. A normal distribution is used to represent the prior information of b. The variance of the prior distribution represents the uncertainty of prior knowledge. The other two categories of prior information, i.e., road grade and rolling resistance, are divided into subcategories as shown in Table 3.1.

The values for rolling resistance coefficients in Table 3.1 were obtained by offline experiments using the PackBot and collecting data from several road segments of different road types. For more details of the experiments see Section 3.5. The design of the prior knowledge table for the road

grade was motivated by visual perception. It has been shown that human visual perception of a road grade is biased toward overestimation (Proffitt et al., 1995). In our experiments, we could comfortably visually discern the flat roads, average slope of up to $\pm 3^\circ$, from roads with slope of $\pm 3^\circ$ to $\pm 5^\circ$ degrees, labeling them as up/downhill. Similarly, roads with slopes ranging from $\pm 6^\circ$ to $\pm 12^\circ$ visually appeared steep up/downhill, although our verbal estimates of the grade were higher than the measured grade. Thus, while the visual perception of the numerical value of the slope may be biased, it was able to effectively classify roads into the correct categories of flat, up/downhill and steep up/downhill. For instance, an operator may state that the next road segment of the mission is on average flat and the road surface is grass. This prior information is matched with its associated prior distributions in Table 3.1. The normal distribution is used to represent the prior information for each parameter subcategory. The variances of the prior distributions are estimated by experiment, but rough estimates can also be extracted from the literature (Wong, 2008). Also, the prior information of the average vehicle velocity during the mission is obtained by requesting the operator to indicate their driving style as shown in Table 3.2. For instance, a moderate driver is expected to operate the UGV at an average velocity of 1-2 m/s.

Based on (3.3), the prior distribution of C can be expressed as follows:

$$C_i^0 = f_i^0 + \theta_i^0 + {C_I'}^0 \sim N(\mu_{f_i}^0 + \mu_{\theta_i}^0 + \mu_{C_I'}^0, (\sigma_{f_i}^0)^2 + (\sigma_{\theta_i}^0)^2 + (\sigma_{C_I'}^0)^2) \tag{3.10}$$

where $\mu_{f_i}^0$, $\mu_{\theta_i}^0$ and $\mu_{C_I'}^0$ are the means of the prior distributions of rolling resistance coefficient, average grade and vehicle internal resistance respectively for road segment i, and $(\sigma_{f_i}^0)^2$, $(\sigma_{\theta_i}^0)^2$ and $(\sigma_{C_I}^0)^2$ are the corresponding variances of the prior distributions. Unlike RLS, here the linearization affects the distribution of the combined parameter. The linearization around $\theta = 0$, resulted in $C = \theta + f + C_I'$; however, we could linearize (3.1) about the operating condition of the prior mean. This would have resulted in a different relationship between C, f, θ, C_I', and also a different model for each operating condition. The resulting model would have still been linear, so the proposed Bayesian prediction could be applied. Experimental validation (Sadrpour et al., 2013a) showed that the linearization about $\theta = 0$ is adequate for prediction of power in typical operating conditions, i.e., $|\theta| \leq 12^\circ$. Operating in roads with more extreme uphill or downhill grades resulted in robot slippage and tipping. We assume that the prior distributions of C_i and b_i are independent, and $\sum_{C_i,b_i}^0 = \begin{bmatrix} (\sigma_{b_i}^0)^2 & 0 \\ 0 & (\sigma_{C_i}^0)^2 \end{bmatrix}$ represents their prior covariance matrix.

Assume that a mission is composed of $i = 1, 2, ..., s$ road segments as shown in Figure 3.5; R_i

represents the remaining distance of road segment i; n_i and $t_i = n_i \Delta t$ are the final measurement index, and the end time of road segment i, respectively.

Table 3.1: Experimentally established prior knowledge (Sadrpour et al., 2013a)

Prior distribution of average road grade (degrees)			Prior distribution of rolling resistance coefficient		
Road grade	Mean	Standard deviation	Road conditions	Mean	Standard deviation
Steep-Uphill	8	3	Sidewalk	0.056	0.025
Uphill	4	2	Asphalt	0.062	0.026
Flat	0	2	Tile	0.066	0.025
Downhill	-4	2	Grass	0.099	0.025
Steep-Downhill	-8	3			
Vehicle Parameters					
	Mean	Standard deviation		Mean	Standard deviation
Internal resistance	0.22	0.003	Sensors & Electronics	28.29	1.73

Table 3.2: Driving style prior information (average speed)

Driving type	Conservative	Moderate	Aggressive
u	0-1 m/s	1-2 m/s	2-3 m/s

The posterior distribution of C_i and b_i at k $(n_{i-1} < k \leq n_i)$ can be obtained recursively based on the measurements only from its road segment (Congdon, 2003):

$$\begin{aligned}
\hat{\Sigma}_{\boldsymbol{\beta}_i}(k|n_{i-1}+1:k) &= (\boldsymbol{x}^T(k)\boldsymbol{x}(k)\sigma_\varepsilon^{-2} + \hat{\Sigma}_{\boldsymbol{\beta}_i}^{-1}(k-1|n_{i-1}+1:k-1))^{-1} \\
\hat{\mu}_{\boldsymbol{\beta}_i}(k|n_{i-1}+1:k) &= \hat{\Sigma}_{\boldsymbol{\beta}_i}(k|n_{i-1}+1:k)(\boldsymbol{x}^T(k)y(k)\sigma_\varepsilon^{-2} \\
&\quad + \hat{\Sigma}_{\boldsymbol{\beta}_i}^{-1}(k-1|n_{i-1}+1:k-1)\hat{\mu}_{\boldsymbol{\beta}_i}(k-1|n_{i-1}+1:k-1))
\end{aligned} \tag{3.11}$$

where for ease of notation we have defined $\boldsymbol{x}(k) = [1\ x(k)]$ and $\hat{\boldsymbol{\mu}}_{\beta_i}(k|n_{i-1}+1:k) = [\hat{\mu}_{b_i}(k|n_{i-1}+1:k)$ $\hat{\mu}_{C_i}(k|n_{i-1}+1:k)]$, and $\hat{\mu}_{\beta_i}(k|n_{i-1}+1:k)$ and $\hat{\Sigma}_{\beta_i}(k|n_{i-1}+1:k)$ represent the $(k-n_{i-1})^{th}$ update of the mean and covariance matrix of b_i and C_i, respectively. The initial values of the mean and variance are obtained according to (3.10). On road segment i, n_{i-1} has been observed and is not estimated.

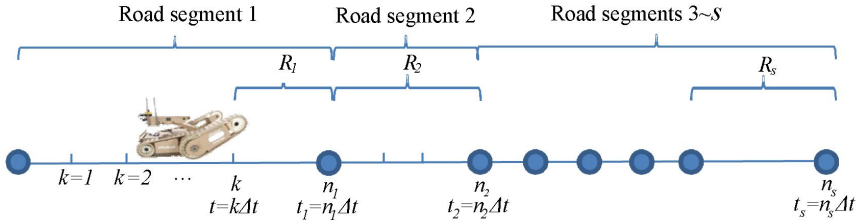

Figure 3.5: UGV on a mission comprised of s road segments.

Before any measurements are collected from a road segment, the power prediction distribution

for road segment i has a normal distribution as follows (see Appendix A.3):

$$P_i(j|0) \sim N(Wu^0\mu^0_{C_i} + \mu^0_{b_i}, (W\mu^0_{C_i})^2 var(u(j|0)) + \sigma^2_\varepsilon) \tag{3.12}$$

Equation (3.12) is conditioned on the mission prior knowledge of $\mu^0_{b_i}$,$\mu^0_{C_i}$, u^0 and $var(u(j|0))$; where $\mu^0_{C_i}$ is the prior mean of the combined parameter according to (3.10); u^0 is the velocity prior value obtained from Table 3.2, and $var(u(j|0))$ can be obtained as described in Appendix A.1.

When measurements are collected from a road segment, the power prediction distribution is sequentially updated. The combined parameter and constant energy terms are assumed to be deterministic and equal to the posterior mean, e.g., $\hat{\mu}_{b_i}$ and $\hat{\mu}_{C_i}$. For instance, the power prediction distribution for road segment i at k ($n_{i-1} < k \leq n_i$) can be shown to be normally distributed (see Appendix A.3) as follows:

$$P_i(k+j|k) \sim N(\hat{\mu}_{p_i}(k+j|k), \hat{\sigma}^2_{p_i}(k+j|k)) \tag{3.13}$$

where

$$\hat{\mu}_{p_i}(k+j|k) = W\hat{u}(k+j|k)\hat{\mu}_{C_i}(k|n_{i-1}+1:k) + \hat{\mu}_{b_i}(k|n_{i-1}+1:k)$$
$$\hat{\sigma}^2_{p_i}(k+j|k) = (W^2\hat{\mu}^2_{C_i}(k|n_{i-1}+1:k)var(u(k+j|k)) + \sigma^2_\varepsilon$$

3.4.2 Prior Updating for Future Missions Based on Past Measurements

An additional advantage of the Bayesian prediction framework is that the information uncertainty about the mission operating condition can be improved over time as the UGV traverses more road segments. The prior distributions of the combined parameters, presented in Table 3.1, can be updated based on the measurements from earlier road segments. Initially, the prior values of the rolling resistance coefficients, the vehicle internal resistance, and sensors and electronic equipment in Table 3.1 might not be accurate for the specific UGV or mission. However, these values are continuously updated during the execution of the mission. The combined parameter's posterior distribution can be used as the prior distribution for the road segments in future missions when a similar combination of road grade and surface condition is encountered.

In addition to updating the combined parameter distribution, the prior distributions of rolling resistance coefficients can be updated. A very likely scenario is when the UGV returns to its initial location at the end of a mission through the same road segment it initially undertook. An uphill road segment in the departure trip usually means a downhill road segment in the return trip. If the

combined parameter of the road segment in the departure trip is represented as $C_i = f_i + \theta_i + C_I^{'}$, then $C_j = f_i - \theta_i + C_I^{'}$ represents the combined parameter in the return trip from the same road segment. Thus, $(C_i + C_j)/2$ provides an estimate of the road rolling resistance and vehicle internal resistance coefficient $f_i + C_I^{'}$. Since the internal resistance, i.e., $C_I^{'}$, is independent of the road segment surface condition and grade, it is convenient to think of $f_i + C_I^{'}$ as one parameter and carry out predictions. This approach allows us to update the prior distribution of $f_i^0 + {C_I^{'}}^0$ for future missions.

3.4.3 Prediction of Mission Energy Requirement

The mission total energy requirement has three parts:

$$\hat{E}_m(k) = E_c(k) + \hat{E}_{rs_i}(k) + \sum_{\ell=i+1}^{s} \hat{E}_{s_\ell}(k) \tag{3.14}$$

where $\hat{E}_{rs_i}(k)$ is the prediction of the energy requirement for the remainder of the i^{th} road segment, and $\hat{E}_{s_\ell}(k)$ is the prediction of the energy requirement for the future road segment ℓ ($\ell > i$). At k, $(n_{i-1} < k \leq n_i)$, the expected values of $\hat{E}_{rs_i}(k)$ and $\hat{E}_{s_\ell}(k)$ are:

$$\hat{E}_{rs_i}(k) = (\hat{n}_i - k)(W\hat{u}(k+1|k)\hat{\mu}_{C_i}(k|n_{i-1}+1:k) + \hat{\mu}_{b_i}(k|n_{i-1}+1:k))\Delta t \tag{3.15}$$

$$\hat{E}_{s_\ell}(k) = (\hat{n}_\ell - \hat{n}_{\ell-1})(W\hat{u}(k+1|k)\mu^0_{C_\ell} + \mu^0_{b_\ell})\Delta t \tag{3.16}$$

The variance of prediction is computed according to Appendix A.3. The predicted energy is updated sequentially with real-time measurements, and the probability of completing the mission given the stored energy in the UGV batteries is calculated. If the estimated total energy requirement exceeds the failure threshold, i.e., E_{th}, it indicates that the UGV will exhaust its energy before completing its mission. The mission completion probability, at time step k, can be estimated by:

$$\Pr(\hat{E}_m(k) \leq E_{th}) \tag{3.17}$$

3.4.4 Application Scope of Proposed Methods

The prediction methodologies previously introduced can be applied to a variety of scenarios, and the scope and range of their applications is discussed next. The naive approach, which was introduced in the introduction, does not require a model for making predictions; however, unlike our

proposed methods, it does not consider any information about the road surface condition changes. Therefore, the naive approach, can neither handle situations when the characteristics of a road surface suddenly change, nor provides an estimate of the energy prediction uncertainty.

Compared to the naive approach, the RLS approach based on a stochastic model, adapts more quickly to both large and small changes in operating conditions using a forgetting factor and covariance resetting. Also, since it uses the vehicle model for prediction, it provides an estimate of prediction uncertainty. However, both the RLS and naive approaches only use real-time measurements for prediction without considering the available prior knowledge of road conditions.

In the absence of prior knowledge, the Bayesian approach will resemble the RLS approach. However, when prior knowledge is available, the Bayesian approach typically outperforms RLS even with moderately imprecise prior knowledge. Moreover, the Bayesian approach is most valuable when the following conditions are satisfied: (a) the energy requirement for locomotion accounts for a large percentage of the total energy requirement for completion of the mission. If this condition is not true, the impact of variations in road condition and its prior information on the overall energy will be small. If electronic components on-board the vehicle consume the majority of energy instead, other strategies can be utilized to minimize the energy consumption (Mei et al., 2005); (b) The internal resistance of the vehicle is not so large as to overshadow the energy requirement for overcoming the road rolling resistance and grade (see Section 3.6.2); (c) Road segments are structured, such as paved and unpaved surfaces made of grass, asphalt and cement, and indoor surfaces, e.g., carpet and tile. However, road surfaces that are unstructured, such as earth-quake affected areas, a forest floor with many obstacles, or roads whose surface condition or grade change very often, are difficult to characterize or to obtain reliable prior information about.

3.5 Experimental Validation of the Model

The objective of this section is to validate, through physical experiments, the theoretical framework that were established in previous sections. Experiments and statistical analyses have been performed to validate the theoretical models as a precursor for utilizing the proposed methodology in prediction of mission energy requirement. First, the sensor and measurement system are tested to analyze their repeatability. Next, the linearity of power consumption with respect to vehicle speed and road grade is verified to ensure that a linear regression model is suitable for prediction of energy. Also, the UGV internal resistance caused by frictional losses is investigated. In addition, the effect of different road surface types on energy consumption is tested and used to categorize roads based

on their roughness. Finally, procedures for estimation of prior distributions are presented.

Simulation validations of robotic systems can be categorized into three approaches: (1) studies that are based on inspection and qualitative comparison between the simulated model behavior and the real vehicle; (2) studies in which quantitative data has been collected, but analyses are qualitative or based on the visual inspection of graphs; (3) studies in which quantitative and statistical validations are used to verify the models or simulation results.

The objective of the majority of studies in the first and second approaches is to determine if the gross behavior of both the physical and simulated platforms are similar (Balakirsky et al., 2009). For instance, validation studies of multi-body dynamic simulations (Sadrpour et al., 2011) have been presented in Rossetti et al. (1998), Mei et al. (2005), Carpin et al. (2006), Carpin et al. (2007), Taylor et al. (2007), Pepper et al. (2007), Chen et al. (2009), and Balakirsky et al. (2009). Pepper et al. (2007) mainly relies on visual inspection in a few scenarios, to test whether the simulated vehicle behaves in a similar way as the physical robot and does not take advantage of real-time sensory information. In Carpin et al. (2007), validation focuses on aspects such as mission completion time on different road segments, but quantitative comparison among completion times are not performed. Similar limitations also appear in Rossetti et al. (1998) where validation is performed based on experts' inputs.

Some examples of the studies based on the third approach are Wang et al. (2005), Crandall et al. (2005), Lendvay et al. (2008), and Seixas-Mikelus et al. (2010). Simulation and validation of human robot interactions (HRI) is presented in Wang et al. (2005), but due to insufficient data, statistical comparisons between the simulated and physical platforms were not conducted. Validation of simulations/simulators involving medical robots have been considered in Seixas-Mikelus et al. (2010), and Lendvay et al. (2008). While Seixas-Mikelus et al. (2010) focuses on face validity (i.e., a measure of the realism of the simulator) of a Robotic Surgery Simulator, Lendvay et al. (2008) goes a step further and presents the first demonstration of face and construct validity of a virtual-reality robotic simulator. Some preliminary statistical analysis based on confidence intervals for HRI was presented in Crandall et al. (2005); however, most validation studies were based on simulations.

Although validation studies of UGV simulations have been the focus of several past studies, the majority of analyses only provide qualitative results based on the visual inspection of differences between simulation results and the behavior of the physical robot. The contribution of this section is to systematically design validation experiments to verify the linear approximation model using quantitative statistical methods. Thus, the validation study presented here is the first for UGVs that can be categorized into the third approach of quantitative and statistical validations. An additional

challenge of our validation experiments was that they were subject to human-robot interactions because the PackBot is tele-operated by a human. The presence of a human operator can add to the complexity of validation experiments due to human to human variations. In our research, we avoid the variations induced through the operator by automatically prescribing a pre-specified drive cycle to the vehicle, as commonly employed for automobiles (Ulsoy et al., 2012). This technique allows us to repeat a test multiple times with exactly the same specified speed profile under different operating conditions.

3.5.1 Measurement System Capability Analysis

To evaluate the capability of the sensor that is used to collect battery power measurements, the gauge capability test was conducted according to Montgomery (2005). The robot was placed on an indoor flat carpet floor, and was run at a constant velocity for a pre-specified time (10 seconds) to collect 3 battery power measurements. Since power measurements were collected at 0.3 Hz, the 3 measurements were taken consecutively every 3 seconds. The process was repeated at 20 different velocity levels ranging from very slow (0.1 m/s) to the maximum speed of 2 m/s. To avoid operator-to-operator variations, the speed profile, which is shown in Figure 3.6, was automatically prescribed to the robot.

Table 3.3 shows samples of power measurements at each velocity level. The range, denoted by R, is the difference between the largest and smallest power measurement at each velocity level. The average range $\bar{R}$ is the average of the collected R values under 40 different velocities. The measurements total variance was calculated as: $\hat{\sigma}^2_{total} = \sum_{i=1}^{N}(P_i - \bar{P})^2/(N-1)$ where P_i, $\bar{P}$, and N denote the individual, the average, and the total number of power measurements in the study, respectively.

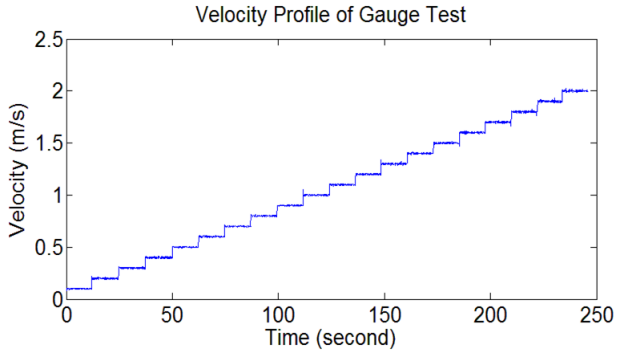

Figure 3.6: Experimental data for measurement system capability test. Speed was varied at 20 different levels for about 10 seconds.

Table 3.3: Sample of power measurements for measurement capability test.

Speed (m/s)	Measurements (Watts)			R
	1	2	3	
0.1	36.6650	35.4940	36.1446	1.1710
0.2	38.6947	39.1428	40.2078	1.5130
0.3	41.6615	42.0259	42.1558	0.4943
0.4	46.0947	44.7206	47.8057	3.0851
0.5	47.7671	49.0350	50.0959	2.3288
0.6	53.7481	54.9878	54.6262	1.2397
...	...	...	...	...
$\bar{R} = 3.02, \hat{\sigma}_{sensor} = 1.784, \hat{\sigma}_{total} = 24.90, \hat{\sigma}_{test} = 24.83$				

For data analysis, the total variance of the test, i.e., $\hat{\sigma}^2_{total}$, and the average range, i.e., $\bar{R}$ are firstly calculated. Then, the standard deviation of the sensor was calculated using (3.18). The constant d_2 in (3.18) is estimated for samples of 3 measurements as described in Montgomery (2005).

$$\hat{\sigma}_{sensor} = \frac{\bar{R}}{d_2} = \frac{\bar{R}}{1.693} \tag{3.18}$$

Next, the variance of the test, i.e., σ^2_{test}, was estimated using (3.19). The test variance is about 616 W^2, and the sensor variance is about 3.2 W^2.

$$\sigma^2_{total} = \sigma^2_{test} + \sigma^2_{sensor} \tag{3.19}$$

Finally, the signal to noise ratio, SNR, was found to be 19 using (3.20). A SNR of 5 or greater is recommended and a value less than two indicates that the measurement system is not capable (Montgomery, 2005; Burdick, 2008).

$$SNR = \sqrt{2(\sigma^2_{test}/\sigma^2_{sensor})} \tag{3.20}$$

Thus, a smaller part of the observed data variation results from the measurement system variability, and the sensor has good capability.

3.5.2 Model Linearity with Respect to Velocity

Based on the vehicle dynamic model, when the road surface type and grade are constant, the UGV power consumption changes linearly with respect to velocity. Experiments have been done to validate this assumption. For this purpose, the robot was placed on two surface types: (i) a flat sidewalk and (ii) a flat grass field. For each road surface type, the robot was run for one minute to collect 20 power measurements. The procedure was repeated at 4 speed levels as follows: 0.5, 1, 1.5, and 2 m/s. The power measurements were plotted against speed to visually inspect the linearity.

Linearity of power with respect to velocity for small UGVs was also validated visually in Mei et al. (2005). Figure 3.7 and Figure 3.8 show the strong linear relationship between velocity and power which is indicated by the values of R-squared, i.e., coefficient of determination. Analysis of variance (ANOVA) verified that speed has a significant effect on power (P-value < 0.01). Next, the estimated slope and intercept were obtained using regression analysis, which were used for analysis presented in section 3.5.6. Higher models, such as a quadratic model in velocity were also fitted but were rejected using a t-test (P-value > 0.37). The analysis confirmed that a linear model for UGV power consumption against velocity is adequate.

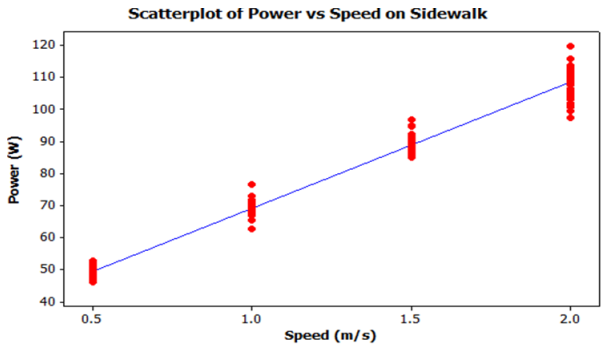

Figure 3.7: Power versus speed plot on sidewalk shows linearity (R-Squared is 98%).

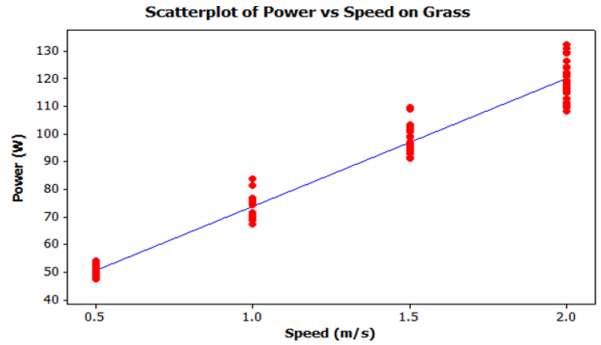

Figure 3.8: Power versus speed plot on grass shows linearity (R-Squared is 97%).

3.5.3 Model Linearity with Respect to Road Grade

Based on the vehicle dynamic model, if velocity and road surface are kept constant, the UGV energy consumption is linearly changed with the road grade for grades less than 12 degrees. To validate this relationship, the robot was run on flat, uphill, downhill, steep uphill and steep downhill sidewalk, and asphalt surfaces at each speed of 0.5 m/s and 1 m/s. The road grade was measured along the road segment in 1 meter intervals, and the mean grade was used for the analysis. For each road surface type and each speed level, power consumption was plotted against road grade, as

shown in Figure 3.9. The figure depicts that steeper uphill roads result in higher energy requirement for the UGV as expected. Although a quadratic model is slightly better fit to the data in terms of the model fitting errors, the margin of improvement is small and the linear model is considered to be an acceptable approximation based on high R-squared values.

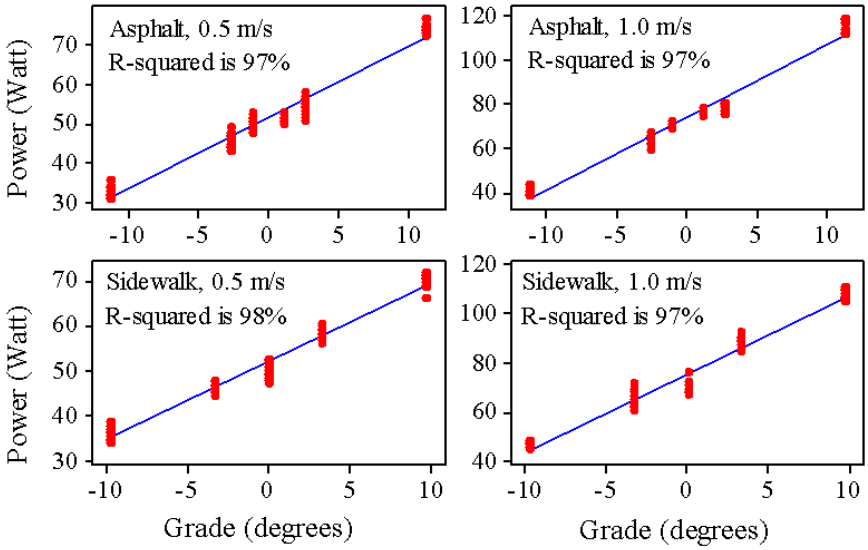

Figure 3.9: Power versus grade for sidewalk and asphalt roads at 0.5 and 1 m/s.

3.5.4 Effect of Road Surface Condition on Power Consumption

In Section 3.4, we proposed that road segments can be categorized into several groups based on their surface conditions such as: paved, roughly paved, rough and very rough. Since roads with different surface types exhibit different rolling resistances, the objective of this experiment was to categorize common surface types based on their rolling resistances. Some preliminary comparisons of power used by the PackBot while traveling over different terrains at different speeds were reported in Boice et al. (2010). Roads with a similar rolling resistance will have comparable power consumption. To avoid the variations induced by road grade, the robot was placed on a flat segment of roads of the following surface types: sidewalk, grass, tile, asphalt and carpet. On each road segment, the robot was run at several speed levels. The power consumptions on different roads were then compared, and based on whether the difference was significant, similar surface types were grouped into one category using Tukey and Fisher tests (Montgomery, 2004). More details of this test are provided in Appendix A.4. The boxplot of power consumption on different surfaces is presented in Figure 3.10. Based on Tukey's test, sidewalk and carpet roads have lower rolling resistances and are in group 1, and tile, asphalt and grass surface types have higher rolling resistance and are placed in group

2. It should be noted that the grass test was performed in a football field. While the grass of a football field is well groomed and is short, this is not generally true for all grass roads. The power consumption is not only affected by the material from which the surface is made, but also by the quality of the surface.

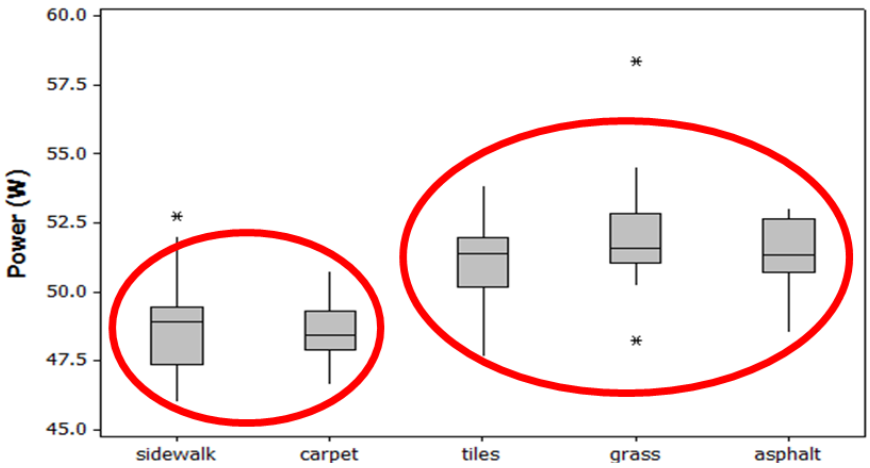

Figure 3.10: Boxplot of power consumption on different road surfaces at 0.5 m/s (stars represent data outliers). Similar surface types can be grouped together based on power consumption as shown.

The results are used for defining prior distributions for roads rolling resistances, i.e., μ_f^0, σ_f^0. For example, based on these results, we can either define prior distributions for each surface type separately, or we can define a prior distribution for each of the two categories of surface types shown in Figure 3.10. The latter should have a higher standard deviation since it encompasses several road surface types.

3.5.5 Estimating the Internal Power Consumption

In addition to rolling resistance and road grade, a part of UGV energy consumption is caused by the internal resistance of the robot, e.g., frictional losses in the transmission and actuators. For this test, the robot was lifted and placed on a wooden block so that the wheels were off the ground. The UGV was run at a constant speed for one minute. The procedure was repeated at four speed levels as follows: 0.5, 1.0, 1.5 and 2.0 m/s. Power measurements were graphed against the velocity to check for linearity. Then, the slope and intercept were estimated. The off ground power consumption was found to be linear with velocity having an R-squared greater than 98%, and the estimated slope, i.e., the internal resistance C_I', was 0.22.

3.5.6 Prior Knowledge

Prediction of the energy requirement for a UGV based on the Bayesian framework requires the prior knowledge of the mission road conditions and the robot characteristics such as its internal resistance, power consumption of sensors and electronic components. Based on the above planned experiments for various road surface types, grades and vehicle speeds, the prior information was estimated and is presented in Table 3.1. This information can be used to construct the prior distributions for the following parameters: The combined parameter (i.e., C), the rolling resistance coefficients of different road surface types (i.e., f), the electronic equipment power consumption term (i.e., b), as well as the UGV internal resistance coefficient (i.e., C_I').

The data in Table 3.1 is organized according to the factors that can be attributed to the vehicle, i.e., vehicle parameters, and also based on external factors, e.g., road surface condition. To obtain the estimated parameters, the road grade, i.e., θ, was manually measured, and C, the slope in (3.4), was obtained by least squares estimation. The rolling resistance coefficient f can be calculated using $f = C - (\theta(t) + C_I')$, where C_I' was estimated in the previous section. The overall mean and variance for each road rolling resistance were calculated using the weighted average and variance of the estimated rolling resistance coefficients, i.e., f, respectively, in which the weight is equal to the number of observations in the test. The estimated mean and standard deviations in Table 3.1 can be used to define the mean and standard deviation of the prior normal distributions. Due to differences in each vehicle internal resistance, and robot characteristics, the values in Table 3.1 are only valid for the PackBot. For other types of UGVs, the distribution parameters can be similarly established by using the above suggested experimental testing procedures.

3.6 Experimental and Simulation Studies

In the previous section, we presented results from experimental tests using the PackBot to validate several key aspects of the proposed prediction approaches: (a) the linear approximation of the vehicle longitudinal dynamic model with respect to velocity and grade was validated, (b) statistical tests were used to categorize and classify typical surface types based on their rolling resistances, (c) procedures for collecting prior knowledge in the Bayesian approach were discussed.

In this section, a few surveillance scenarios are used to illustrate different features of the proposed methods shown in Table 3.4. First, we demonstrate and compare the performances of the RLS and Bayesian prediction approaches when precise prior knowledge of the mission is available. We demonstrate that improved predictions are achievable in the Bayesian approach even with moderately

imprecise mission prior knowledge. Additionally, since the vehicle dynamic model was validated in Section 3.5, we use the model to generate surrogate scenarios in which the imprecise prior knowledge can be corrected *in-advance* by using the similarities among road segments in a round trip mission. In each study, the mission energy requirement is predicted and updated using (3.8) and (3.9) when prior knowledge is unavailable and (3.15) and (3.16) when prior knowledge is available. In addition, the 95% confidence intervals in each case are computed according to Appendix A.5. The two surveillance scenarios that are used for these studies are as follows:

1. *Short (surveillance) mission:* This scenario was carried out using a small size UGV. The mission is composed of two road segments as shown in Figure 3.11. In this mission, the UGV visits A-B-C, respectively. The robot uses two different road segments to accomplish this mission. The first road segment is a downhill sidewalk, and the second road segment is a flat grass field.

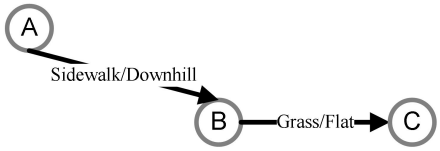

Figure 3.11: The short mission is composed of two road segments.

2. *Long (surveillance) mission:* The vehicle dynamic model is used to generate power data for this scenario. The mission is composed of four road segments as shown in Figure 3.12. During the round-trip mission, the UGV visits points A-B-C-B-A, respectively. The path from A to B is steep uphill and from B to C is downhill. Unlike the short mission scenario, in this round trip, the vehicle returns to its initial location using the same road segments, e.g., A-B-C and C-B-A are the same. Thus, the rolling resistance and road surface condition are assumed to be consistent for all the road segments in the long mission. The prior parameters of each road segment are also depicted.

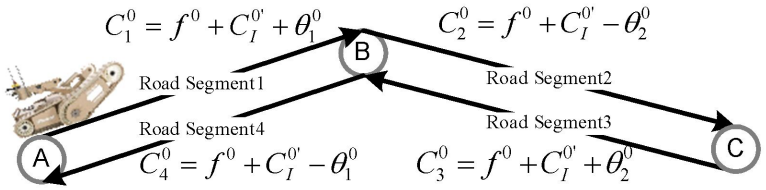

Figure 3.12: The long mission (a round trip) is composed of four road segments.

Table 3.4: Features presented in the study

Study	Type	Mission type	Feature presented in the simulation
1	Experiment	Short	Precise mission prior knowledge
2	Experiment	Short	Imprecise mission prior knowledge
3	Simulation	Long	In-advance parameter updating

3.6.1 Experimental Study 1: Impact of Mission Prior Knowledge on Energy Prediction

The goal of this experimental study is to demonstrate the advantage of using mission prior knowledge in prediction of mission energy requirement. The robot used for this study is the PackBot (Figure 3.13) manufactured by iRobot.

In this scenario, the drive cycle shown in Figure 3.4, the scaled aggressive EPA US06, was prescribed to the PackBot. The first road segment was a downhill sidewalk (-3 degrees on average) and the second road segment was a flat grass field. Since the power measurement frequency was about 0.3 Hz, which is too low to capture power consumption fluctuations within a short time interval, the fast-changing speed profile could not be prescribed directly. Instead of performing the speed profile directly, the UGV was run on both road segments (i.e., grass and sidewalk) at 40 different speed levels from 0.05 m/s to 2 m/s with an interval of 0.05 m/s. Multiple power measurements were taken at each speed level, and their mean values at each 40 speed levels were determined. For any speed data in the speed profile, the corresponding power consumption was found by interpolating between the two closest speed levels among the experimental speed levels. Then corresponding power consumption profile, which is shown in Figure 3.14, was generated for both road segments. Letters A, B and C indicate the position of the UGV in the mission as shown in Figure 3.11. The fluctuations in the profile correspond to the EPA US06 drive cycle shown in Figure 3.4. Next, the prediction approaches were applied to the data using the prior knowledge information presented in Table 3.5. The mission schematic is shown in Figure 3.11.

In Figure 3.15, the estimated *total* mission energy, $\hat{E}_m(k)$, and the corresponding 95% upper and lower confidence intervals, i.e., *UCI* and *LCI*, based on the RLS approach are compared against that of the Bayesian approach. In addition, we have shown the prediction based on the naive approach introduced in the introduction. The naive approach only provides an estimate of the expected energy requirement using the following relationship $\hat{E}_m(k) = E_c(k) + \overline{P}(k)(\hat{t}_e - k\Delta t)$, where $\overline{P}(k)$ and $(\hat{t}_e - k\Delta t)$ are the average power measurements up to time k using the current draw and voltage of the battery, and the estimated remaining duration of the mission, respectively. Letters A, B and C indicate the position of the UGV in the mission as shown in Figure 3.11. An out-of-control signal

(covariance resetting) occurs at the onset of the transition from the sidewalk road to the grass field about 15 minutes into the mission. The naive approach has the least accurate prediction throughout the mission, but the RLS approach also excessively underestimates the mission energy requirement in the first road segment due to lower power consumption in the first road segment compared with the second road segment. This problem is resolved when the measurements from the second road segment are collected and predictions quickly converge to actual total mission energy requirement, i.e., $\hat{E}_a$. The Bayesian predictions take advantage of the prior knowledge of the second road segment before its actual measurements become available, which results in more accurate predictions allowing the operator to prevent unanticipated mission failures due to a shortage of energy. The trends in the prediction profiles are due to change in (a) the estimated parameters of the vehicle model with real-time measurements, (b) predicted remaining duration of the mission. An increase in the duration of mission increases the predicted mission energy requirements because the contribution of electronics in the overall mission energy requirements is a function of remaining duration of mission.

(a) (b)

Figure 3.13: The PackBot used on a grass surface and a sidewalk surface for power data collection

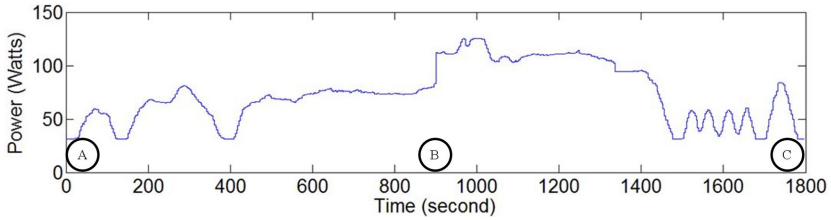

Figure 3.14: UGV power profile

The failure threshold, E_{th}, can be defined to be 1.5 times the expected total mission energy based on the initial prior information. Relying on the real-time data alone in the RLS approach may result in mis-detection of failures at the initial stage of the mission since the predicted end-of-mission

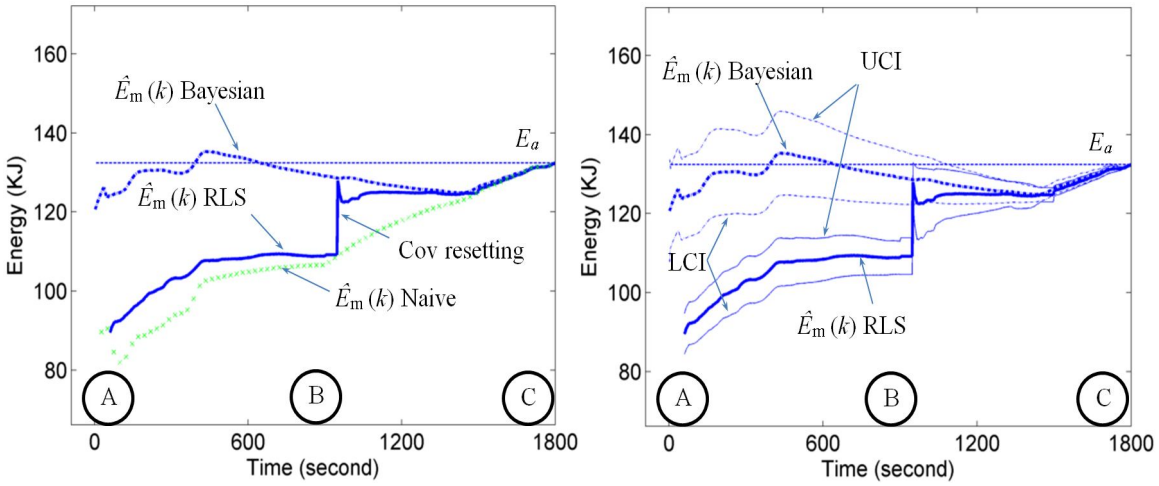

Figure 3.15: (a) Energy prediction mean vs. time using the Bayesian, RLS, and naive approaches. Unlike Bayesian predictions, the naive and RLS approaches underestimates the mission energy requirement. The dashed line at 135 KJ indicates the actual total energy consumed for the mission, E_a. (b) Energy prediction vs. time using the Bayesian and RLS approaches with prediction confidence intervals utilizing correct prior information.

Table 3.5: Parameters of Experimental Study 1.

Parameters	Value
Sidewalk surface prior parameters $(\mu_{f1}, \sigma^2_{f1})$	$(0.056, 0.025^2)$
Grass surface prior parameters $(\mu_{f2}, \sigma^2_{f2})$	$(0.099, 0.025^2)$
Sidewalk grade prior (downhill) $(\mu_\theta, \sigma^2_\theta)$	$(-4, 2^2)$ degrees
Grass grade prior (flat) $(\mu_\theta, \sigma^2_\theta)$	$(0, 2^2)$ degrees
UGV mass	35 lb
Road segments length	1074 meters
λ_{ff}	0.98
λ_u	0.002
σ_ϵ	5 watts
Sampling time Δt	3 seconds

energy is below the failure threshold. In contrast, the Bayesian approach provides more accurate predictions, allowing the operator to prevent unanticipated mission failure due to shortage of energy.

3.6.2 Experimental Study 2: Effect of Mission Imprecise Prior Knowledge on Energy Prediction

The impact of imprecise prior knowledge on the mission energy prediction is studied here. The scenario of the first study is used again. In this study, we consider the type of imprecision that arises from inaccurate prior information regarding the road surface type or the road grade.

In the Bayesian approach, imprecise prior knowledge can lead to less accurate predictions. For instance, categorizing the downhill-sidewalk road as flat-grass for the first road segment will result

in the over-estimation of mission energy requirement as shown in Figure 3.16a. Since actual measurements can be collected from this road segment quickly after the start of the mission, the poor prior information is corrected after a few measurements. However, if the prior knowledge of the second road segment is imprecise, for instance categorizing the grass road as sidewalk, the predictions cannot be corrected until measurements are collected from that road segment at the end of the first road segment, as shown in Figure 3.16b. Even in this case, the Bayesian prediction still typically outperforms the RLS. In the first road segment, the RLS approach, which does not use the mission prior knowledge, assumes the remaining mission, including the second road segment, is a downhill sidewalk similar to the past observations.

In the Bayesian approach, miscategorizing the second road segment as sidewalk still leads to an estimate of the combined parameter which is closer to its actual value compared to the linear regression approach because of the correct prior knowledge about the road grade. As long as the prior knowledge yields parameter estimates that are closer to the true parameters compared to the case of not having any prior knowledge, i.e., the RLS approach, the Bayesian predictions will outperform the RLS predictions.

The criticality of the prior information of the road grade and the rolling resistance after the start of a mission and data collection can be intuitively assessed using the linearized vehicle dynamic model (3.3) and (3.4). Both the RLS and the Bayesian approaches can estimate parameter b in the model accurately using the real time data. Thus, the advantage of the Bayesian approach lies in the combined parameter C. Two factors can weaken the importance of mission prior knowledge: (i) weight of the vehicle. If the vehicle is very light, the ratio of $\frac{Cx(t)}{b}$ becomes small, and so does the importance of C in the overall energy consumption of the vehicle. (ii) The internal resistance of the vehicle. If the internal resistance, $C_I^{'}$, is too large, it will dominate the effect of $\theta + f$, reducing their importance in the overall energy consumption. In these two cases, the difference between the RLS and the Bayesian predictions will be less pronounced.

3.6.3 Simulation Study: In-advance Parameter Updating Using the Vehicle Surrogate Model

In some commonly encountered scenarios, such as the long mission scenario shown in Figure 3.12, it is possible to update the imprecise prior knowledge of road segments in the Bayesian approach *in-advance* before actual measurements are collected based on similarities among roads. The goal of this simulation study is to demonstrate this capability. In-advance updating is performed using the concepts introduced in section 3.4.2, which are listed in Table 3.6. For instance when the UGV is

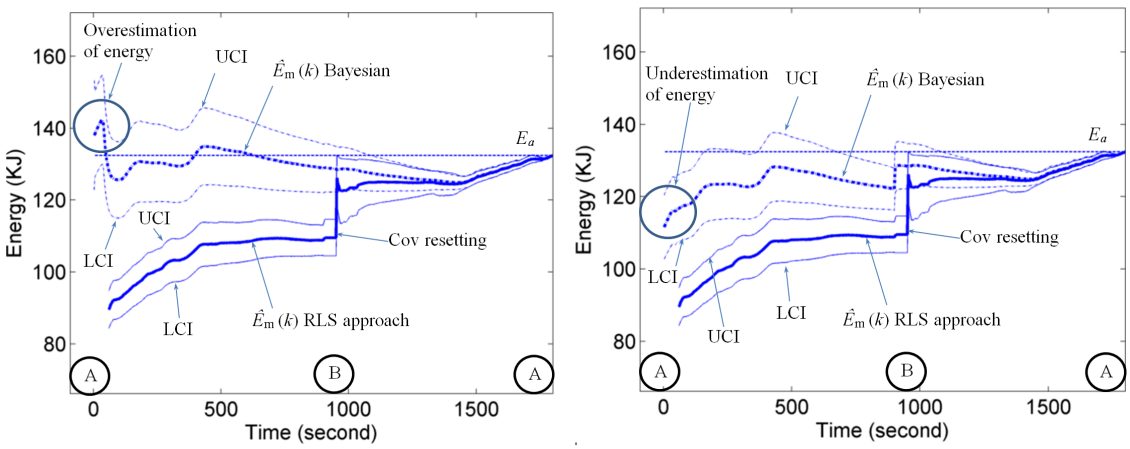

Figure 3.16: (a) Categorizing the first road segment as flat-grass instead of downhill-sidewalk results in overestimation of power consumption in the Bayesian approach, which is quickly corrected with a few measurements from the road. The Bayesian approach still outperforms the RLS approach. (b) Categorizing the second road segment as sidewalk instead of grass results in underestimation of power consumption in the Bayesian approach. The Bayesian predictions still outperform the RLS predictions, but the underestimation cannot be corrected while traversing the first road segment.

on the first road segments, two in-advance updating strategies are outlined in the first row of Table 3.6.

Table 3.6: Strategies for in-advance updating of road combined parameter

UGV position	Update 1	Update 2
Road segment 1(early)	$\hat{C}_4 = 2(f^0 + C_I^{'0}) - \hat{C}_1$	$\hat{C}_4 = \hat{C}_1 - 2\theta_1^0$
Road segment 2(early)	$\hat{C}_3 = 2(f^0 + C_I^{'0}) - \hat{C}_2$	$\hat{C}_3 = \hat{C}_2 - 2\theta_2^0$
Road segment 3	$\hat{C}_4 = \hat{C}_2 + \hat{C}_3 - \hat{C}_1$	$\hat{f} + \hat{C}_I^{'} = (\hat{C}_2 + \hat{C}_3)/2$

In this study, the power data is generated using the nonlinear vehicle dynamic model in (3.1) with the parameters shown in Table 3.7 and the scaled EPA US06 drive cycle. The value of rolling resistance was generated from its corresponding prior distribution. Other parameters, such as road grade, vehicle internal resistance, and consumption of electronic components are also assumed fixed, and the randomness in the simulated data is due to the $\varepsilon(t)$ term. The remaining parameters, i.e., the vehicle weight and the model noise variance, were previously presented in Table 3.5.

The accuracy of prior knowledge is critical for the in-advance updating introduced in the first two rows of Table 3.6. This *early* in-advance updating should be carried out only if the prior knowledge of the road rolling resistance coefficients or average grade is accurate. As shown in Table 3.6, $\hat{C}_3$ or $\hat{C}_4$ can be updated in two different ways. The first alternative, $\hat{C}_4 = 2(f^0 + C_I^{'0}) - \hat{C}_1$, should be used in scenarios with high confidence in the precision of f^0 and less confidence in θ_i^0, while $\hat{C}_4 = \hat{C}_1 - 2\theta_1^0$

Table 3.7: Simulation parameters

Simulation parameters	Value
Grass rolling resistance $\sim (0.099, 0.025^2)$	0.109
Segment 1 and 4 road grade ($\theta_{1,4}$)	$\pm$7.5 degrees
Segment 2 and 3 road grade ($\theta_{2,3}$)	$\pm$6 degrees
Internal resistance coefficient ($C_I^{'}$)	0.22
Sensors & Electronics (b)	28.29 watts
Road segments length	537 meters

should be used in scenarios with more confidence in the prior knowledge of θ_i^0 and less confidence in f^0. The in-advance updating introduced in the third row of Table 3.6, is entirely based on the estimated parameters and does not rely on the mission prior knowledge. Thus, $\hat{C}_4 = \hat{C}_2 + \hat{C}_3 - \hat{C}_1$ can be carried out even without a precise prior knowledge of grade or rolling resistance.

Since early in-advance updating relies on precise prior knowledge, it is not utilized in this simulation, and we demonstrate the improvements by using only the update introduced in the third row of Table 3.6. The prior information of this mission is shown in Table 3.8. We assume imprecise prior knowledge of f^0, i.e., categorizing the grass road as sidewalk. Additionally, although the grades of all four road segments are categorized correctly using the mission prior knowledge, the means of their corresponding prior distributions do not match with the grade parameter value that was used to simulate the data, shown in Table 3.7. Thus, the initial prior knowledge of combined parameters, i.e., C_i^0, $i = \{1, \ldots, 4\}$, is imprecise and does not match their true values.

Table 3.8: Prior information for simulation study

Prior knowledge category	Operator response
First road segment average grade	Steep uphill
Second road segment average grade	Downhill
Third road segment average grade	Uphill
Forth road segment average grade	Steep downhill
Road segments surface condition	Sidewalk (imprecise)
Driving style	Moderate

Figure 3.17a compares the mission energy prediction for the long mission scenario using the Bayesian prediction approach with and without in-advance updating. Letters A through C indicate the position of the UGV corresponding to Figure 3.12. As shown in Figure 3.17a, since early in-advance updating is not used, the predictions in the first two road segments are identical in both approaches. Due to the imprecise prior knowledge of road condition, C_4^0 is underestimated and is corrected when the UGV is traversing the third road segment using the available measurements and in-advance updating $\hat{C}_4 = \hat{C}_2 + \hat{C}_3 - \hat{C}_1$. Figure 3.17a depicts more accurate results on the third road segment as a result of in-advance updating compared with the earlier approach without in-advance

updating. The predictions on the third road segment converge to the proximity of the mission true energy requirement approximately five minutes earlier than the previous approach, which is a significant improvement for mission planning and an early detection of failure. Also, Figure 3.17b compares the mean of predictions in the Bayesian approach with in-advance updating against the RLS approach, and shows that the prediction based on the Bayesian approach is more accurate throughout the mission. Figure 3.17c and 3.17d depict the same predictions with the confidence intervals.

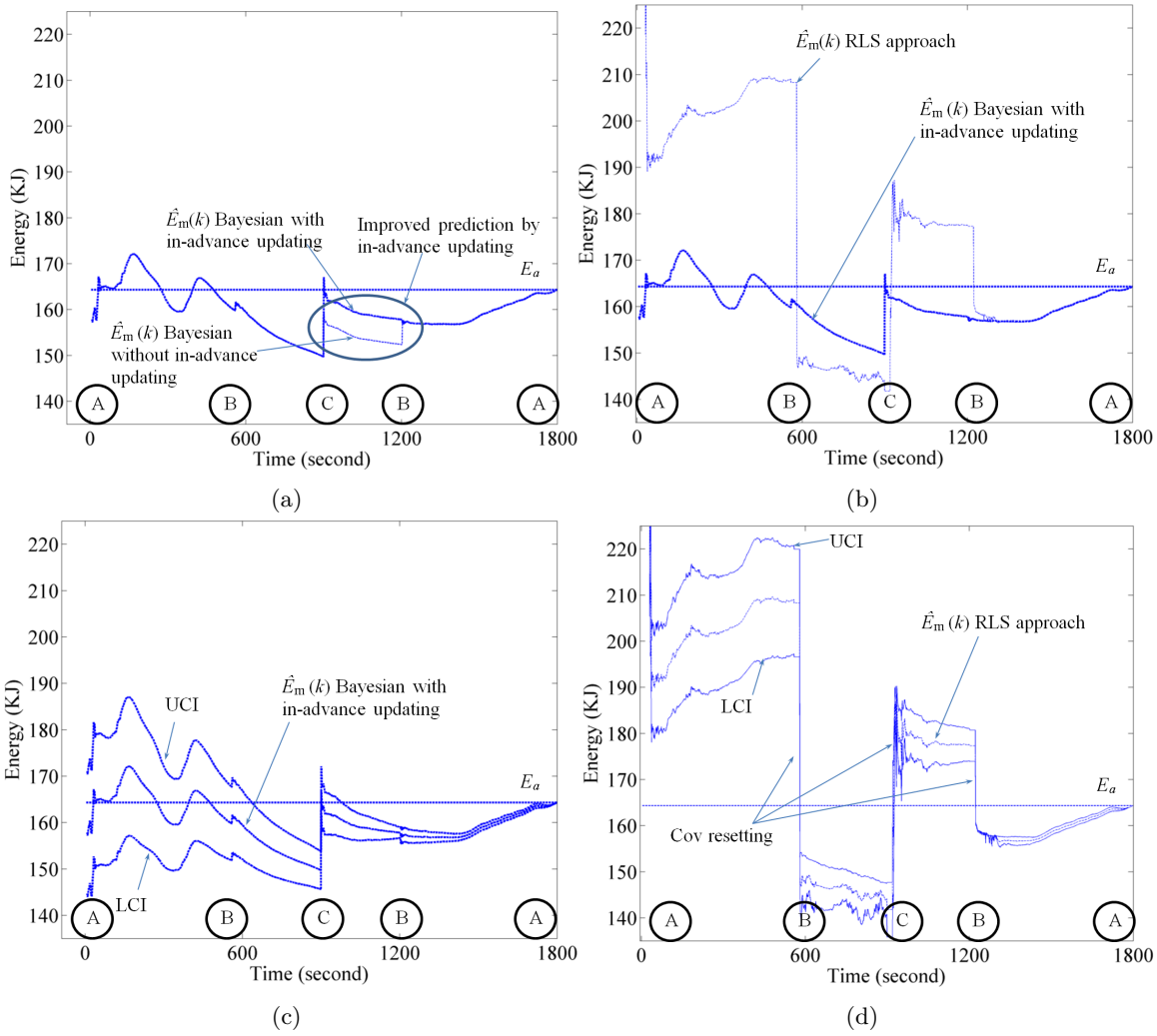

Figure 3.17: End-of-mission energy prediction vs. time. (a) Prediction mean vs. time with and without in-advance parameter updating using the Bayesian prediction approach. In-advance updating corrects the imprecise prior knowledge, resulting in more accurate predictions in the third road segment. (b) Prediction mean from the Bayesian approach with in-advance updating compared against the RLS prediction mean. The Bayesian prediction outperforms the RLS prediction in all road segments. (c) Bayesian prediction with in-advance updating with confidence intervals. (d) RLS prediction with confidence intervals.

In practice, we expect round trip missions, similar to the one presented in this study, to occur frequently, and demonstrate the twofold benefit of the Bayesian approach in such scenarios: (a) direct use of prior knowledge to improve the prediction; (b) use of the mission overall structure to exploit the dependencies and similarities between road segments for in-advance updating of parameters.

A Appendix

A.1 Velocity Prediction

The velocity is predicted using an exponentially smoothing model as follows: $E[u(k+1)|u(1:k)] = \hat{u}(k+1|k) = \lambda_u u(k)+(1-\lambda_u)\hat{u}(k|k-1)$, where $u(1:k)$ is the vector of velocity measurements 1 to k, whose initial value is obtained from the prior information of driving style, and λ_u is the EWMA weight. It follows that at measurement k, $\hat{u}(k+j|k) = \hat{u}(k+1|k), \forall j \geq 1$. The variance of prediction error, i.e., $var(u(k+j)|u(1:k))$, is $\sigma_w^2 \sum_{i=1}^{j-1} G_i^2$ where σ_w^2 is the variance, and $G_i = \begin{cases} 1 & \text{for } i = 0 \\ \lambda_u & \text{for } i \geq 1 \end{cases}$ is the Green's function of the underlying EWMA model (Pandit and Wu, 1983).

A.2 Energy Prediction with Linear Regression Model (RLS approach)

Let $\hat{\boldsymbol{\beta}}(k) = [\hat{b}(k)\ \hat{C}(k)]^T$be the estimated parameters at k. $\hat{y}(k+j|k) = E[y(k+j|k)] = E[y(k+j)|x(1:k), \hat{\boldsymbol{\beta}}(k)]$ is the j-step-ahead prediction of response. Additionally, $\hat{P}(k+j|k) = E[p(k+j)|x(1:k), \hat{\boldsymbol{\beta}}(k)]$ is the j-step-ahead prediction of power. $\hat{x}(k+j|k) = W\hat{u}(k+j|k)$ is the j-step-ahead prediction of predictor, and we assume $\hat{y}(k+j|k) \approx \hat{P}(k+j|k)$. The prediction mean is calculated as follows:

$$\begin{aligned} E[y(k+j|k)] =& E\left[E[y(k+j|k, x(k+j))]\right] = \hat{b}(k) + \hat{C}(k)E\left[x(k+j|k)\right] \\ =& \hat{b}(k) + \hat{C}(k)\hat{x}(k+j|k) \end{aligned} \tag{A-1}$$

The variance of prediction error at k is calculated as follows:

$$\begin{aligned} var[y(k+j|k)] =& E\left[var[y(k+j|k, x(k+j))]\right] + var\left[E[y(k+j|k, x(k+j))]\right] \\ =& \sigma_\varepsilon^2 + \hat{C}^2(k)\sigma_w^2 W^2(1 + (j-1)\lambda^2) \end{aligned} \tag{A-2}$$

The covariance of prediction error at k is calculated as follows:

$$
\begin{aligned}
cov[y(k+j|k), y(k+i|k)] =& E\left[cov[y(k+j|k, x(k+j)), y(k+i|k, x(k+i))]\right. + \\
& cov\left[E[y(k+j|k, x(k+j)), E[y(k+i|k, x(k+i))]\right. \\
=& \begin{cases} \hat{C}^2(k)\sigma_w^2 W^2(1+(j-1)\lambda_u^2) + \sigma_\varepsilon^2 & \text{if } i = j \\ \hat{C}^2(k)\sigma_w^2 W^2(\lambda + \min\{i-1, j-1\}\lambda_u^2) & \text{if } i \neq j \end{cases}
\end{aligned} \tag{A-3}
$$

The variance of end of mission energy prediction at k is computed as follows:

$$
\begin{aligned}
var(\hat{E}_m(k)) &= var\left(\sum_{j=1}^{\hat{n}-k} y(k+j|k)\right)\Delta t^2 \\
&= \left(\sum_{j=1}^{\hat{n}-k} var(y(k+j|k)) + \sum_{i=1}^{\hat{n}-k}\sum_{j\neq i} cov(y(k+j|k), y(k+i|k))\right)\Delta t^2
\end{aligned} \tag{A-4}
$$

A.3 Energy Prediction with Bayesian Regression Model

The predictive distribution is obtained by computing the integration below:

$$
\pi\left(y(k+j|k)\right) = \int \pi\left(y(k+j|k, x(k+j))\right)\pi\left(x(k+j|k)\right)dx(k+j) \tag{A-5}
$$

where $x(k+j|k) \sim N(\hat{x}(k+j|k), W^2\sigma_w^2(G_0^2 + G_1^2 + \cdots + G_{j-1}^2))$

For a mission with two road segments, when $k \leq \hat{n}_1$ the integration results in:

$$
y(k+j|k) \sim
$$

$$
\begin{cases}
N(\hat{\mu}_b(k|k-1) + \hat{\mu}_{C_1}(k|k-1)\hat{x}(k+j|k),\ \hat{\mu}_{C_1}^2(k|k-1)W^2\sigma_w^2(G_0^2 + \cdots + G_{j-1}^2) + \sigma_\varepsilon^2) \\
\quad \text{if } j \leq \hat{n}_1 - k \\
N(\hat{\mu}_b(k|k-1) + \mu_{C_2}^0\hat{x}(k+j|k),\ (\mu_{C_2}^0)^2W^2\sigma_w^2(G_0^2 + \cdots + G_{j-1}^2) + \sigma_\varepsilon^2) \\
\text{if } j > \hat{n}_1 - k
\end{cases} \tag{A-6}
$$

When $k > n_1$ the integration results in:

$$
\begin{aligned}
& y(k+j|k) \\
& \sim N(\hat{\mu}_b(k|k-1) + \hat{\mu}_{C_2}(k|n_1+1:k)\hat{x}(k+j|k), \\
& \qquad \hat{\mu}_{C_2}^2(k|n_1+1:k)W^2\sigma_w^2(G_0^2 + \cdots + G_{j-1}^2) + \sigma_\varepsilon^2)
\end{aligned} \tag{A-7}
$$

The covariance of predictions is computed as follows:

$$
\begin{aligned}
&cov(y(k+j|k), y(k+i|k)) = \\
&E\left[cov[y(k+j|k, x(k+j)), y(k+i|k, x(k+i))]\right] + \\
&\qquad\qquad cov\left[E[y(k+j|k, x(k+j))], E[y(k+i|k, x(k+i))]\right] =
\end{aligned}
\tag{A-8}
$$

$$
\text{if } k \le \hat{n}_1 \begin{cases}
\hat{\mu}^2_{C_1}(k|k-1)\sigma^2_w W^2(\lambda_u + \min\{i-1, j-1\}\lambda^2_u) \\
\text{if } \ i, j \le \hat{n}_1 - k \text{ and } j \ne i \\
\sigma^2_\varepsilon + \hat{\mu}^2_{C_1}(k|k-1)\sigma^2_w W^2(1 + (j-1)\lambda^2_u) \\
\text{if } \ i, j \le \hat{n}_1 - k \text{ and } j = i \\
\hat{\mu}_{C_1}(k|k-1)\mu^0_{C_2}\sigma^2_w W^2(\lambda_u + \min\{i-1, j-1\}\lambda^2_u) \\
\text{if } i \le \hat{n}_1 - k, \ i > \hat{n}_1 - k \quad \text{or if } \ i > \hat{n}_1 - k, \ i \le \hat{n}_1 - k \\
(\mu^0_{C_2})^2\sigma^2_w W^2(\lambda_u + \min\{i-1, j-1\}\lambda^2_u) \\
\text{if } i, j > \hat{n}_1 - k \text{ and } j \ne i \\
\sigma^2_\varepsilon + (\mu^0_{C_2})^2\sigma^2_w W^2(1 + (j-1)\lambda^2_u) \\
\text{if } \ i, j > \hat{n}_1 - k \text{ and } j = i
\end{cases}
$$

$$
\text{if } k > n_1 \begin{cases}
\hat{\mu}^2_{C_2}(k|n_1+1:k)\sigma^2_w W^2(\lambda_u + \min\{i-1, j-1\}\lambda^2_u) & \text{if } j \ne i \\
\sigma^2_\varepsilon + \hat{\mu}^2_{C_2}(k|n_1+1:k)\sigma^2_w W^2(1 + (j-1)\lambda^2_u) & \text{if } j = i
\end{cases}
$$

The variance of prediction for missions that are composed of more than two road segments is a straightforward extension of the presented equations. The variance of mission energy prediction can be computed in a similar way as was discussed in the case of regression.

A.4 Surface Type Grouping Using Tukey's Test

The following results were generated using the Minitab software (Minitab, 2010).

```
Source   DF      SS     MS      F      P
Surface   4  234.72  58.68  23.68  0.000
Error   110  272.63   2.48
Total   114  507.35

S = 1.574   R-Sq = 46.26%   R-Sq(adj) = 44.31%


                          Individual 95% CIs For Mean Based on Pooled StDev
Level      N    Mean  StDev    -+---------+---------+---------+--------
asphalt   23  51.367  1.317                          (----*----)
carpet    23  48.579  1.035    (-----*----)
grass     23  52.053  1.946                                    (-----*----)
sidewalk  23  48.702  1.685     (-----*----)
tiles     23  50.997  1.721                        (----*----)
                            -+---------+---------+---------+--------
                           48.0      49.2      50.4      51.6
Pooled StDev = 1.574

Grouping Information Using Tukey Method

Surface   N    Mean  Grouping
grass     23  52.053  A
asphalt   23  51.367  A
tiles     23  50.997  A
sidewalk  23  48.702    B
carpet    23  48.579    B

Means that do not share a letter are significantly different.
Tukey 95% Simultaneous Confidence Intervals
All Pairwise Comparisons among Levels of Surface
```

A.5 Energy Prediction Confidence Interval

The confidence intervals of energy prediction for both models are computed using $E[\hat{E}_m] \pm z_{1-\alpha}\sqrt{var(\hat{E}_m)}$. We have assumed that $\sum_{j=1}^{\hat{n}-k} y(k+j|k)$ is approximately normal.

CHAPTER IV

Dynamic Energy-Reliable Path Planning for Unmanned Ground Vehicles

4.1 Introduction

4.1.1 Problem Statement

One of the key factors that limit the utility of small tele-operated battery-powered UGVs in surveillance missions is the available on-board energy. The vehicle locomotion is the main source of energy consumption for most UGVs (Sadrpour et al., 2013a). Typical mission duration is currently on the order of 1-2 hours, while it is often desirable to carry out much longer missions (e.g., 8-10 hours) between lengthy recharging stops. A typical surveillance mission consists of various tasks and several alternative paths. Due to limited energy storage capacity, it is essential to predict the energy requirement of alternative paths to help the operator with path planning. The goal of surveillance missions studied here is to start from a known location on a map and reach a destination point using one of the available alternative paths. The objective of this research is to identify the path with the highest probability of successfully completing the mission using the information available at any given time. One failure mode of interest is the unanticipated depletion of the UGV's stored energy, which results in failures to reach the destination point. The shortest path is not always the most energy-efficient since in addition to length, other factors such as road roughness and grade and driving style affect the energy consumption. Additionally, the recommended criterion of the lowest failure probability, instead of the minimum expected energy consumption, considers the prediction uncertainty as well as the expected path energy requirement in decision making.

In this chapter, a surveillance mission is represented by a network where arcs symbolize road segments and nodes represent intersections of road segments. The cost of each arc is the energy

required to traverse the arc. This energy requirement is affected by variable random factors such as road surface conditions and grades with unknown probabilistic distributions. Mei et al. (2005) measured the power consumption of different components of UGVs and presented strategies for saving of energy that take advantage of UGV idle time, speed, etc. However, their deterministic energy models cannot consider random road grade variations, and no case study is presented on applying such strategies for real-time path planning.

Our problem falls within the general class of shortest path problems (SPP). Deterministic shortest path problems (Denardo, 2003) as well as stochastic shortest path problems (SSPP) with known cost distributions (Powell, 2011; Fan et al., 2005) have been extensively studied. A stochastic most reliable path problem with normally and correlated random costs were investigated in Seshadri and Inivasan (2010), however, the distributions of costs were assumed to be precisely known prior to the mission. Here, we relax the assumption of known path cost distributions, and further consider the uncertainty of path costs in the planning stage.

When the distributions of paths' costs are not known, adaptive learning via exploration becomes a viable approach in decision-making. Exploration is a process by which an arc cost distribution is estimated more precisely by collecting actual operating data for a short period from the arc. Ryzhov and Powell (2011) introduced an exploration policy based on the Knowledge Gradient (KG) in a stochastic shortest path problem with unknown cost distributions, in which exploration could be performed on any arc in the network at any given time. In contrast, UGV can only collect measurements from the sequential road segments that it traverses. Also, our exploration cost increases when additional sampling information is needed.

The following papers investigate variations of the traveling salesman problem (TSP) (Applegate et al., 2011) for UGV path planning with energy consideration. In Wei et al. (2012), a path planning problem was discussed for mobile robots with the objective of minimizing the energy requirement using docking stations with deterministic arc costs. A TSP for mobile robots was considered in Sipahioglu et al. (2008) with dynamically changing paths using a deterministic cost model. Moreover, energy-based path planning for cabled robots was studied in Borgstrom et al. (2008). Their goal was to maximize the accumulated rewards by visiting a sequence of nodes in a network. A similar concept is utilized in our proposed approach during the exploration stage. We prefer road segments whose exploration yields the maximum reduction of the prediction uncertainty by considering a stochastic cost model.

Another class of energy-efficient path planning for small UGVs deals with a coverage task problem. In a coverage task, the UGV is required to move through an area and travel within a certain

distance of predefined way-points. Broderick et al. (2012) investigated an energy-efficient coverage task using optimal control. Unlike a shortest path formulation, the UGV must visit every point on the map. Coverage tasks were also studied in Mei et al. (2004) with a focus on minimizing the energy for locomotion by optimally tuning the vehicle velocity and trajectory. However, their models were deterministic and did not consider the impact of terrain variations on power consumption.

Reinforcement learning (RL) is a class of online learning approaches, where an agent interacts with a stochastic and dynamic environment and learns a policy to maximize a measure of its long term reward (Sutton and Barto, 1998; Dearden et al., 1999, 1998). Many RL approaches deal with the tradeoff between exploration and exploitation. There are three major differences between those traditional RL frameworks and the proposed learning scheme to be discussed in this chapter: (1) in our problem, the risk associated with exploration grows with additional measurements due to limited on-board energy; (2) since there is no inherent exploration risk in RL when dealing with Markov Decision Processes, most exploration strategies have an oscillatory behavior in which alternatives or states are visited in an alternating fashion. With a UGV, due to physical constraints, such exploratory strategies are not energy-efficient; (3) our reward function uses the criterion of lowest failure probability (highest reliability) that considers both the expected energy requirement of road segments and their covariance, resulting in a reward structure that is not independent of past or future states of the vehicle. Seshadri and Inivasan (2010) showed, through a counterexample, how the inclusion of covariance in the structure of the reward function results in inapplicability of traditional shortest path algorithms for finding the most reliable path.

The objective of this research topic is to present a novel path planning problem for UGVs, under a network of alternative paths with the following characteristics: (a) The arc cost distributions are not precisely known *a priori*; (b) The arc costs may be correlated; (c) The distributions of arc costs can be updated online based on real-time measurements; and (d) UGVs can only collect measurements from the road segment that they traverse. To identify an energy-efficient path in the network, we propose a heuristic approach that integrates mission prior knowledge and real-time measurements for adaptively predicting the energy requirement distributions of alternative paths. The proposed method is described in the next section.

The rest of this chapter is organized as follows: Section 4.2 is an overview of the proposed methodology. Section 4.3 describes in detail the proposed Bayesian algorithm for the most energy-efficient path planning. Section 4.4 presents a comparative simulated case study to illustrate the advantages of the approach.

4.2 Methodology Overview

Figure 4.1a illustrates the framework of the proposed approach. Let us assume the vehicle has reached an intersection (node) in a network, see Figure 4.1b, from which alternative road segments emanate. A vehicle longitudinal dynamic model and mission prior knowledge are used for estimating the initial distribution (e.g., mean and variance) of energy requirement of alternative paths (Sadrpour et al., 2012). The first step uses the initial distributions to remove paths that are very unlikely to be the most energy-efficient from consideration through a process termed *pruning*. For instance, Figure 4.2a depicts the initial distributions of three alternative paths of the network in Figure 4.1b, i.e, $Q = \{q_1, q_2, q_3\}$, where the set q_i contains the indexes, for example $\{a, b, c, \dots\}$, of road segments of path i, based on mission prior knowledge assuming that the vehicle is at node 1. The figure shows that the distribution of the third path exceeds and does little overlap with the first two paths. If this situation arises, in favor of $\{q_1, q_2\}$, path q_3 (i.e., path 3) can be pruned without a need for exploration. If initial pruning results in only one unpruned path, no further action is needed and UGV can use the remaining path to reach the destination. However, some paths may still remain overlapping after pruning due to large energy prediction uncertainty. In this case, *exploration* of the remaining paths may become necessary, in which some of the available energy is used to explore the remaining alternatives (i.e., traverse and backtrack if necessary), to reduce their prediction uncertainty and bias.

The exploration step includes two substeps. First is to evaluate the exploration feasibility, i.e., to determine if exploration of alternative road segments emanating from the current node is feasible considering the predicted energy of the paths and the remaining stored energy in the UGV. If exploration is not feasible, the most fuel efficient path is selected based on the available information. The criterion for ranking and selection of energy-efficient paths is defined by the ratio $z = \left(\frac{\text{failure threshold - predicted energy expectation}}{\text{prediction standard deviation}}\right)$, which is termed the z-score and considers both the (expected) predicted path energy requirement as well as the prediction uncertainty. If exploration is feasible, in substep 2, the number of exploration measurements from each road segment, i.e., the exploration budget assignment, is determined using an energy efficient strategy based on the reduction of the energy prediction uncertainty. By collecting the measurements, the energy distributions are updated. For example, Figure 4.2b shows the updated distribution of the remaining paths, i.e, $\{q_1, q_2\}$, after exploring road segments $\{a, b\}$. Since the distributions of $\{q_1, q_2\}$ no longer overlap, using the pruning criterion, path q_2 is eliminated in favor of q_1. The exploration may not always lead to one remaining unpruned path. In either case, the road segment of the most energy-efficient

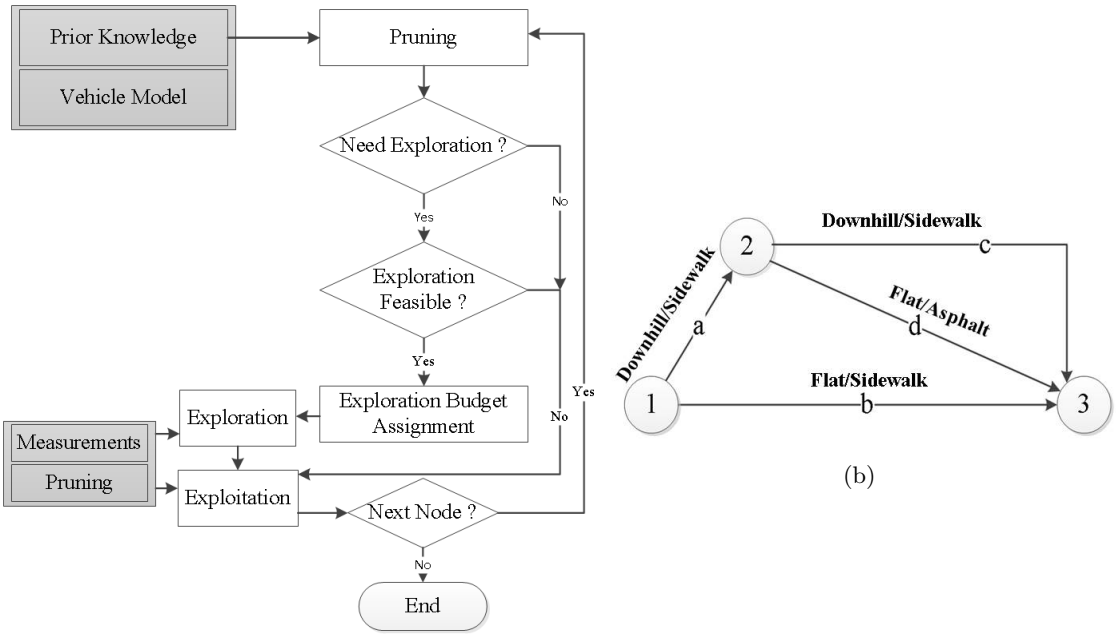

Figure 4.1: (a) Methodology overview, (b) Example of a simple network with 3 nodes, 4 road segements, start node 1, and end node 3. The alternative paths are $Q = \{q_1 = \{a, c\}, q_2 = \{b\}, q_3 = \{a, d\}\}$

path based on the updated energy distributions is selected to be *exploited*.

The exploitation step includes traversing a road segment until the vehicle reaches the next intersection in the network. During exploitation, pruning still continues in real-time. The exploration and exploitation steps are repeated whenever the vehicle reaches a node with multiple alternative paths until it arrives at the destination node. For instance, based on Figure 4.2b, path $q_1 = \{a, c\}$ is selected to be exploited since it has the highest efficiency (highest z-score) and because other alternatives paths have been pruned. It should be noted that the balance between exploration and exploitation is achieved by feasibility analysis and exploration budget assignment. Feasibility analysis assures that exploration does not significantly reduce mission completion probability. Moreover, the budget assignment ensures that only roads with large remaining prediction uncertainty are explored to preserve energy in exploitation. Section 4.3 will describe the above steps in detail.

4.3 Methodology

4.3.1 Vehicle Model

A linearized vehicle longitudinal dynamics model, as typically used for power consumption studies in automobiles, is also utilized here (Ulsoy et al., 2012). The UGV power consumption is modeled

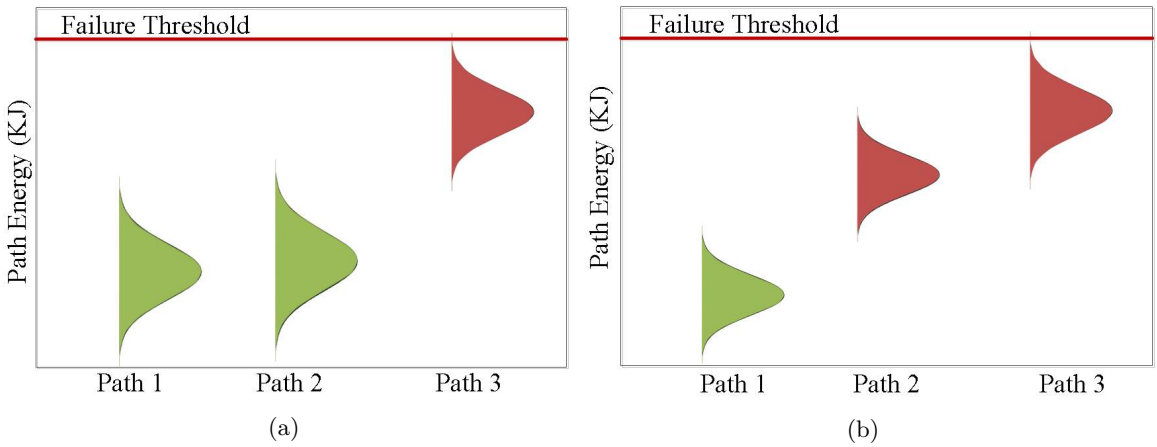

Figure 4.2: (a) The initial energy requirement distribution of a hypothetical mission with 3 alternative paths (see Figure 4.1b) based on mission prior knowledge. Path q_3 (i.e., path 3) energy requirement is clearly higher than $\{q_1, q_2\}$. However, it is not clear which of the remaining paths is more energy-efficient. (b) The updated distributions of energy requirement of $\{q_1, q_2\}$ after exploring them. q_2 can be pruned in favor of q_1 which is estimated to have the highest probability of success.

as follows (Sadrpour et al., 2013b):

$$P(t) = (W\theta(t) + fW + ma(t) + C_I)u(t) + \beta + \epsilon(t) \tag{4.1}$$

where $P(t)$ is the power at time t, W is the vehicle weight, $\theta(t)$ is the road grade, f is the road rolling resistance coefficient, m is the vehicle mass, $a(t)$ is the acceleration, C_I is the internal resistance coefficient, $u(t)$ is the velocity, β represents other constant sources of energy depletion, such as electronic sensors on-board the vehicle, and $\epsilon(t)$ is the model error following NID$(0, \sigma_\epsilon^2)$. Other time varying factors, which have a smaller relative significance, such as aerodynamic drag, are neglected here due to the low operating speed of small UGVs. According to experimental results presented in Sadrpour et al. (2013a), the vehicle slippage is negligible on steep uphill and downhill roads, and the current vehicle longitudinal dynamics model does not consider slippage.

In practice, the actual instantaneous UGV power consumption can be obtained in real-time by multiplying the measured current and voltage of the battery. The vehicle velocity can also be measured using a wheel velocity encoder. The acceleration can be estimated based on the difference between two consecutive velocity measurements. Generally, the exact values of rolling resistance coefficient, road grade, and vehicle internal resistance are difficult to know beforehand; however, some rough knowledge of the vehicle characteristics and road conditions, which can be generally expressed by a prior probability distribution, might be available.

Equation (4.1) can be rewritten as a linear regression model:

$$y(t) = Cx(t) + \epsilon(t) \tag{4.2}$$

where $y(t) = P(t) - ma(t)u(t) - \beta$, $x(t) = u(t)W$, and $C = \theta(t) + f + C_I^{'}$ is the regression model parameter that combines the grade, rolling resistance coefficient, and internal frictional losses. For ease of notation and without loss of generality, we have defined $C_I^{'} = C_I/W$. The proposed vehicle model was validated by experimental studies in Sadrpour et al. (2013a,b).

Parameter C in (4.2) represents the average combined parameter of a road segment. This model (i.e., fixed effect represented by C) does not capture the natural variations in the grade and rolling resistance coefficients within a road segment. Consequently, the prediction variance is underestimated. To overcome this shortcoming, a mixed effect (random slope) model, i.e., $y = (C + \mathfrak{C}_\ell)x + \epsilon$, where $\mathfrak{C}_\ell$'s are i.i.d with $\mathfrak{C}_\ell \sim N(0, \sigma^2)$ is used where the estimate of σ^2 can be obtained by experiments such as the ones presented in Sadrpour et al. (2013a) and procedures in Appendix A.1. A road segment is divided into smaller sub-segments $\ell = 1, 2, \ldots, L$, and n_ℓ measurements are collected from each sub-segment ℓ. In the mixed effect model, parameter C captures the average combined parameter (slope) and $\mathfrak{C}_\ell$ captures the deviations of each sub-segment slope from the average slope. The mixed effect model provides a more reasonable estimate of the prediction uncertainty compared to the fixed effect model; however, parameter estimation for the mixed effect model is more complex computationally since the posterior distributions of parameters do not have a closed-form expression (see Appendix A.1). We assume the random effect have a negligible effect on estimation of C, and will use the fixed effect model to update the posterior distribution of C. The random effect model is used to obtain more accurate estimate of the prediction variance, and the model parameter, σ^2, does not need to be updated with every measurement as discussed in Appendix A.2.

4.3.2 Problem Definition

Consider a directed network $G(N, A)$ with nodes $N = \{1, 2, \ldots, n\}$, and edges $A = \{a, b, \ldots\}$, where edges represent road segments. A road segment is defined as a sector of a road that has the same distribution of grade and rolling resistance (e.g., uphill/grass, level/paved, downhill/unpaved). The goal of a UGV operator is to traverse from a starting node to a final node using one of the alternative paths. Our objective is to provide the operator with a path that has the highest probability of reaching the destination without running out of energy.

4.3.3 Bayesian Prediction of Energy Requirement

The energy requirement of road segment i, i.e., E_i where $i \in A$, can be calculated by integrating the instantaneous power over the time spent on the segment, i.e.,

$$E_i = \int_0^{t_e} P(t)dt \approx \sum_{j=1}^{n} P(j)\Delta t \tag{4.3}$$

where E_i is the total energy requirement of the road segment i, and t_e, n, and Δt are the end time, number of measurements, and the sampling interval, respectively. Let us assume that the vehicle has collected k measurements from road segment i. E_i can be estimated by:

$$\hat{E}_i(k) = E_i^o(k) + \hat{E}_i^r(k) \tag{4.4}$$

where $E_i^o(k)$ is the measured actually consumed energy up to time $t = k\Delta t$, and $\hat{E}_i^r(k)$ is the predicted expected energy requirement for the remainder of the segment.

Based on (4.3-4.4), to estimate E_i, predictions of power for each road segment in the network is carried out using the vehicle model (4.2). In Sadrpour et al. (2012, 2013b), Bayesian recursive estimation was used to estimate and update the unknown parameter C of Eq. (4.2) using real-time velocity and power measurements and mission prior knowledge. In (4.2), the prior distribution of C is assumed as follows:

$$C_i^0 = f_i^0 + \theta_i^0 + {C_I'}^0 \sim N(\mu_{f_i}^0 + \mu_{\theta_i}^0 + \mu_{C_I'}^0, \sigma_{f_i}^{0\,2} + \sigma_{\theta_i}^{0\,2} + \sigma_{C_I'}^{0\,2}) \tag{4.5}$$

where $\mu_{f_i}^0$, $\mu_{\theta_i}^0$ and $\mu_{C_I'}^0$ are the means of the prior distributions of rolling resistance coefficient, average grade and vehicle internal resistance, respectively for road segment i, and $\sigma_{f_i}^{0\,2}$, $\sigma_{\theta_i}^{0\,2}$ and $\sigma_{C_I'}^{0\,2}$ are the corresponding variances of the prior distributions. In Sadrpour et al. (2013a), we experimentally estimated the prior distributions of the parameters for various typical road surfaces using an iRobot Packbot. Assuming k measurements of velocity and power have been collected from road segment i, the posterior distribution of C_i in model (4.2) is updated as follows (Congdon, 2003):

$$\hat{C}_i(k|k-1) \sim N\left(\hat{\mu}_i^C(k|k-1), [\hat{\sigma}_i^C(k|k-1)]^2\right) \tag{4.6}$$

where

$$\hat{\mu}_i^C(k|k-1) = ([\hat{\sigma}_i^C(k-1|k-2)]^{-2} + \sigma_\epsilon^{-2}x^2(k))^{-1} \times([\hat{\sigma}_i^C(k-1|k-2)]^{-2}\hat{\mu}_i^C(k-1|k-2) + \sigma_\epsilon^{-2}x(k)y(k))$$
$$[\hat{\sigma}_i^C(k|k-1)]^2 = ([\hat{\sigma}_i^C(k-1|k-2)]^{-2} + {\sigma_\epsilon}^{-2}x^2(k))^{-1}$$

where $\hat{\mu}_i^C(k|k-1)$ and $[\hat{\sigma}_i^C(k|k-1)]^2$ represent the k^{th} update of the mean and variance of C_i, respectively. Note that for real-time prediction, the estimates of C are obtained from the fixed effect model. The CPU time for estimation is negligible, as is the case for most recursive algorithms. The computer holds the estimated posterior mean and variance of C from the last iteration, and updates them using the closed form expressions in (4.6). Using the posterior predictive distribution of $y(k)$, we can estimate the distribution of energy requirement of each road segment as follows (see Appendix A.2):

$$\hat{E}_i(k) \sim N(\hat{\mu}_i^E(k), [\hat{\sigma}_i^E(k)]^2) \tag{4.7}$$

where

$$\hat{\mu}_i^E(k) = E_i^o(k) + \hat{t}_i(k)\beta_i + \hat{r}_i(k)W\hat{\mu}_i^C(k|k-1)$$
$$[\hat{\sigma}_i^E(k)]^{\,2} = W^2\hat{r}_i^2(k)[\hat{\sigma}_i^C(k|k-1)]^2 + \hat{t}_i(k)\hat{\sigma}_\epsilon^2\Delta t + \phi_i\hat{r}_i(k)$$

where $\hat{\mu}_i^E(k)$ and $[\hat{\sigma}_i^E(k)]^2$ represent the k^{th} update of the mean and variance of $\hat{E}_i$, respectively, $\hat{t}_i(k)$ and $\hat{r}_i(k)$ are the estimated remaining time and remaining distance of road segment i, and ϕ_i is a constant (see Appendix A.2). To obtain an estimate of $r_i(k)$, we assume that real-time localization is available using Global Positioning System (GPS) or Simultaneous Localization and Mapping (SLAM) techniques.

We declare two road segments similar if they have the same prior distributions for rolling resistance and grade (i.e., they share the same parameter C). Measurements from one road segment is used to update the energy requirement distribution of all similar road segments in the network (see Appendix A.3). The covariance of energy prediction between two similar road segments i and i' is

given as follows (Appendix A.4):

$$\hat{\sigma}^E_{(i,i')}(k) = W^2 \hat{r}_i(k)\hat{r}_{i'}(k)[\hat{\sigma}^C_i(k|k-1)]^2 \tag{4.8}$$

The covariance between roads that are not similar is set to zero. Using (4.7-4.8), we construct the joint distribution of energy requirement of road segments. The next step is to enumerate all paths from the start node to the destination node to construct the set $Q = \{q_1, q_2, \dots\}$. The computational complexity for enumerating all the paths from the start to end node, where all N nodes are connected is exponential in the number of nodes. However, in real-world applications the computational complexity is expected to be much less since most nodes are not connected and many paths can be pruned against obviously more reliable ones. For example, Figure 4.5b depicts a network with 7 nodes in which the UGV travels across the University of Michigan's north campus from node 1 to node 7. Since a path is composed of one or more road segments, its energy requirement distribution is predicted by the sum of energy requirement distributions of its corresponding road segments as follows:

$$\hat{E}_{q_j}(k) = \sum_{i \in q_j} \hat{E}_i(k) \tag{4.9}$$

Let us denote $\hat{\mu}^E_{q_j}(k)$ and $\hat{\sigma}^E_{q_j}(k)$ as the estimated mean and standard deviation of the path energy requirement at time k. When energy distributions are not known, $\hat{\mu}^E_{q_j}(k)$ and $\hat{\sigma}^E_{q_j}(k)$ will be updated with each new measurement, which in turn changes the estimated success probability of path q_j. Thus, there may be a situation that while traversing a path with a previously estimated high probability of success, it becomes unreliable. Moreover, some paths that are not initially selected, may actually have higher probability of success and measurements may not be collected from them to update their energy distributions. To reduce the impact of the above issues, paths are explored with an energy-efficient strategy.

Let us define $z_{q_j}(k) = \left(\frac{T - \hat{\mu}^E_{q_j}(k)}{\hat{\sigma}^E_{q_j}(k)} \right)$ where T is the available energy prior to the mission. This index is commonly known as the z-score, which is used to reflect the reliability (i.e., probability of success) of a path indicated by $\hat{R}_{q_j}(k) = \Phi(z_{q_j}(k))$ where $\Phi(\bullet)$ is the cumulative distribution function of the standard normal distribution. The benefits of using the z-score is that it not only captures the reliability of a path (i.e, a path with a higher reliability has a higher z-score), but it is a more informative measure to identify the minimum energy path with high certainty. To rank

paths based on their probability of success, we will use the z-score of the paths.

4.3.4 Pruning of Undesirable Paths

Pruning requires calculation of the lower and upper confidence intervals of the energy requirement of each path, i.e., $LCI_{q_j}(k)$, $UCI_{q_j}(k)$, using $\hat{\mu}^E_{q_j}(k) \pm z_\alpha \hat{\sigma}^E_{q_j}(k)$, where z_α, $0 \leq \alpha \leq 1$, is the $100(1-\alpha)^{th}$ percentile of the standard normal distribution. Using a pair-wise comparison of upper and lower confidence intervals if $\{\exists\ q_j, q_{j'} \in Q\ : LCI_{q_j}(k) > UCI_{q_{j'}}(k)\}$ then path q_j is eliminated from Q. The road segments of the remaining paths may be traversed in the exploration stage. Occasionally, in addition to the energy criterion mentioned above, the duration of time spent on a path should be considered for pruning. Although the analytical details is beyond the scope of this chapter, the remaining duration of a path is a random variable for which confidence bounds can be estimated. Paths whose required minimum (lower confidence bound) of completion times are greater than the desired mission completion time can be pruned at the pruning stage. In the case studies of this chapter, we only consider the energy criterion for pruning and not the mission completion time.

4.3.5 Exploration Feasibility & Exploration Budget

Prior to exploring a path, the uncertainty of energy predictions, i.e., $\{\hat{\sigma}^E_{q_j} : j \in Q\}$, can be very large. As a result, the prediction confidence intervals of energy requirements of many alternatives paths may overlap. The main objective of exploration is to separate some overlapping energy distributions. The separation is a result of reduction in the energy prediction uncertainty and bias from imprecise prior knowledge.

To determine the feasibility of exploration, we need to ensure that energy spent on exploration does not reduce the probability of mission success below a desirable threshold. The exploration feasibility study provides a threshold for the maximum allowable exploration energy expenditure, i.e., an exploration budget

The exploration budget, i.e., $Ex_{q_j}(k)$, is path dependent. Not all the road segments will be visited during a mission. To obtain the exploration budget, we modify the reliability function $\hat{R}_{q_j}(k)$ of q_j by adding $Ex_{q_j}(k)$ to its expected exploitation energy requirement. For each remaining path after pruning, we determine $Ex_{q_j}(k)$ satisfying the following condition $\Phi\left(\frac{T-\hat{\mu}^E_{q_j}(k)-Ex_{q_j}(k)}{\hat{\sigma}^E_{q_j}(k)}\right) > 1-\gamma$. Parameter γ is the probability of mission failure after conducting both exploration and exploitation if path q_j is ultimately selected for exploitation and is calibrated by the user. Solving the relationship

for $Ex_{q_j}(k)$ results in:

$$Ex_{q_j}(k) < T - \left(\hat{\mu}^E_{q_j}(k) + z_\gamma \hat{\sigma}^E_{q_j}(k)\right) \tag{4.10}$$

Since at this stage, any of the remaining paths may potentially be the most energy-efficient, the exploration budget is selected so that even in the worst case scenario the chance of completing the mission is still $1-\gamma$ using $Ex_m(k) = \max\{\min_{q_j}\{Ex_{q_j}(k) : \forall q_j \in Q\}, 0\}$. This is the smallest exploration budget found by calculating $Ex_{q_j}(k)$ for all paths in Q.

4.3.6 Exploration Budget Assignment

Suppose the vehicle is at a node from which alternative road segments emanate, i.e., an exploratory node. The objective of exploration budget assignment is to determine how many measurements to collect from each road segment emanating from an exploratory node. Let $q^{Ex}_{j,n}$ denote the set of road segments along path q_j that can be potentially explored when UGV is at node n. For instance, based on Figure 4.1b, $q^{Ex}_{1,1} = \{a, b, c, d\}$ and $q^{Ex}_{1,2} = \{c, d\}$.

Two competing criteria in the exploration budget assignment are: (a) the reduction in $\hat{\sigma}^E_i$ as a result of additional measurements, and (b) the energy consumed for collecting the measurements. Equation (4.6) provides a closed-form relation for posterior variance of C_i as a function of predictor $x(k)$. $\hat{\sigma}^E_i$ is expected to decrease with more measurements because $\hat{r}_i(k), [\hat{\sigma}^C_i(k|k-1)]^2, \hat{t}_i(k)$ are all generally expected to decrease with additional measurements. The variance updates depend on the input $x(t)$ (weighted drive cycle), which is not known *a priori*. However, we can still estimate the reduction of $\hat{\sigma}^E_i$ by simulating a drive cycle from a velocity model. In this study, we assumed that the velocity follows a normal distribution $u \sim \text{NID}(\mu_u, \sigma^2_u)$, but other models such as time series models can also be used. The expected reduction of $\hat{\sigma}^E_i$ at time k can then be estimated as (see Appendix A.5):

$$\begin{aligned}[\breve{\sigma}^E_i(\breve{k}_i)]^2 = W^2(d_i - \mu_u \breve{k}_i \Delta t)^2 \left([\hat{\sigma}^C_i(k|k-1)]^{-2} + \sigma_\epsilon^{-2} \breve{k}_i W^2 \left(\mu_u^2 + \sigma_u^2\right)\right)^{-1} \\ + \left(\frac{d_i}{\mu_u} - \breve{k}_i \Delta t\right) \sigma^2_\epsilon \Delta t + \phi_i (d_i - \mu_u \breve{k}_i \Delta t)\end{aligned} \tag{4.11}$$

where $[\breve{\sigma}^E_i(\breve{k}_i)]^2$ represents the simulated variance as a function of $\breve{k}_i$, which is the number of simulated velocity measurements from road segment i, and d_i is the length of road segment i. An estimate

for the expected cost of collecting $\breve{k}_i$ measurements from road segment i at time k is obtained by:

$$E_i^{Ex}(\breve{k}_i) = 2(\hat{\mu}_i^C(k|k-1)\mu_u W + \beta)\breve{k}_i \Delta t \tag{4.12}$$

The multiplier 2 in (4.12) is used because we assume exploration is a round trip operation, and the vehicle returns to the exploratory node after exploring a road segment. Figure 4.3 shows that $f(\breve{k}_i) = \breve{\sigma}_i^E(\breve{k}_i) + \xi E_i^{Ex}(\breve{k}_i)$ is a convex function for a typical road segment where $\xi \geq 0$ represents the relative importance of exploration cost with respect to variance reduction. To assign the exploration budget to $q_{j,n}^{Ex}$, we solve the following optimization problem for path q_j:

$$\min \sum_{i \in q_{j,n}^{Ex}} \breve{\sigma}_i^E(\breve{k}_i) + \xi E_i^{Ex}(\breve{k}_i) \tag{4.13}$$

$$\text{subject to: } \sum_{i \in q_{j,n}^{Ex}} E_i^{Ex}(\breve{k}_i) \leq Ex_m(k), \breve{k}_i \in \mathbb{Z}$$

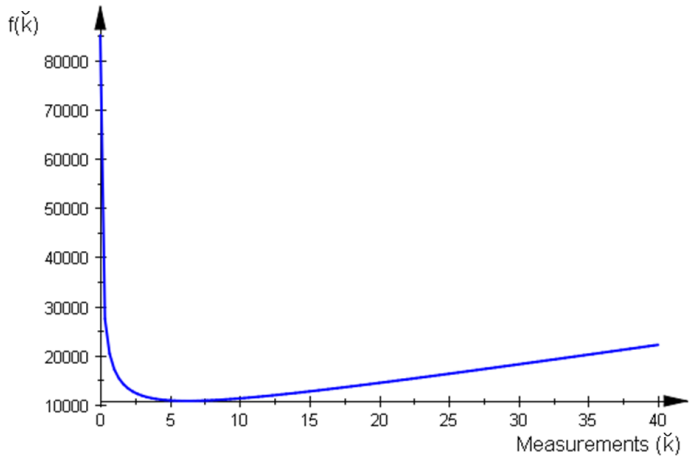

Figure 4.3: The convex structure of $f(\breve{k}) = E^{Ex}(\breve{k}) + \breve{\sigma}^E(\breve{k})$ for a road segment with the following parameters: $d = 4000m$, $\Delta t = 1sec$, $\sigma^C(0) = 0.043$, $\hat{\mu}^C(0) = 0.3$, $W = 400N$, $\sigma_\epsilon = 5$Watts, $\mu_u = 1.5m/s$, $\sigma_u = 0.3m/s$, $\beta = 28$Watts, $\phi = 4800$. The value of $\breve{k}$ corresponding to minimal $f(\breve{k})$ is the ideal number of exploring measurements from the road segment.

The decision variable in this optimization, $\breve{k}_i$, is the number of measurements to collect from road segment i during exploration. Carrying out the optimization for all paths that pass through node n, the output is the assignment of the exploration budget to the explorable road segments in the network. Although only the immediate road segments can be explored, future road segments are considered to assure sufficient energy is available for future exploration. The optimization is repeated

whenever the vehicle reaches an exploratory node. The mission completion and exploration times can also be incorporated in the optimization. The additional time for exploration is approximately $2\breve{k}_i\Delta t$ for road segment i, which can be added to expected completion time of a path if it contains road segment i. Consequently, another constraint can be included in the optimization. The right hand of the constraint reflects the paths completion times including the exploration times, and the left hand side is a scalar reflecting the desirable mission completion time. In the case studies that follows, we do not consider the above constraint (i.e., the mission completion time).

4.3.7 Exploitation

In the exploitation stage, using the collected information during the mission execution and exploration, the path with the highest z-score, i.e., $\arg\max_{q_j \in Q} z_{q_j}(k)$, is selected to be traversed or exploited. The z-score of all the remaining paths in Q can be calculated as follows:

$$z_{q_j}(k) = \frac{T - \hat{\mu}^E_{q_j}(k) - \sum_{i \in q^{Ex}_{j,n'}} 2\breve{k}_i(\hat{\mu}^C_i(k|k-1)\hat{x}(k) + \beta)}{\hat{\sigma}^E_{q_j}(k)} \tag{4.14}$$

where $\hat{x}(k)$ is the expected input using a weighted average of past input measurements, and n' is the next node to be visited along path q_j. Equation (4.14) considers the energy to traverse the path as well as an estimate of the cost of future exploration for road segments along this path, i.e., $\sum_{i \in q^{Ex}_{j,n'}} 2\breve{k}_i(\hat{\mu}^C_i(k|k-1)\hat{x}(k) + \beta)$.

It should be noted that although the mission duration is not directly considered in our case studies, electronics on board the vehicle consume power throughout the mission and their overall energy requirements are a function of mission duration. Therefore, energy predictions are affected by the mission duration. For instance, longer roads have higher energy requirements not only due to locomotion, but also due to longer time requirements.

4.4 Simulated Case Study

In this section, we compare our method with four other approaches for identifying an energy-efficient or reliable path in a network.

I. *Naive approach*: This approach does not consider any model for prediction and relies only on mission qualitative prior knowledge. It uses intuition for comparing the energy requirements of alternative paths. For instance, unpaved roads require more energy per unit distance traveled

compared to paved roads.

II. *Minimum expected energy without updating*: This approach assumes the distribution of energy requirement of road segments cannot be updated and are known *a priori*. Dijkstra's algorithm can be used to identify the optimal path (Denardo, 2003).

III. *Most reliable path without updating*: The goal is to find the path with maximum reliability using mission prior knowledge only (Seshadri and Inivasan, 2010).

IV. *Most energy-efficient path with exploitation only*: In this approach, the path with the highest z-score is exploited. The distribution of energy requirement of road segments are updated using real-time measurements, but exploration is not utilized. The vehicle cannot change its course once undertaking a path unless the path is pruned by real-time measurements. If this situation does not occur, the UGV continues its course until it reaches another node.

V. *Most energy-efficient path with exploration and exploitation (proposed method)*: In this approach, we implement the methodology introduced in the previous section

The prior distributions of road segments are obtained from experimental studies in Sadrpour et al. (2013a). For simulation, the power data is generated using the surrogate model introduced in Sadrpour et al. (2013b). The scaled aggressive EPA US06 driving cycle is used to represent the velocity profile of the UGV over each segment as shown in Figure 4.4. The rolling resistance coefficients are generated using the normal distribution to capture the variations within the segment. The actual grade profiles were extracted from Geocontext (2013).

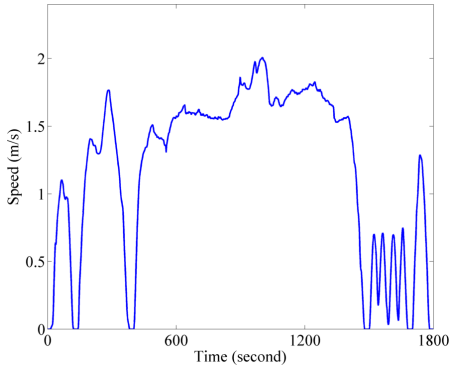

Figure 4.4: The EPA drive cycle was scaled both in time and speed magnitude in the simulation studies.

To validate the proposed approach, we demonstrate its application to a real-world scenario. In this scenario, the UGV traverses part of the University of Michigan's north campus shown in Figure

4.5a. The goal is to reach node 7 from node 1, using one of the 5 alternative paths listed in Figure 4.5a. The parameters of the study are listed in Table 4.1. Although, the road segments' grade profiles were extracted from a database, it is assumed that this exact information is not generally available to the UGV operator. Figure 4.5b shows the schematic of the mission network with road segments' qualitative prior information, i.e., roads' average grades and surface conditions, and the length of each road, which are shown with numbers along each road segment. Road segment d is a new shortcut that the operator is not familiar with. The operator knows that the segment is sidewalk-(steep) uphill, and expresses their lack of knowledge by assigning a larger road grade prior variance (i.e., 1.5 times larger than a typical road grade variance). Also, value of ξ shows if the operator is more interested in reducing the prediction uncertainty by exploration or is more concerned about the battery remaining energy. Assigning a weight of $\xi = 0.1$ indicates that we are more interested in the reduction of uncertainty. A justification is that finding the minimum energy path is likely to save more energy in the long run, outweighing the potential energy savings from shorter exploration.

Table 4.1: Parameters of the simulated case study.

m	40 kg	β	28 Watts	ξ	0.1
$C_{I'}$	$N(0.22,\ 0.003^2)$	σ_ϵ	7 Watts	Δt	1 second
z_α	2	T	85 KJ	γ	0.025
Examples of typical prior distributions of C					
Grass/flat	$N(0.319,\ 0.043^2)$		Asphalt/flat	$N(0.282,\ 0.044^2)$	
Sidewalk/flat	$N(0.276,\ 0.043^2)$		Grass/steep-uphill	$N(0.459,\ 0.058^2)$	
Asphalt/uphill	$N(0.352,\ 0.044^2)$		Sidewalk/uphill	$N(0.346,\ 0.043^2)$	

Figure 4.6a represents the initial distributions of energy requirements of paths based on the mission prior knowledge as well as the actual energy requirement of the paths along with the failure threshold. Using the naive approach, it is not clear which path should be selected since direct comparison of alternative paths is not conclusive. Using approaches II-III, path q_2 has both the highest reliability and the lowest expected energy requirement. However, clearly, this path is not actually the most energy-efficient. Using approach IV also, path q_2 is selected, and without exploration remains unpruned until the vehicle reaches the destination. Figure 4.6b depicts the updated energy requirement distribution of path q_2 using approach IV. While traversing road segments $\{e, f\}$ the predicted energy requirement generally has an increasing trend. The drop in the predicted energy at around observation 75 is because the initial part of road segment e is flat while the rest of it is steep-uphill and the operator states that the road is steep-uphill. The increase in the predicted en-

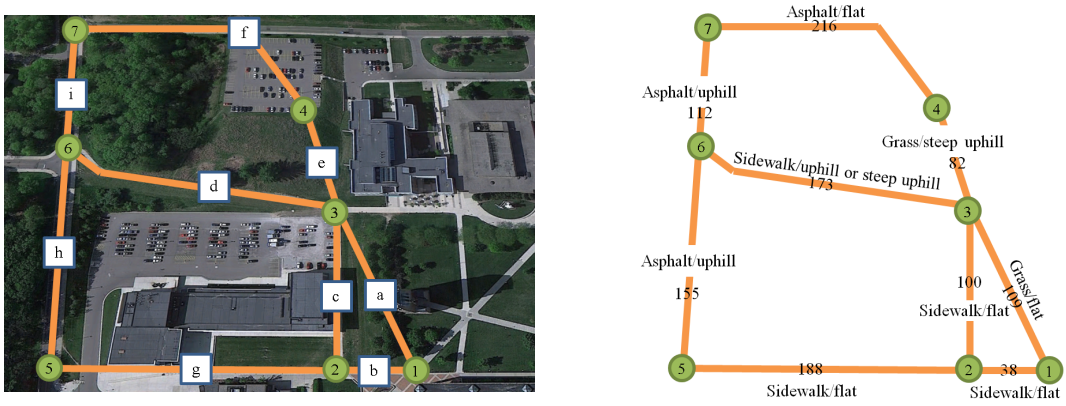

(a) (b)

Figure 4.5: (a) The simulated case study network of alternative paths from node 1 to node 7. Five altermative paths have been identified as follows: $Q = \{q_1 = \{b, c, d, i\}, q_2 = \{a, e, f\}, q_3 = \{b, c, e, f\}, q_4 = \{a, d, i\}, q_5 = \{b, g, h, i\}\}$. (b) The mission network schematic with prior information about each road segment surface condition. The number along each road represents the length of the road in meteres.

ergy at around observation 175 is due to slightly larger actual grade and rolling resistance compared to their prior distribution means.

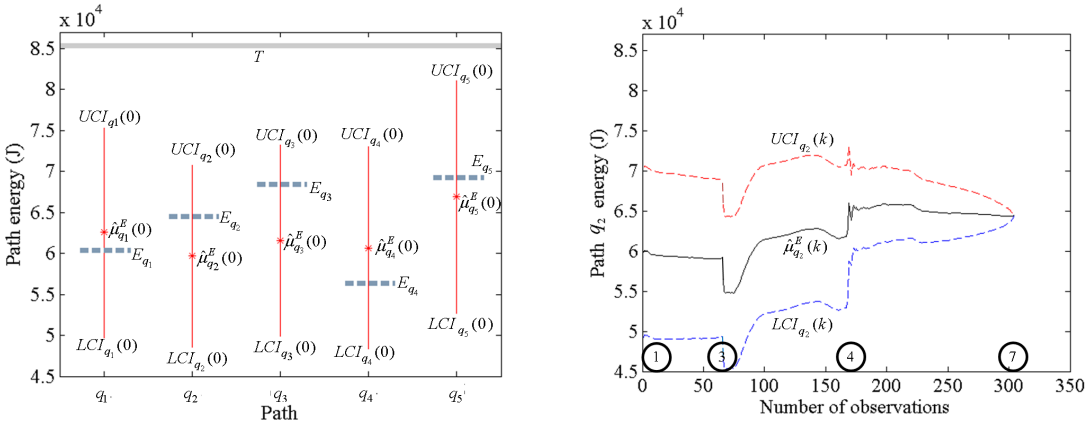

(a) (b)

Figure 4.6: (a) The initial energy requirement distribution of paths based on mission prior knowledge. The distributions are represented by their mean and confidence intervals. The actual energy requirement of each path, i.e., E_{q_i}, is shown with a dashed line, and the energy failure threshold, i.e., T, is shown with a solid line. (b) The energy requirement of path q_2 vs observations from this path using approach IV. The numbered circles correspond to the nodes in the network. This path cannot be pruned against the alternative paths and is traversed to reach to node 7.

Based on approach V if either paths $\{q_1, q_2, q_3, q_4\}$ are selected, the UGV will explore all four road segments along them. Thus, the budget assignment optimization needs to be solved at node 1 and 3 only. The number of measurements from $\{a, b\}$ are $[4, 2]$. The CPU time to perform the optimization was approximately 2 seconds using a quad-core Intel core i-7 processor. After exploring

road segments $\{a, b\}$, path q_2 still has the highest z-score. The UGV then exploits road segment a until it reaches node 3. The vehicle then explores the alternative road segments $\{e, d\}$ and collects $[3, 4]$ measurements from each, respectively. The z-score associated with each path after the second exploration is shown in Figure 4.7a. Clearly, from Figure 4.7a, path $q_4 = \{a, d, i\}$, which actually has the least energy requirements (see Figure 4.6a for actual energy requirements), should be selected. Figure 4.7b depicts the predicted energy requirement of path q_4. The change in the decision from path q_2 to path q_4 after exploration is due to a drop in the predicted energy requirement of road segment d, shown with a circle in Figure 4.7b, which initially perceived to have an average grade of 6 degrees compared to an actual average grade of around 3 degrees uphill.

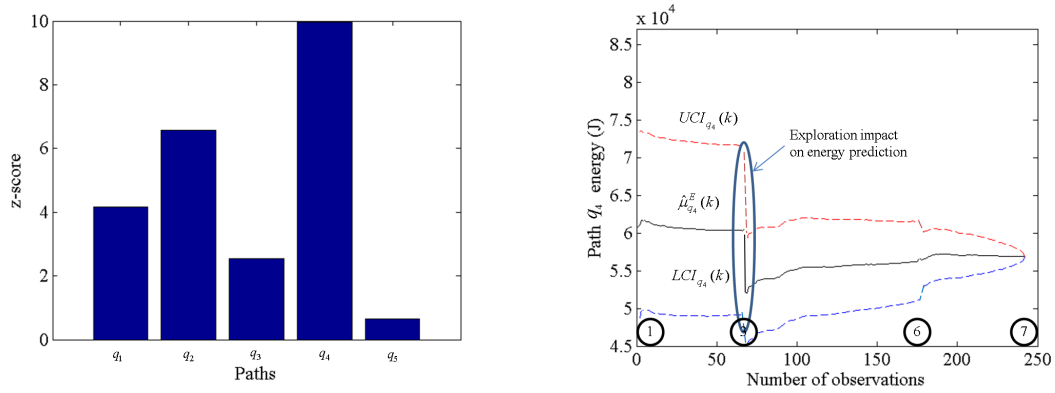

(a) (b)

Figure 4.7: (a) Updated z-score of each path after exploring road segments $\{e, d\}$. The exploration stage requires a total of 13 measurements. Path $q_4 = \{a, d, i\}$ has the highest z-score and is subsequently selected to be traversed. Note that for example, path q_5 can be clearly eliminated at this stage due to very low z-score (b) Path q_4 energy distribution updates using approach V.

This case study shows the effectiveness and flexibility of the proposed approach. Operators can express their lack of knowledge of road surface conditions with large prior variances. These road segments will be assigned larger exploration budgets when solving the budget allocation optimization problem. Also, we noticed that when generating alternative paths for different real-world scenarios, many alternative paths can be intuitively eliminated using the naive approach. Consequently, the number of alternative paths requiring exploration does not necessarily increase exponentially with the number of nodes and road segments.

A Appendix

For ease of notation, we drop the index i that indicates the road segment whenever possible in the Appendix.

A.1 Parameter Estimation for Random Slope

Let us denote $\mathfrak{C}'_\ell = C + \mathfrak{C}_\ell$ where $\mathfrak{C}_\ell \sim N(0, \sigma^2)$ and thus $\mathfrak{C}'_\ell \sim N(C, \sigma^2)$. The estimation involves finding the posterior distribution of $\mathfrak{C}'_\ell$, C, and σ^2. The joint distribution of the data and parameters is proportional to:

$$\begin{aligned}\pi(\{\mathfrak{C}'_\ell\}_\ell, C, &\sigma^2 | \{y_{i\ell}\}_{i\ell}, \{x_{i\ell}\}_{i\ell}, \sigma^2_\epsilon, \mu^C, \sigma^C, \varrho, \kappa) \\ &\propto \left(\prod_{\ell=1}^{L} \left(\prod_{i=1}^{n_\ell} \pi(y_{i\ell} | \mathfrak{C}'_\ell, x_{i\ell}) \right) \pi(\mathfrak{C}'_\ell | C, \sigma^2) \right) \pi(C | \mu^C, \sigma^C) \pi(\sigma^2 | \varrho, \kappa)\end{aligned} \tag{A-1}$$

Where $\pi(y_{i\ell}|\mathfrak{C}'_\ell, x_{i\ell}), \pi(\mathfrak{C}'_\ell|C, \sigma^2)$, and $\pi(C|\mu^C, \sigma^C)$ are normal distributions, and $\pi(\sigma^2|\varrho, \kappa)$ (i.e., the prior distribution of σ^2) is an inverse-gamma distribution, and $x_{i\ell}, y_{i\ell}$ are the measured input and output from sub-segment ℓ. Parameters ϱ, κ can be chosen so that the mean and variance of prior distribution matches an estimated value obtained through offline experiments.

Since the posterior distribution does not have a closed-form solution, we will use Gibbs sampling to draw samples from the full conditional distributions of parameters. Let us assume that data from $\ell = 1, \ldots, j'$ sub-segments within the road segment have been collected. The full conditional distribution of $\mathfrak{C}'_\ell$ and C are as as follows (Hoff, 2009):

$$\begin{aligned}&\pi(\mathfrak{C}'_\ell | \bullet) \\ &\quad \sim N((\sigma^{-2} + \sigma_\epsilon^{-2} \sum_{i=1}^{n_\ell} x_{i\ell}^2)^{-1} (\sigma^{-2} C + \sigma_\epsilon^{-2} \sum_{i=1}^{n_\ell} x_{i\ell} y_{i\ell}), (\sigma^{-2} + \sigma_\epsilon^{-2} \sum_{i=1}^{n_\ell} x_{i\ell}^2)^{-1})\end{aligned} \tag{A-2}$$

where $\bullet$ indicates that the distribution is conditioned on all the remaining parameters.

$$\begin{aligned}&\pi(C | \bullet) \\ &\quad \sim N((\sigma^{C^{-2}} + j'\sigma^{-2})^{-1} (\sigma^{C^{-2}} \mu^C + \sigma^{-2} \sum_{\ell=1}^{j'} \mathfrak{C}'_\ell), (\sigma^{C^{-2}} + j'\sigma^{-2})^{-1})\end{aligned} \tag{A-3}$$

And, the full conditional distribution of σ^2 is as follows:

$$\pi(\sigma^2 | \bullet) \sim \text{Inverse-Gamma}(\varrho + j'/2, , \kappa + \sum_{\ell=1}^{j'} (\mathfrak{C}'_\ell - C)^2/2) \tag{A-4}$$

The CPU time to perform the Gibbs sampling varied between 3-12 seconds using a quad-core

Intel core i-7 processor. The computation time depends on: (a) number of draws in the Gibbs sampling, (b) size of the sub-segments, and (c) size of the road.

A.2 Predictive Distribution of Output

Suppose the vehicle has collected k measurements from a road segment, and $\hat{x}(k+j|k), \forall j \geq 1$ is the expected input at time $k+j$, which is estimated by the weighted average of velocity measurements up to time k. The mean and variance of the j-step-ahead prediction of output are estimated as follows:

$$\begin{aligned} E[y(k+j|k, \{\mathfrak{C}_\ell\}_\ell = 0)] &= E\left[E[y(k+j|k, \hat{x}(k+j|k), C(k|k-1), \{\mathfrak{C}_\ell\}_\ell = 0)]\right] \\ &= \hat{\mu}^C(k|k-1)\hat{x}(k+j|k) \end{aligned} \tag{A-5}$$

We use the fixed effect model to estimate the expected energy requirement of a road segment in real-time. The variance of prediction for j step-ahead prediction of power, which is assumed to belong to sub-segment ℓ, at k is calculated as follows:

$$\begin{aligned} var(y(k+j|k)) = E\left[var(y(k+j|k, \hat{x}(k+j), C(k|k-1), \mathfrak{C}_\ell)\right] \\ + var\left(E[y(k+j|k, \hat{x}(k+j|k), C(k|k-1), \mathfrak{C}_\ell)]\right) \\ \approx \sigma_\epsilon^2 + ([\hat{\sigma}^C(k|k-1)]^2 + E[\sigma^2|k])\hat{x}^2(k+j|k) \end{aligned} \tag{A-6}$$

where $C(k|k-1)$ is estimated in real-time using the fixed effect model, and $E[\sigma^2|k]$ is posterior mean of σ^2, which is estimated less frequently using the mixed effect model. The covariance of prediction error of j and j' step-ahead predictions if both belong to the same sub-segment ℓ is calculated as follows:

$$\begin{aligned} &cov(y(k+j|k), y(k+j'|k)) = E[cov(y(k+j|k, \hat{x}(k+j), C(k|k-1), \mathfrak{C}_\ell), \\ &y(k+j'|k, \hat{x}(k+j'|k), C(k|k-1), \mathfrak{C}_\ell))] \\ &+ cov\left(E[y(k+j|k, \hat{x}(k+j|k), C(k|k-1), \mathfrak{C}_\ell)], \right. \\ &\left. E[y(k+j'|k, \hat{x}(k+i|k), C(k|k-1), \mathfrak{C}_\ell)]\right) \\ &\approx ([\hat{\sigma}^C(k|k-1)]^2 + E[\sigma^2|k])\hat{x}(k+j|k)\hat{x}(k+j'|k) \end{aligned} \tag{A-7}$$

if j and j' do not belong to the same sub-segment their covariance is estimated by

$$cov(y(k+j|k), y(k+j'|k)) = [\hat{\sigma}^C(k|k-1)]^2 \hat{x}(k+j|k)\hat{x}(k+j'|k) \tag{A-8}$$

Since at k, $\hat{x}(k+j) = \hat{x}(k+j')$ the last term in the equation above becomes $[\hat{\sigma}^C(k|k-1)\hat{x}(k+j|k)]^2$. In Sadrpour et al. (2012), we showed power consumption can be estimated by $P(k+j|k) \approx y(k+j|k) + \beta$. The term $\hat{E}^r(k)$ in (4.4) is estimated as follows:

$$\hat{E}^r(k) \approx \sum_{j=1}^{n} P(k+j|k)\Delta t \tag{A-9}$$

where n is the expected number of remaining measurements from the road segment and is estimated by $\hat{r}(k)/(\hat{u}(k)\Delta t)$ where $\hat{u}(k)$ is the weighted average of past velocity measurements. Let us assume the vehicle is at subsegment ℓ', and let r_ℓ denote the remaining distance from sub-segment ℓ. Using (A-5)-(A-8), the expected value and variance of $\hat{E}^r(k)$ are as follows:

$$\begin{aligned} E[\hat{E}^r(k)] &= (\hat{\mu}^C(k|k-1)\hat{x}(k+j) + \beta)(\hat{r}(k)/(\hat{u}(k)\Delta t))\Delta t \\ &= \hat{r}(k)W\hat{\mu}^C(k|k-1) + \hat{t}(k)\beta \end{aligned} \tag{A-10}$$

$$\begin{aligned} var(\hat{E}^r(k)) = var(\sum_{j=1}^{n} P(k+j|k))\Delta t^2 &= W^2\hat{r}^2(k)[\sigma^C(k|k-1)]^2 \\ &+ \hat{t}(k)\hat{\sigma}_\epsilon^2\Delta t + W^2E[\sigma^2|k]\sum_{\ell=\ell'}^{L} {r_\ell}^2 \end{aligned} \tag{A-11}$$

If we assume that each sub-segment has roughly an equal length r_c, we can simplify the term $W^2E[\sigma^2|k]\sum_{\ell=\ell'}^{L} {r_\ell}^2$ to $W^2E[\sigma^2|k]r_c\hat{r}(k)$ where $W^2E[\sigma^2|k]r_c$ is a constant denoted by ϕ.

Based on experiments using a large number of data from various road segments to estimate posterior distribution of σ^2 by Gibbs sampling through relations (A-1)-(A-4), we realized that 0.02 is a reasonable estimate for the expected value of σ^2 for a large majority of roads. Updating the posterior distribution of σ^2 frequently and without adequate data from a road segment, results in over estimation of the true expected value of σ^2 (inflates the prediction confidence interval). Consequently, we recommend starting with an initial value of 0.02 for all roads, and updating the posterior distribution of σ^2 only when measurements from at least 5-10 sub-segments are collected. It was also observed that with sufficient data, the estimated expected value of σ^2 does not change

significantly among updates. Thus, there is little advantage for estimating the posterior distribution of σ^2 frequently.

A.3 Posterior Updating Using Similarities

Consider the following distribution for combined parameters of two road segments, i, i', $\pi\left(C_i, C_{i'}\right) \sim N(\boldsymbol{\mu}, \Sigma)$. Using realizations from C_i , the distribution of $C_{i'}$ can be updated by the conditional distribution $\pi\left(C_{i'}|C_i\right)$. However, realizations of combined parameter $C_{i'}$ are not available. The only measurable quantities are the input and output of model (4.2). Let us assume k measurements are collected from road segment i denoted by obs_i. The distribution of $C_{i'}$ is updated as follows:

$$\pi\left(C_{i'}|obs_i\right) = \int \pi\left(C_{i'}|C_i\right) \pi\left(C_i|obs_i\right) dC_i \tag{A-12}$$

where $\pi\left(C_i|obs_i\right)$ is the posterior distribution of C_i. While this updating scheme can be applied to any multivariate normal distribution, in our case, we assume that two similar roads share the same combined parameter having a correlation of one. Thus, any realization of C_i from $\pi\left(C_i|obs_i\right)$ is a realization from $C_{i'}$, and based on (A-12), the combined parameter of both road segments can be simultaneously updated using measurements from one of them.

A.4 Covariance of Energy Requirement of Road Segments

Two road segments are similar if they share the same C. Let us assume k measurements have been collected from road segment i and the vehicle has not yet started to traverse similar road segment i'. Two predictions from road segments i and i' has a covariance of $[\hat{\sigma}^C(k|k-1)]^2\hat{x}(k+j|k)^2$. Thus, covariance of energy prediction can be calculated using the derivations from Section A.2 as follows:

$$\begin{aligned} &cov(\sum_{j=1}^{n_i-k} y(k+j|k)\Delta t, \sum_{j'=1}^{n_{i'}} y(j'|k)\Delta t) \\ &=(n_i-k)n_{i'}[\hat{\sigma}^C(k|k-1)]^2\hat{x}(k+j|k)^2\Delta t^2 = W^2\hat{r}_i(k)\hat{r}_{i'}(k)[\hat{\sigma}^C(k|k-1)]^2 \end{aligned} \tag{A-13}$$

where $n_i, n_{i'}$ are the number of measurements from road segments i and i'.

A.5 Estimating the Reduction in Uncertainty

For estimating the reduction of energy prediction variance, we use the prediction variance relation in (4.7). We assume based on prior knowledge of driving style, the velocity follows a normal distribution $u \sim \text{NID}(\mu_u, \sigma_u^2)$. The posterior distribution of C after k measurements is estimated by $[\hat{\sigma}^C(k)]^2 = ([\hat{\sigma}^C(0)]^{-2} + \sigma_\epsilon^{-2} \sum_{i=1}^{k} x^2(i))^{-1}$. The expected value of $E[\sum_{i=1}^{k} x^2(i)] = kW^2({\mu_u}^2 + \sigma_u^2)$. The two other parameters of (4.7) $\hat{r}(k)$ and $\hat{t}(k)$ are estimated by $(d - \mu_u k\Delta t)$ and $(d/\mu_u - k\Delta t)$, respectively. Replacing these estimates in (4.7), we obtain (4.11).

CHAPTER V

The Role of Operator Style on Mission Energy Requirements for Tele-Operated Unmanned Ground Vehicles

5.1 Introduction

One of the key factors that limit the utility of small tele-operated battery-powered Unmanned Ground Vehicles (UGVs) is the available on-board energy. Typical mission duration is currently on the order of 1-2 hours, while it is often desirable to carry out much longer missions (e.g., 8-10 hours) between lengthy recharging stops. The energy consumption is affected by several factors such as (Sadrpour et al., 2012, 2013a,b,d): (1) road surface condition, (2) driving style, (3) the on-board electronic equipment, and (4) vehicle internal resistance. Since most UGVs are tele-operated, this chapter focuses on the impact of remote operating style on energy requirements in a typical patrol mission for a small UGV.

The impact of driving style on emissions and fuel consumption has been extensively studied for conventional vehicles. Holmen and Niemeier (1998) showed that duration and intensity of acceleration events impact the emission levels significantly in a study with 24 drivers. An on board gas analyzer to monitor emissions was used in DiGenova et al. (1994) and despite using only two drivers, concluded that driver behavior can alter average per-mile emissions significantly. Evidence that aggressive driving increases emissions and fuel consumption, but without detailed statistical analyses, was presented in Vojtíšek et al. (2009, 2008). In Van Mierlo et al. (2004) and Reichart et al. (1998), the effect of driving style on emissions and fuel consumption was shown to result in 5%-40% difference in fuel consumption. Also, actual drive cycles were compared with the ideal and smoothed reference velocities in Manzoni et al. (2010). They showed an increase of about 275% and 20% in energy requirements with respect to each reference velocity when actual drive cycles were utilized. Syed et al. (2009) proposed an adaptive real-time advisory system for hybrid vehicles as

guidance for selecting the optimal driving strategy and reported 21%-28% in fuel reduction.

An intelligent energy management agent was introduced in Langari and Won (2005) that used statistical features of a drive cycle to determine driving style and improve fuel consumption by identifying critical driving features. Also, Ericsson (2000) used regression analysis to show that the driving pattern characteristics significantly affect the fuel consumption of conventional vehicles. Vlieger et al. (2000) categorized driving styles based on their average acceleration ranges and concluded that fuel consumption rose by 7%-40% for aggressive drivers. Also, Automobile Association (2012), Barkenbus (2010), and Gos (2011) showed 10-33% reduction in fuel consumption when an eco-driving style was employed. However, due to the small size of UGVs and tele-operation, those results are not directly valid for UGVs.

Several studies investigate factors that contribute to the energy consumption for conventional vehicles. For instance, Van Mierlo et al. (2004) indicated a fluent driving style with low engine speed, and eco-drive (2010) showed changing gears and smooth driving, increase energy efficiency, while Berry (2010) pointed that harsh acceleration and high velocity reduces efficiency. Some of these factors are not directly applicable to UGVs, and the UGV's light weight, and low velocity range result in a smaller contribution of acceleration in overall power consumption.

There has been little work on the impact of driving style on electric vehicles (EVs) (Knowles et al., 2012). Compared to conventional vehicles, EVs have a smaller range of around 145 kilometers, and in the case of small UGVs the range shrinks to only a few kilometers. The dependency between EV range and driving style was studied in Knowles et al. (2012) using 11 drivers with different road types. The result showed a significant change in the operating range among drivers. Walsh et al. (2010) investigated energy consumption in EVs showing large variations on tracks with high opportunities for regenerative braking. They also showed that driver training can result in an average of 87% more energy regeneration on certain road conditions. However, the results cannot be extended to UGVs because regenerative braking is not currently available for most UGVs.

Despite the abundance of literature on conventional vehicles, the impact of remote operating style and skill on UGVs has not been addressed. There are several aspects that distinguish operations with UGVs from conventional, electric, and hybrid vehicles: (1) tele-operation induces delays beyond what is normally observed while driving other types of vehicles. The additional time delay can be attributed to wireless communication or data processing for video streaming; (2) in conventional vehicles the operator receives direct and immediate feedback and cues (visual, haptic and auditory) when turning the wheels, accelerating, or braking. In tele-operated vehicles, the operator may have to rely only on video feedback, which provides limited situation awareness, and may suffer from

a time delay. Therefore, both the quality and quantity of feedback is affected by tele-operation and the operator style and skills; (3) in conventional vehicles, locomotion accounts for the largest percentage of energy consumption. However, due to the smaller size of UGVs, electronic equipment contributes significantly to overall power consumption, which affects the optimal driving style; (4) unlike electric or hybrid vehicles, most UGVs do not have power regenerating capabilities and the operator style has a different impact on energy consumption; (5) UGVs are frequently operated off-road in hazardous and unfamiliar conditions (e.g., nuclear disposal or in battlefields). The intensity of missions and lack of situation awareness make operations more prone to maneuvering mistakes that increase energy requirements, (6) UGVs are used in a very diverse operating conditions with drastically different energy requirements. While this is beyond the scope of this chapter, the vehicle model used here can incorporate a wide range of operating conditions (Sadrpour et al., 2013d).

This study aims to provide a better understanding of the impact of tele-operation on energy consumption of a small UGV. We use a model that incorporates factors such as communication and human delays, random variations in steering, stop-and-go operations and operator aggressiveness. The objectives are (1) to develop an energy optimal drive cycle based on the vehicle model, and study the impact of velocity deviations from the optimal drive cycle, and (2) to determine which factors and their interactions increase the energy consumption significantly.

General recommendations are provided to reduce energy consumption by up to around 100% for operators with different experience levels. This study is carried out through simulation using design of experiments techniques where the effect of driver characteristics on the energy is investigated by using a response surface design. The rest of this chapter is organized as follows. Section 5.2 discusses the simulation framework, and Section 5.3 elaborates on the response surface setup. In Section 5.4, simulation results are presented, and Section 5.5 is devoted to recommendations for improving energy efficiency.

5.2 Simulation Model

5.2.1 Optimal Velocity

The velocity profile that minimizes the energy requirement for traveling a predefined distance on a known straight path is derived here. The assumption is that the optimal solution is symmetric and has a trapezoidal shape (see Manzoni et al. (2010)). As shown in Figure 5.1a, the optimal drive cycle is characterized by two parameters: acceleration, i.e., a^*, and acceleration time, i.e., t_a. The objective is to minimize energy represented by (Sadrpour et al., 2013d): $E = \int_0^{t_m} (M|a(t)|u(t)+CWu(t)+b)dt$,

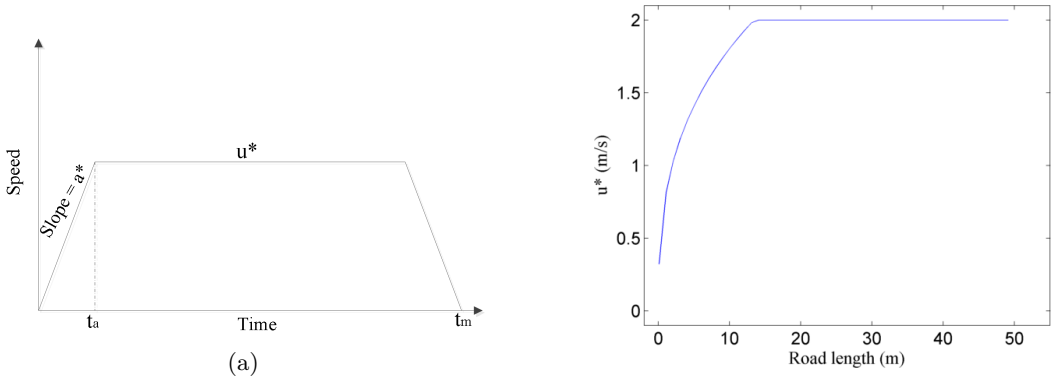

Figure 5.1: Optimal velocity characterization. (a) The general structure of optimal velocity vs time. (b) Maximum velocity according to the optimal drive cycle as a function of road length.

where t_m is the mission completion time, M is vehicle mass, $a(t)$ is the acceleration, $u(t)$ is the velocity profile, C is a parameter that combines the effect of road grade, rolling resistance, and vehicle internal resistance, W is the vehicle weight, and b is the power consumption of electronic equipment on-board the vehicle. The vehicle maximum velocity and acceleration are assumed to be $u_{max} = 2\ m/s$ and $a_{max} = 2\ m/s^2$, respectively for a PackBot platform. Figure 5.1b shows u^*, i.e., the optimal drive cycle maximum velocity, as a function of the road length. For extremely short roads, the vehicle does not accelerate to u_{max}. That is because acceleration and deceleration segments (the beginning and ending segments of Figure 5.1a) have a significant effect on overall mission energy. For road segments that are longer than 15 meters, the optimal velocity and acceleration are u_{max} and a_{max}. Thus, the vehicle accelerates at a_{max} and reaches the velocity u_{max}. It should be noted that these results hold for the specified maximum velocity and acceleration and the PackBot platform while traversing a straight path based on the vehicle model in Sadrpour et al. (2013d). The proposed drive cycle may not be optimal in the presence of sharp turns, or in vehicles with larger masses. For instance, a larger mass increases the influence of acceleration term shifting the kink in Figure 5.1b to the right. Moreover, maximum velocity may not always be attainable in practice due to concerns such as battery overheating or increased probability of other failure modes such as suspension system failures.

Note that the term $\int_0^{t_m} CWu(t)dt$ in the energy equation, is a constant equal to CWd, where d is the road length. For a longer mission duration the term associated with electronics, i.e., $\int_0^{t_m} bdt = bt_m$, dominates the acceleration term $\int_0^{t_m}(m|a(t)|u(t))dt$. Thus, to minimize mission duration, t_m, the vehicle has to move at its maximum velocity.

5.2.2 Vehicle Longitudinal/Lateral Model

We consider a tracked differential-drive vehicle operation on a known terrain. The states of the robot are its x and y position in vehicle-fixed coordinates, with θ heading, u forward velocity, and ω angular velocity. Therefore, the system dynamics can be defined as (Broderick et al., 2012):

$$\begin{bmatrix} \dot{x} \\ \dot{y} \\ \dot{u} \\ \dot{\theta} \\ \dot{\omega} \end{bmatrix} = \begin{pmatrix} u\cos\theta \\ u\sin\theta \\ \frac{f_r+f_l}{M} - \frac{CW}{M} \\ \omega \\ \frac{B(f_r-f_l)}{I_z} - \frac{b_r\omega}{I_z} \end{pmatrix} \tag{5.1}$$

where B is the length from the tracks/wheels to the center of the vehicle, f_r and f_l are the forces exerted by the right and left tracks/wheels, I_z is the moment of inertia, and b_r is the turning friction coefficient. In general, the lateral and longitudinal dynamics are coupled as a result of non-zero products of inertia, but here, we assume the vehicle is symmetric in all planes resulting in the decoupled model (5.1). The value of I_z was estimated from actual dimensions and weight of an iRobot PackBot (iRobot 510 Packbot Specifications). In the longitudinal dynamics, we found experimentally that a constant (i.e., coulomb) friction model is sufficient (Sadrpour et al., 2013a). This is due to low longitudinal velocity of UGVs. The viscous (i.e., linear in u) and aerodynamic (i.e., quadratic in u) effects will occur at higher velocities. In the turning dynamics, the wheel rotation speeds are large enough for viscous friction (i.e., linear in ω) to be the appropriate model. According to experiments conducted in Guo and Peng (2013), the torque required for turning increases with turning velocity (ω), and the value of b_r was estimated from their experiments.

5.2.3 Simulink Model

The simulation model is illustrated in Figure 5.2. The reference velocity and current state of the robot are the inputs to the operator advisory module. The proposed stable tracking control rule for mobile robots in Kanayama et al. (1990) is used in this module. The controller can turn the inputs from the optimal trajectory to the desired forward and angular velocities (outputs) that are easier for an operator to interpret compared to UGV states.

The difference between actual velocity and the desired velocity is the input to the operator and the basis for acceleration or braking, and steering. The operator model accounts for the delays

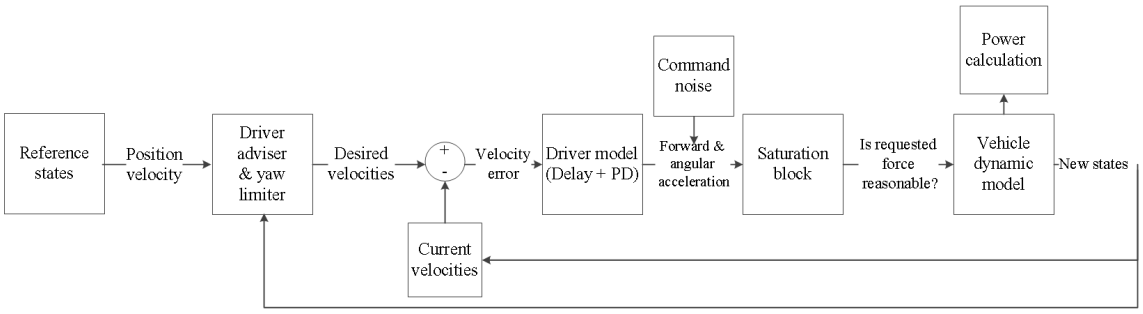

Figure 5.2: The simulation model of the operator and vehicle.

associated with human neuromuscular and cognitive efforts, and uses a PD controller to represent the operator's aggressiveness and style. We also add two sources of variations to represent distractions, mistakes, and lapses by the operator, variations at the vehicle level, and/or equipment inefficiencies. The first variation (i.e., stop-and-go) is in the longitudinal velocity and is simplified and represented by frequent-equal-distance velocity drops in the reference velocity. The second variation is in the lateral direction and is created by frequent angular acceleration inputs (See Section 5.3 for more information).

If the acceleration requested by the operator can be met, the vehicle state is calculated using the vehicle dynamic model. The total power is the summation of power needed to propel the vehicle forward, i.e., $P_{lo} = M|a||u| + CW|u| + b$ and to turn it, i.e., $P_{la} = I_z|\dot{\omega}||\omega| + b_r\omega^2$.

5.3 Response Surface Design

Response surface methodology is a general statistical modeling technique for modeling and analysis of problems, in which a response of interest is influenced by several factors and the objective is to study and optimize the impact of factors and their interactions on the response (Montgomery, 2004).

The model estimation is done by collecting the responses at different configurations of factors. We can design such simulation experiments with suitable statistical properties (e.g., orthogonal designs) to achieve the minimum number of trials using design of experiments techniques. One such a design is the Box-Behnken design from which a second order model can be fitted including the main effects, interactions and the quadratic terms. The Box-Behnken design requires defining a reasonable range for factors under study, but does not require experiments at extreme factor configurations (Montgomery, 2004). Each factor is varied at three levels: low, medium and high. Next, we specifically define the factors and their levels.

Some of the parameters are kept fixed in the simulation while others (i.e., factors) are varied and their effects on the response is captured. Parameters that are not varied are the operator adviser module parameters, I_z, C, b_r, d, M, derivative controller gain, and communication delay. Communication delay can be defined as the time delay between the user's input and its displayed response (Davis et al., 2010). Typical reported lags are between 0.2-1.0 seconds from Army test beds (Davis et al., 2010), and we use a fixed delay of 0.3 seconds.

The factors that are varied are: (A) the frequency and intensity of stop-and-go operations, (B) human operator delay, (C) variance of the lateral noise, (D) duration of the lateral noise, and (E) proportional controller gain. The justification for the choice of levels of each factor is presented next.

A) Stop-and-go: It is expected that some operators accelerate and decelerate often even when the reference velocity is constant. Such stop-and-go operations are common in conventional vehicles where the reference velocity is the road speed limit. The sources of variation can be lack of experience, distractions, communication lags, unstable video streaming, loss of peripheral vision (Kelly et al., 2013), poor joystick calibration or resolution, terrain (i.e., rough or bumpy terrain) and the disturbances at the vehicle level. To simulate such variations, recurring stop-and-go (reducing velocity to a full stop and accelerating to the original velocity) is incorporated in the reference velocity. The frequency of velocity drops ranges from no velocity drops to about one drop every 20 seconds.

B) Human Operator Delay: It reflects the time duration for making a decision and sending out a command. The human operator delay includes neuromuscular and cognitive efforts and exacerbating elements such as distractions, high workload or poor situation awareness. The reaction time of drivers of various ages in the presence or absence of distractions in a stopping maneuver ranged from 0.5-0.9 seconds (Hancock et al., 2003). Moreover, the reaction time tends to increase in older drivers (RAC, 2010; Daigneault et al., 2002). The human time delay in responding to visual stimuli is typically around 150-200 milliseconds (Pick and Cole, 2003). In this chapter, we use a fixed time delay, i.e., the delay does not change during a simulation run, but varies with a range of 0.3-1.0 seconds for different runs.

C-D) Lateral Velocity Variations: Steering in a manned mission, requires overcoming mechanical tolerances and frictional forces in the steering system which creates a feedback for the operator that improves vehicle drivability and control (U.S. Army, 2010). Such feedback is not present during tele-operation by joystick. The operator receives feedback from his command only through the video interface which has inherent delays. The steering inputs for the unmanned operations were not smooth or continuous based on several driving trials using manned and unmanned vehicles in U.S. Army (2010). While in manned missions small angular corrections were observed, less frequent,

but very large steering inputs were necessary to keep the unmanned vehicle on the same path. To capture such steering variability, random noise is added to the driver output periodically. The magnitude of the noise is generated from a uniform distribution whose support ranges from almost zero to $\pm$ 0.4 rad/sec^2 (about 20% of the assumed maximum angular acceleration of the vehicle). The duration of each disturbance ranges from 1 to 5 seconds.

E) Proportional Controller Gain: The controller gain reflects the aggressiveness of the operator response to magnitude of deviation of the vehicle velocity from the desired velocity. The range of values for the gain were obtained by running the simulation at extreme factor configurations and assuring driving stability in the worst case scenarios. We also made sure that the lateral deviations of the vehicle from the reference path is less than $\pm$4 meters in each direction. Table 5.1 summarizes the factors and their ranges.

Table 5.1: Factors and their levels in the simulation study.

i	Factor name	Level	
		low	high
A	Stop-and-go	Absent	Every 20 seconds
B	Human Delay	0.3 Second	1 Second
C	Lateral noise range	No noise	± 0.4 rad/sec^2
D	Lateral noise duration	1 Second	5 Seconds
E	Proportional gain	0.75	1.5

5.4 Simulation Results

MATLAB/Simulink was used for simulation to obtain the energy requirements for completing the mission. The robot is planned to drive on a straight path for 1800 meters.

5.4.1 Model Selection

Based on the Box-Behnken design, the simulation was run n times under the given levels of the factors. The following model was then estimated:

$$E_{tot} = \beta_0 + \sum_i \beta_i x_i + \sum_i \beta_{ii} x_i^2 + \sum_{i<j} \sum \beta_{ij} x_i x_j + \epsilon \tag{5.2}$$

where E_{tot} is the total energy consumed in a particular simulation run. The β's are the parameters that are estimated; β_i is the main effect, β_{ii} is the quadratic coefficient, and β_{ij} is the interaction coefficient. The x_i represents the level of factor i. Commonly, x_i's are coded, taking on the value

of (+1) when the factor is at its highest level, and (−1) when it is at its lowest level. This allows comparison across factors regardless of their natural scales (Montgomery, 2004).

5.4.2 Simulation Results

Scenario 1: the baseline scenario corresponds to the optimal drive cycle in the absence of delay or velocity variations, and E_{tot} was estimated to be 115300 Joules. The optimal drive cycle is given in Figure 5.1a, with $a^* = 2\ m/s^2$, $u^* = 2\ m/s$, and $t_m = 900$ seconds.

Scenario 2: the operator attempts to follow the optimal drive cycle (i.e., maintain $u^* = 2\ m/s$), but their behavior is affected by the 5 factors described in the previous section. For instance, the velocity may drop due to the stop-and-go factor temporarily, but the operator speeds up to 2 m/s quickly. The simulation was run by varying the levels of the 5 factors in each trial with 10 center points (i.e., all factors at (0) level), and 23 replications of all combinations, resulting in a total of 1150 runs.

Analyzing the response surface design, the significant main affects and interactions are shown in Table 5.2. The presented model, with the coefficient of determination of 99.4%, is not a full second order model. This lower order model is not statistically different from the full second order model using an $F-$test. Also, we noticed a maximum of 6.5% increase in energy consumption compared to the baseline scenario when all five factors were at or near their highest levels. This percentage increases when a wider range for factors such as C and D is used in the simulation.

All the main effects are statistically significant, but for the purpose of interpretation, their interactions with other factors should also be considered. The following general results can be stated: (1) the stop-and-go factor has the most significant impact on energy consumption dominating the other factors. This is evident from the magnitude of factor A main effect, which overshadows the negative quadratic effect, i.e., A^2, in Table 5.2, (2) the lateral noise variance and its duration compound each other's impact. That is, if the duration of deviations is large, an increase in the magnitude of the noise has a larger impact on the energy consumption. This is due to the positive interaction between the two factors. To see this, we fix the level of C at (+1) and vary D, which results in a large increase in power consumption. We can repeat the same process when the level of C is fixed at (−1) and vary D, which results in a small change in energy consumption, (3) when the lateral deviation is large while delay and stop-and-go are negligible, the impact of proportional controller gain increases (larger is better). This is due to the positive interaction of the gain with the stop-and-go and delay factors, i.e., AE, BE, and its negative interaction with the lateral noise range and duration, i.e., CE, DE, (4) if the lateral noise is small, the proportional controller gain

impact diminishes. This is because without such lateral variations, the deviations from the reference path are small, (5) the human delay becomes more detrimental when there are many stop-and-go operations. This is due to the positive main and second order effects of the delay in addition to its positive interaction with the stop-and-go factor, (6) when delay and stop-and-go operations are at their high levels, lower gain is beneficial due to positive interactions of gain with delay and stop-and-go. In this configuration, aggressiveness can lead to sharper acceleration and deceleration and also vehicle oscillation.

Table 5.2: Significant factors and their coefficients. Factors are represented by letters, e.g., factor A represents stop-and-go, and AC is the interaction of factors A and C.

Factor	Coefficient	Factor	Coefficient	Factor	Coefficient
A	1845.18	B	170.175	C	290.150
D	384.850	E	186.750	A^2	-1122.49
B^2	118.575	C^2	-215.192	D^2	94.0750
E^2	91.3417	AB	134.300	AE	202.700
BD	-27.3000	BE	238.300	CD	238.400
CE	-63.8000	DE	-71.8000		

Scenario 3: the operator does not know the optimal drive cycle and follows a reference velocity slower than the optimal velocity (i.e., $u^* = 2\ m/s$) ranging from $0.5 - 1.5\ m/s$. To do this, velocity, u, was added as an additional factor at three levels of $0.5, 1.0, 1.5\ m/s$. The tele-operation is still influenced by the 5 factors studied in the second scenario. However, since driving velocity has a dominating effect, which overshadows the initial 5 factors, its effect is studied separately. The objective is to determine whether informing the operator of the optimal velocity significantly affects the mission energy requirements. The average energy requirements across all velocity levels are shown in Figure 5.3. At the lowest velocity level, the energy requirement is approximately twice as large as the optimal ($u^* = 2\ m/s$) level, and the difference decreases as the velocity increases. Consequently, driving at a lower velocity, u, has a significant detrimental impact on the mission energy requirement.

The additional energy requirement among simulation runs can be attributed to four sources. These sources, in order of their magnitudes, can be summarized as follows. (1) Longer mission duration: for every second of additional time spent on the mission, the electronics consume approximately 30 Joules of energy. Any combination of lower reference velocity, u, stop-and-go, or deviation from the main path can increase the mission duration, (2) acceleration effect: fluctuations in velocity levels (acceleration events) require additional energy, (3) larger distance traveled: deviation from the straight line trajectory increases the overall distance that the vehicle travels to reach the destination.

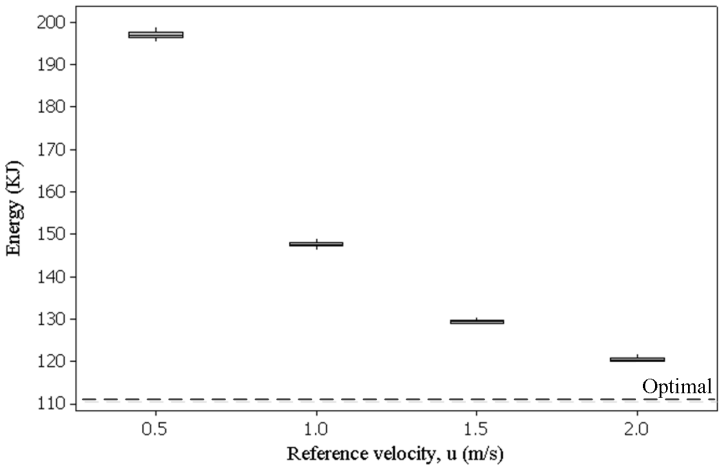

Figure 5.3: Operating at lower reference velocity, u, increases energy requirement significantly. The optimal energy consumption based on Scenario 1 is shown with a dashed line.

Assuming constant velocity and ignoring electronics, for each additional meters traveled, the vehicle consumes CW Joules of energy, where typical values are $C = 0.25 - 0.30$, $W = 200 - 400\ N$, and $CW = 50 - 120$ Joules, (4) lateral deviations: steering the vehicle demands additional energy that increases with the angular velocity of the vehicle.

5.5 Recommendations for Reduction of Mission Energy Requirements

Each configuration of the factors reflects an operator skill or style, and the factors that impact energy requirements for that style can be determined by response surface analyses. The levels of a factor can be altered by training the operator or by improving the user interface. This section addresses improvements that are applicable to most operators.

velocity variations and operation at low velocity can increase energy demand significantly regardless of the value of all other factors. Thus, it is recommended that the operators become aware of the optimal velocity by incorporating visual velocity cues in the interface. In the case of lateral velocity variations, if the variations are due to poor video feedback or latency, the operator can control the vehicle by designating way-points and having the vehicle autonomously drive to each one sequentially without stopping. If the variations are due to equipment, higher resolution equipment and better calibration is beneficial.

In the presence of stop-and-go and delay, the operator should not react aggressively to velocity error to reduce acceleration and deceleration intensity and prevent vehicle from spinning out of control. The operator can adapt their driving style when such situations arise. Also, increasing the frequency and magnitude of lateral deviations increases the energy consumption. Improving

Table 5.3: Summary of recommendations for improving mission energy requirements.

Factor	Training/aid to improve
Nonoptimal velocity	Inform the operator of optimal velocity
	Automated driving via waypoints
	Video stabilization and control aid
	Improve device resolution or calibration
High lateral deviations and delay	Less aggressive steering
	Automated driving via waypoints
High lateral deviations	Video stabilization and control aid
	Map view of the robot's position and trajectory

the user interface (video stabilization) and providing control aids (path following and prediction) reduces the lateral deviation magnitude and frequency, and reduces the mission completion time, i.e., t_m, according to experimental results in Kelly et al. (2013). That paper also shows that the effect of latency can be reduced by adding predictive control and path prediction. Although Kelly et al. (2013) considered driver performance, they did not consider energy consumption as a criteria for evaluating or designing their assistive features.

Table 5.4: Recommendations for improving mission energy requirements based on the type of control.

Improvement through automation	Additional feedback and training to operator
Automated driving via waypoints	Inform the operator of optimal velocity
Automated velocity control	Map view of the robot's position and trajectory
	Video stabilization and control aid
	Improve device resolution or calibration
	Less aggressive steering

Most tele-operated robots offer the operator a view from an on board camera. These video pictures do not allow the operator to establish the orientation or whereabouts of the robot in its environment. Some Operator Control Units offer a second window, in which the trajectory of the robot is plotted in outdoor environments using the Global Positioning System (Borenstein et al., 2010). Also, new approaches for accurate indoor position tracking using dead-reckoning techniques are proposed in the literature (Borenstein et al., 2010). These additional video feedback capabilities can help the operator detect and reduce deviations from the nominal path. A summary of recommendations is provided in Table 5.3.

Table 5.3 suggests that supervisory control can improve energy efficiency. The human delay can be reduced during the automated driving interval with an increased level of autonomy. The optimal velocity can be automatically prescribed to the vehicle to reduce stop-and-go operations. Automated driving via waypoints is also another instance of increased autonomy where supervisory commands

can be provided by the operator. As a result, Table 5.3 can be reconstructed using two categories that involve human operator and automation as shown in Table 5.4.

CHAPTER VI

Concluding Remarks

6.1 Summary of Major Work and Results

This dissertation has focused on developing some elements of a unified methodology for improving the mission reliability of UGVs throughout the following deployment phases: (a) prior to field deployment: remove design deficiencies by acceptance testing, and (b) during field usage: prevent unexpected energy depletion failures during mission execution, and increase energy availability through driver training. A new framework for simulation-based acceptance testing as a complement to physical acceptance testing is proposed. Then, the problem of real-time mission energy prediction in the presence of operational uncertainty was studied. Furthermore, the problem of identifying the most energy reliable path in a network of alternative paths with unknown random mission energy requirements is addressed through a two-stage exploration-exploitation strategy. In the last part of the dissertation, the role of operator style on mission energy requirement was investigated. The main research results of this dissertation are summarized as follows.

(1) *A new simulation-based acceptance testing approach for UGVs.* A simulation-based acceptance testing methodology is introduced that can be used as a complement to physical testing under a number of typical operational failures, which includes joint torque saturation, rollover, flip over, and suspension system breakdown. To capture operational variations and environmental uncertainties, a statistical hypothesis test is proposed to quantitatively test whether the difference between dynamic simulations and static simulations significantly affect the decision of UGV operational states. The results of statistical hypothesis testing show that in the analysis of joint torque saturation and rollover failures, which occur at slow operational speeds, the decisions on the failure states are consistent between the static and dynamic simulations. Therefore, static simulations can be used

as a good approximation of dynamic simulations in these situations. In contrast, in the case of analyzing flip over and suspension failures, dynamic simulations cannot be well approximated by static simulations. Moreover, it is further shown how to develop the boundaries of safe operation based on the simulation results. These results can help provide a guideline in the design of efficient physical testing scenarios, which not only help avoid some unnecessary tests, but can also avoid some scenarios leading to severe damage to UGVs during physical tests.

(2) *A new approach for real-time energy prediction of UGVs using mission prior knowledge and real-time measurements.* A general framework for prediction of end-of-mission energy is presented that will help prevent UGV mission failures due to unexpected battery depletion. Two prediction approaches, based on the availability of mission prior knowledge, were compared. The first approach, based on RLS estimation, only uses online power and velocity measurements for energy prediction. The second approach, based on Bayesian estimation, takes advantage of available mission prior knowledge about road conditions, in addition to real-time measurements, for improving energy predictions. Our comparative experimental and simulation results show that the Bayesian approach can yield more accurate predictions compared to the RLS approach even in the case of moderately imprecise mission prior knowledge. Also, the imprecise mission prior knowledge can be improved from similar road segments in a mission by using in-advance updating strategies before actual measurements become available from the later road segments.

(3) *A new dynamic energy-reliable path planning using two-stage decision-making: exploration and exploitation.* A dynamic energy-reliable path planning approach is proposed to determine the most reliable path for a UGV to traverse for a mission without depleting the on-board energy. Mission prior knowledge and real-time sensory information, such as vehicle instantaneous power consumption and velocity, are used to update the distribution of alternative paths' energy requirements by using two decision making stages. The first is an exploration stage, where prior information may not be sufficiently precise, and an energy expenditure budget is created to reduce the prediction uncertainty of the energy requirement of these paths; at the same time, through a process called pruning, alternative paths are removed from consideration when the lower bound of their energy requirements are higher than the upper bound of a different path. The second stage, i.e., the exploitation stage, involves the UGV traversing the selected most energy-reliable path based on the results of the first stage. Our simulation results outperformed four other methods, which included (1) a naive approach without online updating, (2) an approach based on the initial predicted minimum expected energy,

(3) a method based on the initial maximum predicted path reliability, and (4) an approach that uses online updating but only takes advantage of exploitation for path planning.

(4) *A new statistical study on the role of operator style on mission energy requirement for tele-operated UGVs.* Using a simulation model of the UGV and its operator, the impact of driving style on mission energy requirements is investigated. To determine factors and interactions that significantly increase energy consumption in a surveillance mission, the statistical response surface design is used. The impact of factors such as vehicle reference velocity, stop-and-go operations, lateral velocity variations, human delay, and operator aggressiveness and their interactions is captured with a second order model. The most significant factors are identified as vehicle reference velocity and stop-and-go operations that can double the energy consumption in a typical mission.

6.2 Summary of Major Contributions

(1) *Simulation-based acceptance testing for UGVs.* Currently, acceptance testing or methods for evaluating the mobility capabilities of UGVs are mainly performed using the actual vehicle (Jacoff et al., 2009; Carlson and Murphy, 2003, 2005; Carlson et al., 2004). Due to the limited testing facilities and apparatus, often only a small range of operational requirements can be physically tested. Additionally, conducting physical tests can be time consuming and tedious. Moreover, there are many uncontrollable or hard-to-control factors in physical tests such as variations in different operators' knowledge and operating skills, environmental condition changes, etc., which may lead to inevitable variations in the physical testing results.

To overcome the limitations of physical tests, simulation-based acceptance testing as an effective complement to physical tests is proposed. Simulation-based evaluation methods have played an increasing role in complementing physical tests in other industries, such as aerospace and automotive (Norris, 1995; Guonian et al., 2010). However, even simulation-based acceptance testing can be costly and time consuming in the case of complex dynamic simulations. Static simulation, on the other hand, is more straightforward to construct and to use for development of comprehensive boundaries of safe operations. Despite its advantages, static simulation may not always be an acceptable approximation to dynamic simulation. Currently, there is no systematic method to determine which simulation scheme can be used for a specific failure analysis scenario. The contribution of Chapter II of this dissertation is to propose a systematic method to quantitatively ensure when a

static analysis is satisfactory for failure analysis. For this purpose, dynamic and static simulation results are compared based on a statistical hypothesis testing, which is used to quantitatively judge whether both simulations will make a consistent decision on the failure state for a given scenario.

(2) *Real-time energy prediction of UGVs using mission prior knowledge and real-time measurements.* Because of the inevitable uncertainty in environmental conditions, UGVs will encounter unanticipated environmental changes that can jeopardize expected mission reliability (Carlson and Murphy, 2005). Kramer and Murphy (2006) show that some of the UGV failures can be predicted and prevented through real-time condition monitoring. Real-time performance monitoring typically uses real-time operational data to predict future failures (Saha et al., 2007, 2009a,b). These techniques do not consider prior knowledge of the remaining tasks in real-time prediction. When relying only on real-time measurements, it is assumed that future operating conditions can be represented by the collected measurements. This is not true for many of UGV operations, since the vehicle may encounter tasks later in the mission that have different energy requirements compared to earlier tasks.

The first contribution of this research topic is to propose a physical model-based Bayesian energy prediction approach. The proposed model structure considers terrain characteristics, and allows us to integrate mission prior information with real-time measurements for online energy prediction (Sadrpour et al., 2013c; Ulsoy et al., 2012). The expected prior knowledge consists of qualitative information about the road condition and road grade, which can reasonably be expected to be known prior to a mission. Although at the early stages of a mission, the uncertainty of prior knowledge might be large, this uncertainty is reduced over time using the Bayesian updating framework.

The second contribution of this work is to conduct comprehensive physical and statistical testing to experimentally validate the proposed model and prediction approach. Simulation validations of robotic systems are either based on inspection and qualitative comparison between the simulated model behavior and the real vehicle or based on the visual inspection of graphs from collected measurements (Pepper et al., 2007; Carpin et al., 2007; Taylor et al., 2007; Balakirsky et al., 2009; Chen et al., 2009). The validation studies in Chapter III are the first of its kind for UGVs that is based on comprehensive quantitative statistical analysis.

(3) *Dynamic energy-reliable path planning using two stage decision-making: exploration & exploitation.* Chapter IV of this dissertation presents a unique path planning problem for UGVs, which is represented by a network with the following characteristics and challenges: (a) The arc

cost/energy distribution is not fully known *a priori*. Finding the shortest path between two nodes in a network has been extensively studied in stochastic shortest path problems (Powell, 2011; Fan et al., 2005). However, this problem is different from traditional stochastic shortest path problems that assume the energy distributions are precisely known. Also, The problem of identifying the most reliable path between two nodes in a network was discussed in Seshadri and Inivasan (2010). However, they also assumed that the distributions are known. (b) The arcs' costs/energy requirements can be correlated. It can be shown that due to correlation, principle of optimality which is the basis for sequential optimization techniques, such as dynamic programming, cannot be directly applied to this problem (Seshadri and Inivasan, 2010). (c) The distribution of an arc cost/energy requirement can be updated in real-time by measurements. Real-time updating raises an issue known as the exploration/exploitation dilemma commonly seen in the reinforcement learning literature (Sutton and Barto, 1998). Ryzhov and Powell (2011) provide an efficient exploration strategy in a network with unknown cost distributions, but focus on finding the path with the minimum expected cost, not the path with the highest reliability. Also, there is a physical limitation which was not considered in their paper as follows: (d) UGVs can only collect measurements from the road segment that they traverse. In other words, the vehicle cannot freely explore different part of the network, and a novel exploration strategy had to be developed to overcome this challenge.

The contribution of this research topic is to propose a novel dynamic energy-reliable path planning approach for the above problem that divides the planning decisions into two stages of exploration and exploitation. At the exploration stage, a decision is made to determine where and how many sensor measurements are needed to reduce the prediction uncertainty and bias. Real-time measurements are used to dynamically determine the energy that is allocated to exploration at each road conjunction and to assess and update mission probability of success. At the exploitation stage, the UGV traverses the most reliable path chosen from the exploration stage. Our simulation results show that the proposed approach outperforms commonly used offline methods in which a path is selected using only the mission prior knowledge, as well as a method that does not use the exploration, and only relies on exploitation.

(4) *The role of operator style on mission energy requirement for tele-operated UGVs using the response surface design.* Despite the abundance of literature on the impact of driving style on energy consumption of conventional vehicles (Knowles et al., 2012; Automobile Association, 2012; Barkenbus, 2010; Gos, 2011; Van Mierlo et al., 2004; Berry, 2010), the impact of remote operating style and skill on UGVs has not been addressed. There are several aspects that motivate this

research and distinguish operations with UGVs from conventional, electric, and hybrid vehicles: (1) tele-operation induces delays beyond what is normally observed while driving other types of vehicles. The additional time delay can be attributed to wireless communication or data processing for video streaming; (2) in conventional vehicles the operator receives direct and immediate feedback and cues (visual, haptic and auditory) when turning the wheels, accelerating, or braking. In tele-operated vehicles, the operator may have to rely only on video feedback, which provides limited situation awareness, and may suffer from a time delay; (3) in conventional vehicles, locomotion accounts for the largest percentage of energy consumption. However, due to the smaller size of UGVs, electronic equipment contributes significantly to overall power consumption, which affects the optimal driving style; (4) unlike electric or hybrid vehicles, most UGVs do not have power regenerating capabilities and the operator style has a different impact on energy consumption; (5) UGVs are frequently operated off-road in hazardous and unfamiliar conditions, and the intensity of missions and lack of situation awareness make operations more prone to maneuvering mistakes that increase energy requirements.

The contribution of Chapter V is to use the statistical response surface design to systematically determine factors and interactions in driving style that significantly increase energy consumption in a small UGV. To carry the analyses, a simulation model of the vehicle and its operator is utilized that incorporates factors such as deviation from the vehicle optimal velocity, communication and human delays, random variations in steering, stop-and-go operations and operator aggressiveness. Identifying the significant factors allow us to design training and procedures to reduce energy consumption in typical surveillance missions by half.

6.3 Future Research

The improvement and prediction of system reliability for UGVs considering environmental and operational uncertainty is important and challenging in terms of both methodological development and implementation in real world systems. This provides many future research opportunities in manufacturing, civilian and military applications, which will be of broad interest to public and private agencies and foundations. In this dissertation, some initial efforts have been made and demonstrated in both methodological developments and real-world applications. However, future research is needed in this area, and a few examples of such research topics are listed below.

- The proposed methodologies in this dissertation focused on two deployment phases: design and field operation. The third deployment phase for reliability improvement is post-deployment.

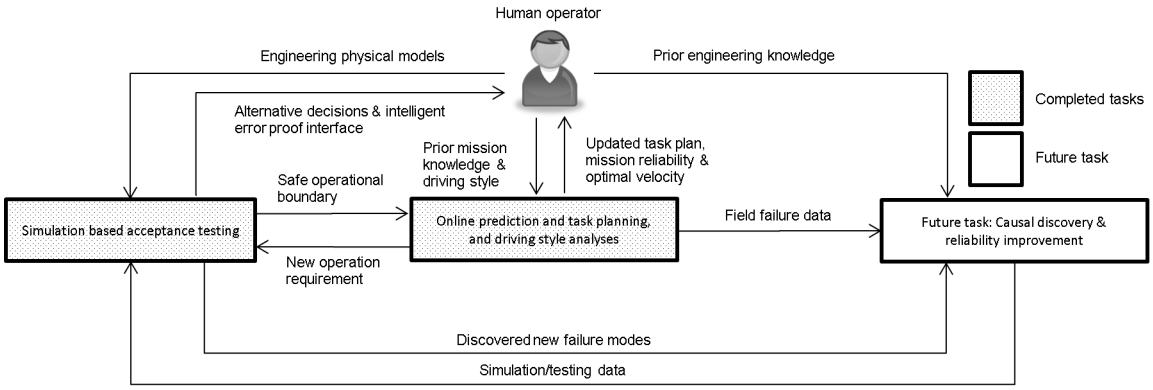

Figure 6.1: The proposed future research direction will focus on post deployment reliability modeling, which complements the accomplished research topics.

At this phase, some field failure data is available, which provides future research opportunity for failure analyses and reliability improvement. The relation among the completed research topics and the proposed future research direction is shown in Figure 6.1. The first future topic will aim to improve UGV reliability by modeling the overall system reliability during the early stages of deployment. This research topic is specifically useful for UGV manufacturers and designers to evaluate the reliability of their products, while considering a diversity of usages and operations. The task focuses on the analysis of the field failure data to model and assess UGV products' reliability by incorporating a wide range of operational conditions applied to UGVs. To construct the UGV system reliability model based on field failure data, a mixture failure distribution model can be used to account for different failure rates of UGVs under different operation conditions. A Bayesian modeling and estimation framework can be used to overcome the shortage of field failure data at the beginning by effectively utilizing the prior knowledge of the components reliability. One of the major challenges is modeling at the system level, which must take into account the variety of system configurations and the poor quality of the field failure data. The field failure data may be available at the system level or at the component level, or the data may have missing information about the operating condition at which the failure occurs.

- The last research topic in this dissertation studied how different driving styles affect the energy consumption in a mission. The second future research topic will build upon those findings to develop an analytical model that integrates the UGV human operator into the system reliability assessment. The model enables the end users to choose the operators that are best suited for a mission, based on their skill level. Traditional reliability analyses of UGVs have

mainly focused on mechanical/electronics failures, but many failures are associated with faulty interactions between the robot and its human operator, which is critical due to tele-operation. The reliability failure model under consideration is composed of three modeling elements: (1) mechanical/electronics, (2) human operator, and (3) interaction of human operator and mechanical/electronics elements. The first modeling element, the mechanical/electronics failures, is based on physical reliability models that are affected by covariates of environmental factors, such as road roughness and duration of the mission. The second modeling element, human operator, includes failures due to human mistakes, lapses and errors affected by the operator experience and mission workload. The third modeling element, interactions, captures the influence of decisions of human operators on mechanical failures. For instance, a novice operator may operate the UGV beyond its design capabilities (see Chapter II for some examples). Another example is the impact of the experience and dexterity of a driver on the duration of a mission (see Chapter V for some examples). The proposed system reliability model will help answer critical questions such as: (1) How much will a change in the environmental conditions/mission workload impact the reliability of the system and the mission? (2) Given the current environmental conditions, how much does the reliability of the mission change if a novice operator is replaced with an expert operator? There is a significant need for this line of research. Also, this research topic is challenging because of its need for integration of mechanical reliability models with less well established human operator models.

- Finally, there are some future work to extend this research. For example:

  - *Model extensions to include practical road and operational complexities*

    One of the requirements of the proposed Bayesian approach is that road segments have a consistent grade and surface condition. Situations may arise in which the UGV traverses unstructured terrains such as a forest or an earthquake-affected area. In these situations, it is difficult to characterize the road conditions. Future work should focus on extending the framework to such scenarios. One potential solution is to rely on real-time methods such as RLS for energy prediction, while the on board camera is used to characterize and classify the immediate surface/road conditions (Manduchi et al., 2005; Muller et al., 2013) for prediction improvements. Moreover, the currently used vehicle model does not consider sharp turning events, wheel slippage, penetration of wheels in the soil, or power regenerative breaking capabilities. Our prediction approach was applied to a scenario with frequent turning and the obtained results were satisfying (Ersal et al., 2014); however,

further improvement is possible if turning maneuvers are explicitly included in the vehicle model. For instance, the vehicle dynamic model of Chapter V considers turning and can be integrated with the proposed Bayesian prediction framework. Moreover, High fidelity wheel-terrain interaction model that can capture penetration of wheels into the soil was developed in Jia et al. (2012), but further advancements are needed to integrate the above model to a mission energy prediction framework. Another interesting situation that can arise is recharging capabilities. The recharging can be performed using recharging docks or energy harvesting capabilities for increasing operational endurance (Page et al., 2010). Recharging capabilities were considered in Wei et al. (2012), but the cost functions were deterministic and did not consider the uncertainty in operating conditions. Those will be considered in future work for the model improvement.

– *Development of general mission optimization criteria*

  While incorporating the mission duration in the optimization framework for path planning was suggested (in addition to energy criterion), it was not implemented in the thesis. Moreover, a fixed failure threshold for calculating the reliability of alternative paths was used in the thesis. Another extension is to use dynamic thresholding to consider the thermal effect of battery on vehicle's state of change, in which the failure boundary may be time varying during the mission execution.

– *Development of an integrated framework to optimally combine autonomous and semi-autonomous operations.*

  This thesis focused on the impact of tele-operation on energy requirement of a small UGV using a simulated model of the vehicle and its operator. A natural extension of this research is to replace the simulation with actual drivers in conjunction with a simulated model of the vehicle. Another extension is to investigate those scenarios in which increased autonomy or lack of thereof improves energy consumption. The level of autonomy can vary from no autonomy (i.e., tele-operation by human operator) to full autonomy (i.e., no human involvement). When the mission profile (e.g., the path trajectory, the terrain surface condition and obstacles) are pre-known, one can derive the optimal drive cycle that minimizes (for instance) the energy usage using methodologies such as optimal control (Broderick et al., 2012) or optimization (Sadrpour et al., 2014). Subsequently, the optimal drive cycle can be prescribed to a UGV for fully autonomous operations. However, when

the mission operating condition is not well-known *a priori*, autonomous navigation and path planning can become quite challenging in the presence of several competing priorities such as safety, mission duration and energy requirements.

Currently, tele-operated or semi-autonomous driving maybe the most viable solution for operating in unknown environments; however, in the past few decades, efforts have been made in developing fully autonomous (conventional) vehicles. For instance, Defense Advanced Research Projects Agency (DARPA) has sponsored DARPA Grand Challenges (Seetharaman et al., 2006). The competitions took place in various operating conditions including off-road and urban environments with great success leading to the first U.S. driven license for driveless cars (Ferreras, 2013). While driveless car research denoted a gas savings from 20% to 50%, the research in this area is still ongoing and DARPA Grand Challenges have not been free of accidents (Levinson et al., 2011). Considering the developing nature of methodologies, the highest priority is typically placed on safety and demonstration of technology capabilities, and future research is needed to study the impact of various autonomous driving algorithms on energy consumption.

BIBLIOGRAPHY

BIBLIOGRAPHY

Gosford City Council project report for the local air education project. (accessed on 1 February 2012) 2011. URL `http://www.gosford.nsw.gov.au/environment/education/documents/Economic%20Driving_Ver2.pdf`.

D. L. Applegate, R. E. Bixby, W. J. Cook, and V. Chvatal. *The Traveling Salesman Problem: A Computational Study*. Princeton University Press, 2011.

Automobile Association. Eco driving advice, (accessed on 14 September 2013) 2012. URL `http://www.theaa.com/motoring_advice/fuels-and-environment/drive-smart.html`.

S. Balakirsky, S. Carpin, G. Dimitoglou, and B. Balaguer. From simulation to real robots with predictable results: Methods and examples. In *Performance Evaluation and Benchmarking of Intelligent Systems*, pages 113–137. 2009.

J. N. Barkenbus. Eco-driving: An overlooked climate change initiative. *Energy Policy*, 38(2):762 – 769, 2010.

M. I. Berry. *The effects of driving style and vehicle performance on the real-world fuel consumption of US light-duty vehicles*. Master's thesis, Massachusetts Institute of Technology, 2010.

K. Boice, A. Leo, J. Lee, Jr. Paulson, M. Skalny, and T. Valascho. Baseline field testing of BB-2590 lithium-ion batteries using an iRobot FasTac 510 robot. Technical report, 2010.

J. Borenstein, A. Borrell, R. Miller, and D. Thomas. Heuristics-enhanced dead-reckoning (HEDR) for accurate position tracking of tele-operated UGVs. In *Proceeedings of Society of Photographic Instrumentation Engineers*, volume 7692, pages 76921R–76921R–12, 2010.

P. H. Borgstrom, A. Singh, B. L. Jordan, G. S. Sukhatme, M. A. Batalin, and W. J. Kaiser. Energy based path planning for a novel cabled robotic system. In *International Conference on Intelligent Robots and Systems*, pages 1745 –1751, 2008.

J. Broderick, D. Tilbury, and E. Atkins. Energy usage for UGVs executing coverage tasks. In *Proceedings of Unmanned Systems Technology*, pages 83871A–83871A, Baltimore, Maryland, USA, 2012.

R. K. Burdick. *Gauge Repeatability and Reproducibility (R&R) Studies, Misclassification Rates*. John Wiley & Sons, Ltd, 2008.

J. Carlson and R. Murphy. Reliability analysis of mobile robots. In *International Conference on Robotics and Automation*, volume 1, pages 274–281, Taipei, Taiwan, 2003.

J. Carlson and R. Murphy. How UGVs physically fail in the field. *IEEE Transactions on Robotics*, 21(3):423–437, 2005.

J. Carlson, R. Murphy, and A. Nelson. Follow-up analysis of mobile robot failures. In *International Conference on Robotics and Automation*, pages 4987–4994, New Orleans, Louisiana, 2004.

S. Carpin, T. Stoyanov, Y. Nevatia, M. Lewis, and J. Wang. Quantitative assessments of usarsim accuracy. In *Proceedings of PerMIS*, Bremen, Germany, 2006.

S. Carpin, M. Lewis, J. Wang, S. Balakirsky, and C. Scrapper. Bridging the gap between simulation and reality in urban search and rescue. In *RoboCup 2006: Robot Soccer World Cup X*, pages 1–12. Springer Berlin Heidelberg, 2007.

M. Ceraolo and G. Pede. Techniques for estimating the residual range of an electric vehicle. *IEEE Transactions on Vehicular Technology*, 50(1):109–115, 2001.

X. Chen, Q. Ou, D. R. Wong, Y. J. Li, M. Sinclair, and A. Marburg. Flight dynamics modelling and experimental validation for unmanned aerial vehicles. *Mobile Robots - State of the Art in Land, Sea, Air, and Collaborative Missions*, pages 177–202, Rijeka, Croatia, 2009.

P. Congdon. *Bayesian statistical modelling.* John Wiley & Sons, Ltd., 2003.

J. W. Crandall, M. A. Goodrich, Jr. Olsen, D. R., and C.W. Nielsen. Validating human-robot interaction schemes in multitasking environments. *IEEE Transactions on Systems, Man and Cybernetics, Part A: Systems and Humans*, 35(4):438–449, 2005.

G. Daigneault, P. Joly, and J-Y. Frigon. Previous convictions or accidents and the risk of subsequent accidents of older drivers. *Accident Analysis & Prevention*, 34(2):257–261, 2002.

J. Davis, C. Smyth, and K. McDowell. The effects of time lag on driving performance and a possible mitigation. *IEEE Transactions on Robotics*, 26(3):590–593, 2010.

R. Dearden, N. Friedman, and S. Russell. Bayesian Q-learning. In *Proceedings of Fifteenth National Conference on Artifical Intelligence*, pages 761–768, Menlo Park, CA, 1998.

R. Dearden, N. Friedman, and D. Andre. Model based bayesian exploration. In *Proceedings of the Fifteenth Conference on Uncertainty in Artificial Intelligence*, pages 150–159, San Francisco, CA, 1999.

E. V. Denardo. *Dynamic Programming: Models and Applications.* Dover Publications, Englewood Cliffs, N.J., 2003.

F. DiGenova, T. Austin, J. Tiden, J. M. Lee, and P. Tarczy. Development of an onboard data acquisition system for recording vehicle operating characteristics and emissions. Technical report, 1994.

F. Dressler and G. Fuchs. Energy-aware operation and task allocation of autonomous robots. In *Proceedings of the fifth international workshop on robot motion and control*, pages 163–168, Dymaczewo, Poland, 2005.

FIAT eco-drive. Eco-driving uncovered: the benefits and challenges of eco-driving based on the first study using real journey data. (accessed on 14 September 2013) 2010. URL `http://www.lowcvp.org.uk/assets/reports/Fiat_Eco-Driving20Uncovered.pdf`.

E. Ericsson. *Urban Transport and the Environment in the 21st Century : The relation between vehicular fuel consumption and exhaust emission and the characteristics of driving pattern.* WIT Press, 2000.

T. Ersal, Y. Kim, J. Broderick, T. Guo, A. Sadrpour, A. Stefanopoulou, J. Siegel, D. Tilbury, E. Atkins, H. Peng, J. Jin, and A. G. Ulsoy. Keeping ground robots on the move through better battery and mission management. In *DSC Magazine (to appear)*, 2014.

Y. Y. Fan, R. E. Kalaba, and J. E. Moore. Shortest paths in stochastic networks with correlated link costs. *Computers and Mathematics With Applications*, 49:1549–1564, 2005.

L. Ferreras. *Autonomous Vehicles: A Critical Tool to Solve the XXI Century Urban Transportation Grand Challenge*, chapter 36, pages 405–412. 2013.

D. W. Gage. UGV history 101: A brief history of unmanned ground vehicle (UGV) development efforts. Technical report, 1995.

Geocontext. Geocontext center for geographic analysis, May 2013. URL `http://www.geocontext.org/publ/2010/04/profiler/en/`.

I. Godler, K. Ohnishi, and T. Yamashita. Repetitive control to reduce speed ripple caused by strain wave gearing. In *International Conference on Industrial Electronics, Control and Instrumentation*, volume 2, pages 1034–1038, Bologna, Italy, 1994.

J. Gondor, T. Markel, A. Simpson, and M. Thornton. Using global positioning system travel data to assess real-world energy use of plug-in hybrid electric vehicles. *Transportation Research Record*, pages 26–32, 2007.

Google-Earth, May 2013. URL `earth.google.com`.

N. Gorjian, L. Ma, M. Mittinty, P. Yarlaqadda, and Y. Sun. A review on degradation models in reliability analysis. In *Proceedings of the Fourth World Congress on Engineering Asset Management*, Athens, Greece, 2009.

T. Guo and H. Peng. A simplified skid-steering model for torque and power analysis of tracked small unmanned ground vehicles. In *American Control Conference*, pages 1106–1111, Washington, DC, 2013.

Y. Guonian, H. Haiying, S. Hao, W. Junhu, and S. Guoji. The whole vehicle system dynamics modeling and simulation for transportation vehicle. In *Mechanic Automation and Control Engineering International Conference*, pages 698–701, Wuhan, China, 2010.

H. Hagras, V. Callaghan, M. Colley, and M. Carr-West. A fuzzy-genetic based embedded-agent approach to learning and control in agricultural autonomous vehicles. In *International Conference Robotics and Automation*, volume 2, pages 1005–1010, Detroit, MI, 1999.

H. Hagras, M. Colley, V. Callaghan, and M. Carr-West. Online learning and adaptation of autonomous mobile robots for sustainable agriculture. *Autonomous Robots*, 13(1):37–52, 2002.

P. A. Hancock, M. Lesch, and L. Simmons. The distraction effects of phone use during a crucial driving maneuver. *Accident Analysis & Prevention*, 35(4):501 – 514, 2003.

P. D. Hoff. *A First Course in Bayesian Statistical Methods*. Springer, 1st edition, 2009.

B. A. Holmen and D. A. Niemeier. Characterizing the effects of driver variability on real-world vehicle emissions. *Transportation Research Part D: Transport and Environment*, 3(2):117 – 128, 1998.

iRobot 510 Packbot Specifications. (accessed on 14 September 2013) . URL `http://www.irobot.com/us/learn/defense/packbot/Specifications.aspx`.

A. Jacoff, E. Messina, H. Huang, A. Virts, and A. Downs. Standard test methods for response robots (pamphlet). *ASTM International Committee on Homeland Security Application; Operational Equipment; Robots (E54.08.01)*, 2009.

Z. Jia, W. Smith, and H. Peng. Terramechanics-based wheel-terrain interaction model and its applications to off-road wheeled mobile robots. *Robotica*, 30(3):491–503, 2012.

Y. Kanayama, Y. Kimura, F. Miyazaki, and T. Noguchi. A stable tracking control method for an autonomous mobile robot. In *International Conference on Robotics and Automation*, volume 1, pages 384–389, 1990.

A. Kelly, N. Chan, H. Herman, and R. Warner. Experimental validation of operator aids for high speed vehicle teleoperation. In *Experimental Robotics*, volume 88, pages 951–962. Springer International Publishing, 2013.

M. Knowles, H. Scott, and D. Baglee. The effect of driving style on electric vehicle performance, economy and perception. *International Journal of Electric and Hybrid Vehicles*, 4(3):228–247, 2012.

J. Kramer and R. Murphy. Endurance testing for safety, security and rescue robots. In *Performance Metrics for Intelligent Systems*, pages 247–254, Washington, DC, 2006.

B. H. Lam, S. K. Panda, and J.-X. Xu. Reduction of periodic speed ripples in PM synchronous motors using iterative learning control. In *International Conference on Industrial Electronics, Control and Instrumentation*, volume 2, pages 1406–1411, Nagoya, Japan, 2000.

R. Langari and J-S. Won. Intelligent energy management agent for a parallel hybrid vehicle-part I: system architecture and design of the driving situation identification process. *IEEE Transactions on Vehicular Technology*, 54(3):925–934, 2005.

J. Larsson, M. Broxvall, and A. Saffiotti. An evaluation of local autonomy applied to teleoperated vehicles in underground mines. In *International Conference of Robotics and Automation*, pages 1745–1752, Anchorage, AK, 2010.

H. J. Lee, J. Jin, and A. G. Ulsoy. Simulation based acceptance testing for unmanned ground vehicles. In *Proceeding of the 209 Ground Vehicle Systems Engineering & Technology Symposium*, page 6, 2009.

T. Lendvay, P. Casale, R. Sweet, and C. Peters. Initial validation of a virtual-reality robotic simulator. *Journal of Robotic Surgery*, 2(3):145–149, 2008.

J. Levinson, J. Askeland, J. Becker, J. Dolson, D. Held, S. Kammel, J. Z. Kolter, D. Langer, O. Pink, V. Pratt, M. Sokolsky, G. Stanek, D. Stavens, A. Teichman, M. Werling, and S. Thrun. Towards fully autonomous driving: Systems and algorithms. In *IEEE Intelligent Vehicles Symposium (IV)*, pages 163–168, 2011.

L. Ljung. *System Identification: Theory for the User*. Prentice-Hall, Inc., Upper Saddle River, N.J., 1999.

H. Lu, W.J. Kolarik, and S. Lu. Real-time performance reliability prediction. *IEEE Transactions on Reliability*, 50(4):353–357, 2001a.

S. Lu, H. Lu, and W.J. Kolarik. Multivariate performance reliability prediction in real-time. *Reliability Engineering and System safety*, 72(1):39–45, 2001b.

R. Manduchi, A. Castano, A. Talukder, and L. Matthies. Obstacle detection and terrain classification for autonomous off-road navigation. *Autonomous Robots*, 18(1):81–102, 2005.

V. Manzoni, A. Corti, P. De Luca, and S. M. Savaresi. Driving style estimation via inertial measurements. In *International Conference on Intelligent Transportation Systems*, pages 777–782, Madeira Island, Portugal, 2010.

Y. Mei, Y. Lu, Y. Hu, and C. Lee. Energy-efficient motion planning for mobile robots. In *International Conference on Robotics and Automation*, volume 5, pages 4344–4349, New Orleans, LA, 2004.

Y. Mei, Y. Lu, Y. Hu, and C. Lee. A case study of mobile robot's energy consumption and conservation techniques. In *International Conference on Advanced Robotics*, pages 492–497, Seattle, WA, 2005.

E. Messina and A. Jacoff. Performance standards for urban search and rescue robots. In *Proceedings of the International Society for Optical Engineering*, volume 6230, pages 62301V–1–12, Orlando, FL, 2006.

Minitab. Minitab 16 statistical software. State College, PA: Minitab, Inc., 2010. URL `www.minitab.com`.

D. Montgomery. *Design and Analysis of Experiments*. Wiley, 6th edition, 2004.

D. Montgomery. *Introduction to Statistical Quality Control*. John Wiley & Sons, Inc., New York, 5th edition, 2005.

U. A. Muller, L. D. Jackel, Y. LeCun, and B. Flepp. Real-time adaptive off-road vehicle navigation and terrain classification. In *SPIE Defense, Security, and Sensing*, pages 87410A–87410A. International Society for Optics and Photonics, 2013.

G. Norris. Boeing's seventh wonder. *IEEE Spectrum*, 32(10):20–23, 1995.

S. F. Page, J. D. Rogers, K. May, D. R. Myatt, D. Hickman, and M. I. Smith. Cooperative energy harvesting for long-endurance autonomous vehicle teams. In *SPIE Defense, Security, and Sensing*, pages 76921X–76921X. International Society for Optics and Photonics, 2010.

S. M. Pandit and S. M. Wu. *Time Series and System Analysis with Applications*. John Wiley & Sons, Inc., New York, NY, 1983.

C. Pepper, S. Balakirsky, and C. Scrapper. Robot simulation physics validation. In *Proceedings of the 2007 Workshop on Performance Metrics for Intelligent Systems*, pages 97–104, New York, NY, 2007.

A. J. Pick and D. J. Cole. Neuromuscular dynamics and the vehicle steering task. In *Proceedings of IAVSD Symposium on Dynamics of Vehicles on Roads and on Tracks*, Kanagawa, Japan, 2003.

W. B. Powell. *Approximate Dynamic Programming: Solving the Curses of Dimensionality*. Wiley, Hoboken, N.J., 2nd edition, 2011.

D. R. Proffitt, M. Bhalla, R. Gossweiler, and J. Midgett. Perceiving geographical slant. *Psychonomic Bulletin & Review*, 2(4):409–428, 1995.

E. Purdy. Ground robotics technology, Presentation slides, 2007.

RAC. available at http://media.rac.co.uk/pdf/rac-rom-2010-06-14.pdf. (accessed on 13 February 2012). 2010.

G. Reichart, S. Friedmann, C. Dorrer, H. Rieker, E. Drechsel, and G. Wermuth. Potentials of BMW driver assistance to improve fuel economy. In *FISITA World Automotive Congress*, Paris, 1998.

Z.-B. Ren, Z-A. Yu, and J-W. Liang. Study and implementation on high accuracy servo system for robot joint. In *Chinese Control and Decision Conference*, pages 1673–1676, Guilin, China, 2009.

M. D. Rossetti, A. Kumar, and R. A. Felder. Mobile robot simulation of clinical laboratory deliveries. In *Proceedings of the 30th Conference on Winter Simulation*, pages 1415–1422, Los Alamitos, CA, 1998.

I. O. Ryzhov and W. B. Powell. Information collection on a graph. *Operations Research*, 59(1): 188–201, 2011.

A. Sadrpour, J. Jin, A. G. Ulsoy, and H. J. Lee. Simulation-based acceptance testing for unmanned ground vehicles. *International Journal of Vehicle Autonomous Systems*, 11(1):62–85, 2011.

A. Sadrpour, J. Jin, and A. G. Ulsoy. Mission energy prediction for unmanned ground vehicles. In *International Conference on Robotics and Automation*, St. Paul, Minnesota, 2012.

A. Sadrpour, J. Jin, and A. G. Ulsoy. Experimental validation of mission energy prediction model for unmanned ground vehicles. In *American Control Conference*, pages 5960–5965, Washington, DC, 2013a.

A. Sadrpour, J. Jin, and A. G. Ulsoy. Mission energy prediction for unmanned ground vehicles using real-time measurements and prior knowledge. *Journal of Field Robotics*, 30(3):399–414, 2013b.

A. Sadrpour, J. Jin, and A. G. Ulsoy. Real-time energy reliable path planning for UGVs using mission prior knowledge. *International Journal of Vehicle Autonomous Systems (in review)*, 2013c.

A. Sadrpour, J. Jin, and A. G. Ulsoy. Real-time energy reliable path planning for UGVs using mission prior knowledge. In *Dynamic Systems and Control Conference*, Palo Alto, CA, 2013d.

A. Sadrpour, J. Jin, and A. G. Ulsoy. The role of operator style on mission energy requirements for tele-operated unmanned ground vehicles. In *American Control Conference (submitted)*, Portland, OR, 2014.

B. Saha and K. Goebel. Uncertainty management for diagnostics and prognostics of batteries using bayesian techniques. In *IEEE Aerospace Conference*, pages 1–8, Big Sky, MT, 2008.

B. Saha, S. Poll, K. Goebel, and J. Christophersen. An integrated approach to battery health monitoring using bayesian regression and state estimation. In *IEEE Autotestcon Conference*, pages 646–653, Baltimore, MD, 2007.

B. Saha, K. Goebel, and J. Christophersen. Comparison of prognostic algorithms for estimating remaining useful life of batteries. *Transactions of the Institute of Measurement and Control*, 31 (3-4):293–308, 2009a.

B. Saha, S. Saha, and K. Goebel. A distributed prognostic health management architecture. In *Proceedings of the Conference of the Society for Machinery Failure Prevention Technology*, Dayton, OH, 2009b.

B. Saha, E. Koshimoto, C. Quach, E. Hogge, T. Storm, B. Hill, S. Vazquez, and K. Goebel. Battery health management system for electric UAVs. In *IEEE Aerospace Conference*, pages 1–9, Big Sky, MT, 2011.

M. W. Sayers. Dynamic terrain inputs to predict structural integrity of ground vehicles. Technical report, 1988.

G. Seetharaman, A. Lakhotia, and E. P. Blasch. Unmanned vehicles come of age: The darpa grand challenge. *Computer*, 39(12):26–29, 2006.

S. A. Seixas-Mikelus, T. Kesavadas, G. Srimathveeravalli, R. Chandrasekhar, G. E. Wilding, and K. A. Guru. Face validation of a novel robotic surgical simulator. *Urology*, 76(2):357–360, 2010.

R. Seshadri and K. K. Inivasan. Algorithm for determining most reliable travel time path on network with normally distributed and correlated link travel times. *Transportation Research Record: Journal of the Transportation Research Board*, 2196:83–92, 2010.

A. Sipahioglu, A. Yazici, O. Parlaktuna, and U. Gurel. Real-time tour construction for a mobile robot in a dynamic environment. *Robotics and Autonomous Systems*, 56(4):289–295, 2008.

S. Stancliff and J. Dolan. Towards a predictive model of mobile robot reliability. Technical report, 2005.

R. S. Sutton and A. G. Barto. *Reinforcement Learning: An Introduction*. A Bradford Book, Cambridge, MA, 1998.

F. U. Syed, D. Filev, F. Tseng, and H. Ying. Adaptive real-time advisory system for fuel economy improvement in a hybrid electric vehicle. In *Annual Meeting of the North American Fuzzy Information Processing Society*, pages 1–7, 2009.

B. K. Taylor, S. Balakirsky, E. Messina, and R. D. Quinn. Design and validation of a whegs robot in USARSim. In *Proceedings of the Workshop on Performance Metrics for Intelligent Systems*, 2007.

D. M. Tilbury and A. G. Ulsoy. A new breed of robots that drive themselves. *ASME Mechanical Engineering Magazine*, 133:28–33, 2011.

S. Tricomo. Army AL&T online, 2009. URL `http://www.usaasc.info/alt_online/article.cfm?iID=0904&aid=12`.

A. G. Ulsoy, H. Peng, and M. Cakmakci. *Automotive Control Systems*. Cambridge University Press, Cambridge, England, 2012.

U.S. Army. Safe operation of mobile ugv systems. Technical report, U.S. Army Aberdeen Test Center, (accessed on 26 September 2013) 2010. URL `http://oai.dtic.mil/oai/oai?verb=getRecord&metadataPrefix=html&identifier=ADA525472`.

J. Van Mierlo, G. Maggetto, E. Van de Burgwal, and R. Gense. Driving style and traffic measures-influence on vehicle emissions and fuel consumption. *Proceedings of the Institution of Mechanical Engineers, Part D: Journal of Automobile Engineering*, 218(1):43–50, 2004.

N. Vichare, P. Rodgers, V. Eveloy, and M. Pecht. Environment and usage monitoring of electronic products for health assessment and product design. *Quality Technology & Quantitative Management*, 4:235–250, 2007.

I. De Vlieger, D. De Keukeleere, and J. G. Kretzschmar. Environmental effects of driving behaviour and congestion related to passenger cars. *Atmospheric Environment*, 34(27):4649 – 4655, 2000.

M. Vojtíšek, M. Fenkl, and M. Dufek. Effect of high-speed, performance driving on exhaust emissions of modern light-duty vehicles. *Advances in Automotive Engineering edited by Pavel Novotný, Tribun EU, Brno*, 2008.

M. Vojtíšek, M. Fenkl, M. Dufek, and J. Mareš. Off-cycle, real-world emissions of modern light duty diesel vehicles. Technical report, Society of Automotive Engineers, Warrensdale, PA, 2009.

C. Walsh, S. Carroll, A. Eastlake, and P. Blythe. Electric vehicle driving style and duty variation performance study. (accessed 15 September 2013), 2010. URL `http://www.nichevehiclenetwork.co.uk/LinkClick.aspx?fileticket=WTmGSFXB8qA%3d&tabid=531`.

J. Wang, M. Lewis, S. Hughes, M. Koes, and S. Carpin. Validating USARsim for use in HRI research. *Proceedings of the Human Factors and Ergonomics Society Annual Meeting*, 49(3):457–461, 2005.

H. Wei, B. Wang, Y. Wang, Z. Shao, and K. C. C. Chan. Staying-alive path planning with energy optimization for mobile robots. *Expert Systems with Applications*, 39(3):3559–3571, 2012.

J. Y. Wong. *Theory of Ground Vehicles*. John Wiley & Sons, Inc., Ottawa, Canada, 2008.